Development of porous membranes for water desalination

Ma, Xianzheng

DOI (link to publication from Publisher):
10.54337/aau499832678

Publication date:
2022

Document Version
Publisher's PDF, also known as Version of record

DEVELOPMENT OF POROUS MEMBRANES FOR WATER DESALINATION

BY
XIANZHENG MA

DISSERTATION SUBMITTED 2022

AALBORG UNIVERSITY
DENMARK

DEVELOPMENT OF POROUS MEMBRANES FOR WATER DESALINATION

by

Xianzheng Ma

AALBORG UNIVERSITY
DENMARK

Dissertation submitted 2022

Dissertation submitted:	September 2022
PhD supervisor:	Associate Prof. Vittorio Boffa, Aalborg University, Denmark
Assistant PhD supervisor:	Associate Prof. Cejna Anna Quist-Jensen, Aalborg University, Denmark
PhD committee:	Associate Professor Donghong Yu Aalborg University
	Professor Giorgio Domenico Maria Micale University of Palermo, Italy
	Professor María José López Muñoz King Juan Carlos University, Spain
PhD Series:	Faculty of Engineering and Science, Aalborg University
Department:	Department of Chemistry and Bioscience

ISSN (online): 2446-1636
ISBN (online): 978-87-7573-831-1

Published by:
Aalborg University Press
Kroghstræde 3
DK – 9220 Aalborg Ø
Phone: +45 99407140
aauf@forlag.aau.dk
forlag.aau.dk

Printed in Denmark by Stibo Complete, 2022

ENGLISH SUMMARY

Membrane desalination is an important technology for the sustainable development of future water resources, yet there are limitations for the most applied membrane desalination technologies in terms of brine discharge, water recovery, and energy consumption. This Ph.D. study has attempted to provide alternative membrane desalination solutions, namely, nanofiltration (NF) and membrane distillation (MD).

Three studies from the Ph.D. project have been concluded in this thesis. The first study focused on the development and testing of nanofiltration membranes for groundwater desalination in the Puglia region, Italy. Groundwater in Puglia suffers from high salinity and potential pollution of organic pollutants. Sol-gel-derived SiO_2-Al_2O_3 membranes with high stability were developed in this study. Both the newly developed ceramic membrane and commercial polymeric NF membrane (Dow NF90) have been screened for the desalination and detoxification of groundwater samples, and NF90 was selected for the construction of the desalination demonstrative site in the local area.

In the second study, membrane distillation was applied for the desalination of an inland mariculture effluent in Eliat, Israel. A polypropylene hollow fiber membrane was applied for the MD process of the effluent. To simulate the chemical condition of the fish farming process in which potentially toxic compounds are accumulated in the fish pounds, formaldehyde was sparked into the effluent samples. Due to the high volatility, this model pollutant could not be retained by the MD membrane. Therefore the MD process was coupled for the first time with UVC/VUV photolysis process to detoxify the membrane permeate.

The third study was the development of a novel inorganic MD membrane with high thermal and chemical stability, but also a high MD performance, including high hydrophobicity, and low thermal conductivity, high water permeability. The membrane was derived from a low-cost industrial material. To the writing date of the thesis, the inorganic MD membrane is undergoing a patenting process, thus, the specific materials, methods, and performance will not be discussed in this thesis. Instead, the thesis will attempt to shed light on the general synthesis strategy to overcome some of the major challenges of the inorganic MD membrane development.

The funder of this Ph.D. project is Project Ô (H2020-CIRC-2017 TwoStage, Grant Agreement n. 776816), an EU project that aims for a circular water economy. Finally, the data and membranes obtained from this Ph.D. study will be contributed to the establishment of the local demo sites.

DANSK RESUME

Afsaltning ved brug af membranteknologi spiller en vigtig rolle for at sikre vandressourcer i fremtiden på en bæredygtig måde. Dog er der flere begrænsninger ved de eksisterende membranteknologier, såsom udledning af koncentratstrømme, vandgenindvinding og energiforbrug. Dette Ph.d. studie omhandler alternative metoder til afsaltning med membraner, som for eksempel nanofiltrering (NF) og membrandestillering (MD).

Tre studier fra dette Ph.d. projekt er medtaget i denne afhandling. Det først studie fokuserer på udvikling og testning af nanofiltreringsmembraner til afsaltning af grundvand fra Puglia i Italien. Puglia har problemer med for højt saltindhold og mulig forurening med organiske stoffer i deres grundvand. I dette studie er SiO_2-Al_2O_3 membraner (keramiske membraner) udviklet, som har en høj stabilitet. Membranerne er blevet testet til afsaltning og rensning af grundvandet i Puglia og herefter sammenlignet med kommercielle polymer NF membraner (Dow NF90).

I det andet studie blev membrandestillering afprøvet til afsaltning af spildevand fra udløb fra akvakultur i Eliat i Israel. En polypropylen membran (polymer membran) blev testet til brug i MD processen og for at efterligne de kemiske betingelser af fiskeindustrien, hvor toksiske forbindelser potentielt kan ophobes, blev formaldehyd tilsat til udløbsprøverne fra Israel. Formaldehyd kunne ikke tilbageholdes med MD membranen grundet dets flygtighed. Derfor blev MD processen integreret med UVC/VUV fotolyse for rense permeatet fra MD.

Det tredje studie omhandler udvikling af nye uorganiske MD membraner, som udviser høj termisk og kemisk stabilitet, men også en høj ydeevne i form af gode hydrofobiske egenskaber, lav termisk konduktivitet og stor vandpermeabilitet. Membranen blev udviklet ud fra billige industrielle materialer. Denne membran indgår i en igangværende patentproces under skriveprocessen af denne afhandling og derfor vil dens materiale, metode til fremstilling og dens ydeevne ikke blive diskuteret i denne afhandling. I stedet vil afhandlingen omhandle den generelle syntetiseringsstrategi i forbindelse med at overvinde nogle af udfordringerne ved fremstilling af uorganiske MD membraner.

Dette Ph.d. projekt er en del af EU projektet; Project Ô, som er bevilliget under Horizon2020 (H2020-CIRC-2017 TwoStage, Grant Agreement n. 776816), hvis formål er et cirkulært vandforbrug og hvor membranerne og membranprocesserne, fremstillet i dette Ph.d. studie, vil blive brugt på lokale demonstrationssteder i f.eks. Italien og Israel.

ACKNOWLEDGMENTS

It’s been a long journey since the first come to Aalborg University in 2016, I would not make it this far without the support of my supervisors, colleagues, friends, and families.

But first, I would show my appreciation for Project Ô for funding my Ph.D. study. I would like to thank I.R.I.S. s.r.l. (Orbassano, Italy), for providing the NF case study for groundwater treatment. And I would also like to thank the National Center of Mariculture (IOLR), Eliat, Israel. For providing the MD case study for mariculture effluent treatment. Additionally, I would like to thank Shandong Guiyuan Advanced Ceramic Co, Ltd, for promoting my studies by providing the membrane samples.

Then, I would like to thank my supervisor Vittorio Boffa. I am grateful for him to be my supervisor at the very beginning of my master's project, and we have been working together ever since. He has taught me a lot regarding inorganic chemistry, membrane technologies, and water treatment. Thanks for believing in me, and giving me many opportunities to improve myself. I would also like to thank my co-supervisor Cejna Anna Quist-Jensen, for always giving me advice and help in my time of need. I would like to thank Yuanzheng Yue as well, to endorse me to come to Aalborg University in the first place.

Also, I am very grateful for all the people that I have met. Therefore, I would like to thank all my friends and colleagues who have always encouraged and inspired me, and for the good time that we had. At last, I would like to thank my family, especially my parents, thanks for their selfless support, and for guiding me throughout my journey!

TABLE OF CONTENTS

CHAPTER 1. INTRODUCTION

1.1. Background

Water scarcity has been a serious challenge for the development of society. Among all the water that is preserved on earth, only less than 1% is accessible for human consumption (1). However, even the remaining freshwater resources are depleted by overuse, pollution, and other anthropogenic activities. Therefore, the issue of water scarcity needs to be addressed from the perspective of both expanding freshwater resources and eliminating water pollution. The oceans represent the majority of the water on earth, yet they cannot be used directly due to their high sanity. Hence, desalination technologies are important for the expansion of accessible freshwater resources.

Over the last decades, membrane technologies have become a popular choice for desalination, since membrane units are easy to operate and require no additional chemical input (2). The membranes can separate different substances based on their sizes, charges, polarity, etc (2, 3). The separation ability of a membrane is largely dependent on its pore size. The molecules and the hydrated ions that are smaller than the pores can be transported through the membrane, while the larger species are retained. Based on the pore size and applications, the membranes can mainly be divided into four categories, namely, microfiltration (MF), ultrafiltration (UF), nanofiltration (NF), and reverse osmosis (RO), which can retain different types of substances, from microparticles to salt ions, as shown in Figure 1-1 (2).

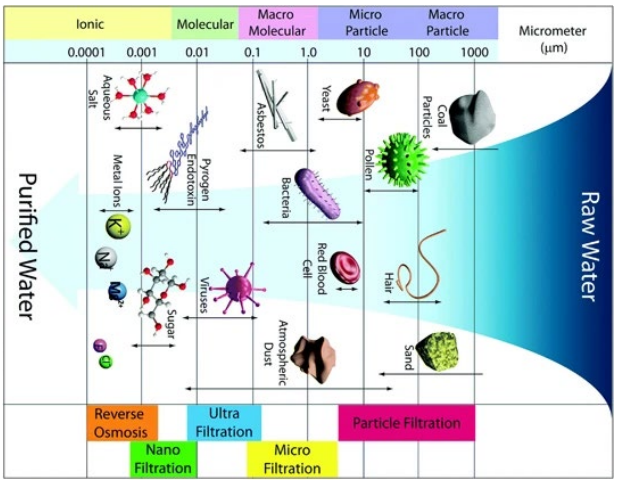

Figure 1-1: Illustration of the membrane classification based on the average pore sizes, including, particle filtration, MF, UF, NF, and RO. And examples of the particles that the membrane can retain under each membrane category (2).

Membranes can be synthesized from polymeric and inorganic materials. At present, polymers are the most available membrane materials (4). However, inorganic membranes are recently gaining increasing attention due to their high stability and long lifespan. Polymeric RO membranes are nowadays the most applied technology for desalination (5). The active layer of RO membranes is usually considered to consist of dense material, water transportation within a RO membrane can be described by the solution-diffusion mechanism (6, 7). RO units are pressure-driven systems, when the pressure applied to the membrane feed overcomes the osmotic pressure, the pressure gradient drives the water molecules to transport through the membrane. While ions and other dissolved species are retained in the feed. RO can typically reach a NaCl rejection of about 99% (8). However, during the desalination process, the concentration of the feed continuously increases, hence, additional pressure is required to overcome the osmotic pressure (5). When the concentration factor reaches a certain point, further increasing the applied pressure will no longer be economically feasible. Therefore, water recovery is commonly limited to the range of 35-85%, and large quantities of brine are produced from the RO system, which is now discharged with potentially negative consequences for the environment (9, 10). On the other hand, different membrane technologies can be applied to address the specific needs of each desalination application. The technologies should achieve a high-water recovery factor, and high energy efficiency while minimizing their environmental impact. In this context, the focus of this Ph.D. project has been desalination by applying membrane technologies based on porous materials, namely, nanofiltration and membrane distillation, to achieve maximum recycling/reuse of resources while minimizing pollution and waste.

The Ph.D. project is funded by Project Ô (H2020-CIRC-2017 TwoStage, Grant Agreement n. 776816), which is an EU project that aims for a circular economy approach to the management of wastewater. The Ph.D. study was conducted based on two case studies, namely (i) the desalination of the groundwater in Puglia, Italy, and (ii) the desalination of an inland mariculture site discharge in Israel, Eilat. The general goal is the establishment of a reproducible water management system in the local area of each case study. In the first study, the groundwater in the local range is suffering from high salinity. The objective is to reduce the salinity of the groundwater to a level that is suitable for human consumption. For this purpose, NF was applied for groundwater desalination. The consideration for applying NF instead of RO is that the NF can obtain a higher flux under the same pressure, due to the porous nature of the membrane layer. Also, the NF can achieve a higher water recovery factor since it will not remove the salt ions completely from the groundwater. For this study, a commercial polymeric membrane and lab-made ceramic NF membrane were tested for this application. In the second study, a closed water loop is attempted for an inland mariculture site in Eliat, Israel. The mariculture site effluent not only has a high salinity but also contains a high amount of organic and inorganic substances that are accumulated in the water during the fish farming process and that can be harmful to the fish in a recirculated system. Therefore, MD was applied to control the salinity of

the effluents of the mariculture site. MD can achieve maximum water recovery. To remove the organic pollutants that could be presented in the effluents, an advanced oxidation process (AOP) is also coupled with the MD process. Furthermore, a novel inorganic MD membrane with a low cost, high stability, and superior performance was developed, for the application of mariculture desalination.

1.2. Scope and objectives

The general scope of this Ph.D. project is to investigate the potential of porous membranes for desalination, from a general perspective and specifically for the two demonstrative sites in Project Ô. Besides commercial polymer membranes, novel inorganic membranes were developed for each study.

In the case of the desalination of groundwater in Puglia, Italy, sol-gel-derived silica-alumina NF membranes were developed and compared to a commercial polyamide membrane. Concerning the effluent desalination of an inland mariculture site in Eliat, Israel, a commercial polymer hollow fiber membrane was tested. It was found that MD cannot reject volatile pollutants such as formaldehyde. Therefore, a new integrated process is proposed in this thesis: the permeate of the MD unit is treated with the VUV/UVC photolysis for the removal of volatile pollutants. Moreover, associated with the second case study, a novel inorganic MD membrane with high performance, high stability, and low cost was also developed and characterized. The results obtained from the new ceramic MD membranes are so promising that Aalborg University has found this product potentially patentable. For this reason, this research development of the new ceramic membrane is not included in this thesis.

Overall, this Ph.D. thesis investigates the potential of porous desalination membranes in the two case studies from the following perspective:

- Investigating the potential of porous membranes in the desalination of real waste systems.
- Screening the potential of polymeric and inorganic NF membranes for the treatment of groundwater with high salinity, estimating their energy consumption, and assessing their feasibility on a real scale.
- Testing the potential of a state-of-the-art polymeric MD membrane for the desalination of a mariculture effluent.
- Studying the VUV/UVC process in removing volatile pollutants in the MD permeate.
- Developing and characterizing a novel inorganic MD membrane with enhanced performances.

This thesis is an overview of the crucial studies that have been conducted by the author. To briefly summarize the content of the thesis for the readers, the thesis starts with a general induction of the membrane technologies and membrane materials for desalination application in Chapter 2. Chapter 3 and Chapter 4 focus on the first study of using NF for groundwater desalination, and the second case study of applying MD combined with VUV/UVC for groundwater desalination/detoxification, respectively. In both case studies, the synthesizing process, membrane characterization, and the testing method will be described, the resulting conclusion will guide the membrane selection to be installed at the demonstrative sites of each study. Chapter 5 describes the development of a novel inorganic MD membrane with low cost and enhanced performance. As of the writing date of this thesis, the developed membrane is undergoing the patenting process, therefore the detailed synthesis method and membrane performance will not be elaborated. Finally, the main finding of this Ph.D. study will be concluded in Chapter 6.

1.3. Thesis content

The majority of the experiments in this thesis were conducted at Aalborg University and the University of Turin (Italy). This thesis consists of three experimental developments, the outcome of the Ph.D. project is concluded in three journal papers, one review paper (the review paper will not be attached to the end of the thesis for the sake of concision), and one patent (either published or ready for submission manuscripts). The papers listed below are cited by their roman numerals throughout the thesis.

I. Xianzheng Ma, Katarzyna Janowska, Vittorio Boffa, Debora Fabbri, Giuliana Magnacca, Paola Calza, Yuanzheng Yue, Surfactant-Assisted Fabrication of Alumina-Doped Amorphous Silica Nanofiltration Membranes with Enhanced Water Purification Performances. Nanomaterials, 9(10), 1368 (2019).

II. Xianzheng Ma, Cejna Anna Quist-Jensen, Aamer Ali, Vittorio Boffa, Desalination of Groundwater from a Well in Puglia Region (Italy) by Al_2O_3-Doped Silica and Polymeric Nanofiltration Membranes. Nanomaterials, 10(9), 1738 (2020).

III. Katarzyna Janowska, Xianzheng Ma, Vittorio Boffa, Mads Koustrup Jørgensen, Victor M. Candelario, Combined Nanofiltration and Thermocatalysis for the Simultaneous Degradation of Micropollutants, Fouling Mitigation and Water Purification. Membranes, 11(8), 639 (2021).

IV. Xianzheng Ma, Lana Flanjak, Xinxin Chen, Cejna Anna Quist-Jensen, Aamer Ali, Peter Roslev, Vittorio Boffa, VUV-UVC Coupled Membrane Distillation for Recirculating of inland Mariculture Effluents (to be submitted)

V. Xinxin Chen, Xianzheng Ma, Vittorio Boffa, and Yuanzheng Yue, Recent Advances in Oxide Membranes for Water Desalination (to be submitted).

CHAPTER 2. THE FUNDAMENTALS OF POROUS MEMBRANES FOR WATER DESALINATION

In this Ph.D. project, new strategies of water desalination for applying porous membranes have been explored. Indeed, the conventional approach for water desalination is based on dense polymeric RO membrane units. The driving force for the permeation of water through these membranes is the chemical potential gradient between the feed and the permeate side, which is largely dependent on the applied hydraulic pressure. The transport in dense RO membranes is governed by a solution-diffusion mechanism, which implies that their selectivity arises from the differences in the solubility and diffusivity of water and the dissolved ions through the membrane material. The polymeric active layer (typically polyamide) is highly permeable to water while hindering the transport of ionic species. Therefore dense membranes can generally achieve a high rejection for salt ions (even higher than 99% for sodium chloride (8)). However, due to the tight membrane structure, high pressure is needed to maintain the water flux across the membranes, which leads to high energy consumption. Additionally, to counter the increased osmotic pressure of the feed solution, the applied pressure also needs to increase during the desalination process, therefore, only a finite amount of water can be recovered. For this reason, the use of NF and MD is here proposed for the desalination of two specific water effluents. The fundamentals of the two membrane technologies and the conventional membrane materials are elaborated on in this section to have a better understanding of their advantages and limitations.

2.1 Nanofiltration

Nanofiltration is defined as a pressure-driven technology based on membranes with a pore size in the range of about 1-2 nm (11). Generally, the NF can achieve a full rejection of divalent ions and partially reject monovalent ions (11). Moreover, NF membranes reject a consistent part of the dissolved organic matter. Membrane performance is generally described in terms of permeability and selectivity. Ideally, a membrane would combine high permeability and selectivity. Nevertheless, a trade-off is often found between the membrane permeability and selectivity, which can be explained by considering the mechanisms governing the mass transfer of the solvent and solute through the membrane layer (12, 13). The flux of water (J_w) through porous membranes is often described by using the Hagen–Poiseuille equation or its modification (Equation 2-1) (14). In this equation, ΔP_{net} is the net pressure difference between the applied transmembrane pressure and the osmotic pressure. The r_{pore},A_k , and Δx refer to the pore size, porosity, and membrane thickness, respectively. While v and ρ_w are the viscosity and the density of the solvent, respectively.

$$J_w = \Delta P_{net}\left(\frac{r_{pore}^2}{8v\rho_w\left(\frac{\Delta x}{A_k}\right)}\right) \qquad 2-1$$

On the other hand, the permeation of ionic species is a more complex phenomenon since it is influenced by factors such as the membrane charge density, the valence of the ions, and the pH (15). Generally, the ionic selectivity of the NF membranes is governed by the ion-membrane interaction at the membrane surface, and the hindered transport within the membrane pores. The former can be described by the Donnan-steric interaction and the latter can be predicted by the extended Nernst-Planck model (16).

At the membrane surface, the NF membrane rejection mechanism is mainly contributed by the combination of steric exclusion, Donnan exclusion, and dielectric exclusion (Figure 2-1 A) (17). For the particles that are larger than the pores, the rejection is mainly dominated by steric exclusion. In NF, the Donnan effect played an important role in the rejection of charged particles and ions, the particles can be repulsed or attracted by the charged membrane surface (17). Dielectric exclusion describes the energy barrier that a particle with a hydration shell needs to overcome when moving from the bulk solution to the inside of membrane pores (17).

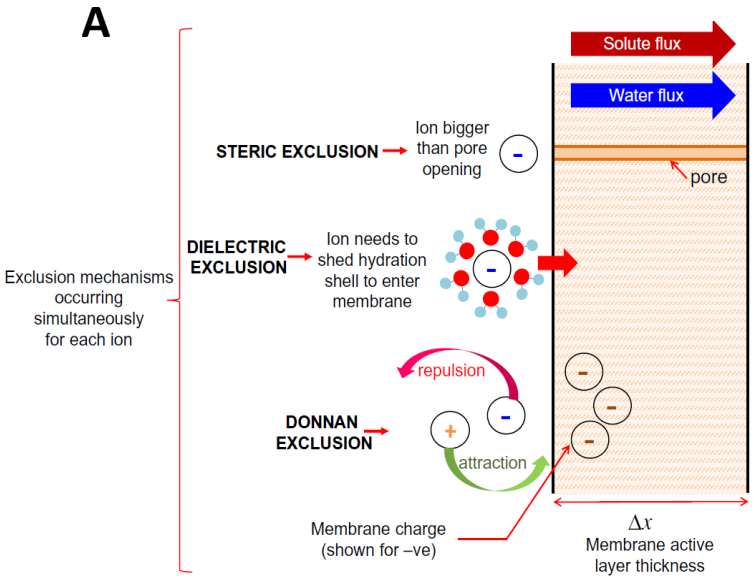

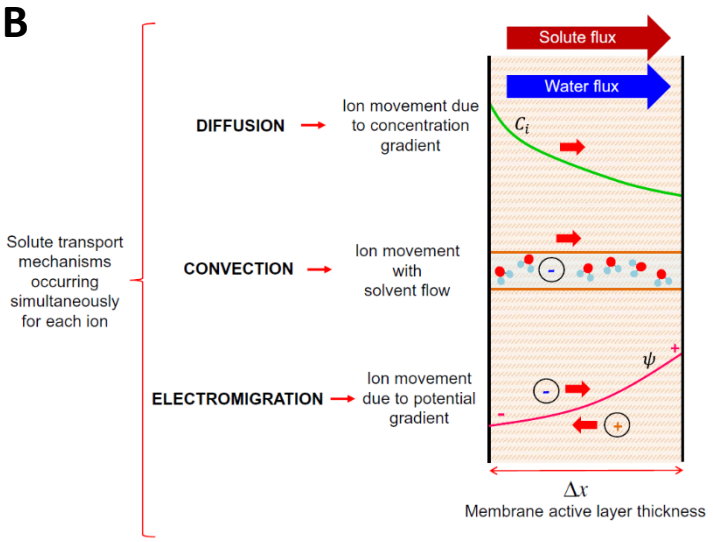

Figure 2-1: (A) The ion rejection mechanism on the membrane surface under equilibrium conduction, including steric exclusion, Donnan exclusion, and dielectric exclusion. (B) The ion transportation mechanism in the membrane is explained by the Nernst–Planck equation under equilibrium conduction, including diffusion, convection, and electromigration (17)

The Donnan-steric pore model can be interpreted as Equations 2-2 and 2-3 (16, 18). This model considers the transport of the ions at the interfaces of the membrane with the feed and the permeate under equilibrium conduction. For the feed-membrane interface (Equation 2-2), $\gamma_{i,pore}$ and $\gamma_{i,m}$ represent the ion activity coefficients at the pore entrance and the feed membrane surface, respectively. While $C_{i,pore}$ and $C_{i,m}$ are the ion concentrations at the pore entrance and the feed membrane surface, respectively. The steric exclusion, Donnan exclusion, and dielectric exclusion are expressed by the steric factor (Φ_i), the Donnan effect term ($\psi_{D,m}$) and the dielectric factor (Φ_B). z_i, F, R, and T are the ion valent, Faraday constant, the universal gas constant, and the absolute temperature, respectively. Equation 2-3 is obtained by taking the same assumptions for the permeate side.

$$Feed: \frac{\gamma_{i,pore}C_{i,pore}}{\gamma_{i,m}C_{i,m}} = \Phi_i\Phi_B \exp\left(-\frac{z_iF}{RT}\psi_{D,m}\right) \qquad 2-2$$

$$Permeate: \frac{\gamma_{i,pore}C_{i,pore}}{\gamma_{i,p}C_{i,p}} = \Phi_i\Phi_B \exp\left(-\frac{z_iF}{RT}\psi_{D,p}\right) \qquad 2-3$$

On the other hand, the transport of ions within the membrane pores is mainly determined by the combination of diffusion, convection, and electromigration (18). As illustrated in Figure 2-1 (B), diffusion and electromigration are ion transportation

coursed by the concentration and potential gradient across the membrane, respectively, while convection of the ions is due to the flow of the solvent. The three factors can be expressed by the extended Nernst–Planck equation (Equation 2-4). J_i representing the ion flux. The diffusion factors in the expression include $D_{i,\infty}$ the ion diffusion coefficient, $K_{i,d}$, the diffusion hindrance factor, and $\frac{dc_i(x)}{dx}$, the concentration gradient across the membrane. The effect of convection in the equation are being expressed as J_p, the solvent flux and $K_{i,c}$, the convection hindrance factor. While ψ is the potential of the membrane.

$$J_i = K_{i,c}c_i(x)J_p - K_{i,d}\frac{dc_i(x)}{dx} - \frac{z_i D_{i,\infty} F c_i(x)}{RT}\frac{d\psi(x)}{dx} \qquad 2-4$$

When mentioned models are considered, a good correlation between the ion rejection and water permeability of the NF membranes can be derived (Figure 2-2) (12). In general, a trade-off between permeability and selectivity can be observed. It can be seen that the membrane permeability has a positive correlation with the pore size and is negatively correlated with thickness and surface charge, and vice versa for selectivity. The permeability-selectivity trade-off can be tuned to design or select the suitable membrane for specific desalination applications.

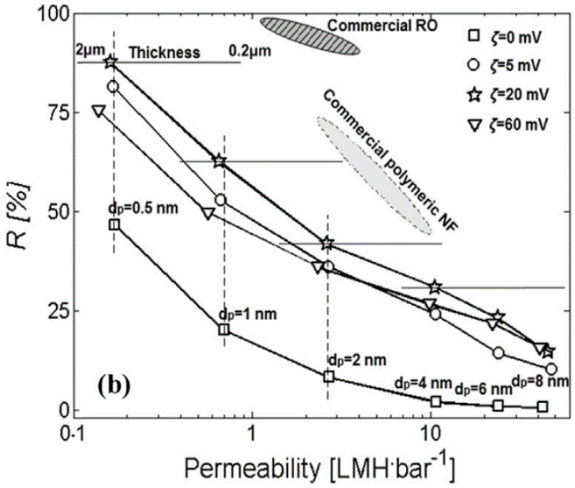

Figure 2-2: Membrane NaCl rejection as a function of the permeability for membranes with different pore sizes, thickness, and zeta potential (12).

2.2 Membrane distillation

With the increasing demand for freshwater, concerns about traditional pressure-driven membrane technologies have also risen over the passing years. The pressure-driven membrane technologies can be energy-intensive, plus, the limation of the water recovery factor means that a large amount of concentrated brine is being discharged into the environment, which could bring negative environmental consequences.

In recent years, membrane distillation, a thermally driven membrane technology, has gained much attention in desalination applications. In the case of a direct contact MD system, a piece of hydrophobic membrane is applied to separate the feed and permeate side. A temperature gradient is established across the membrane by heating and cooling the feed solution and the permeate solution, respectively (19). Liquids can not enter the membrane pores due to the hydrophobicity of the membrane and keep the membrane 'dry'. Instead, water vapor will transport from the feed through the pores and condensed at the permeate side. Over time, freshwater can be collected, and the feed solution is concentrated (19). Compared with a pressure-driven membrane, the effect of the osmotic pressure is much less in an MD system since the main driving force is the vapor pressure coursed by the temperature difference. Wettability is one of the most important parameters of the membrane for MD application (20, 21). Wetting of the membrane can occur when the transmembrane pressure exceeds the liquid enter pressure (LEP), at which point the feed and permeate solution can enter the membrane pores and be miscible with each other (21). The LEP can be expressed as Equation 2-5. B, $cos\theta$, and r_{max} is the pore geometry coefficient, surface contact angle, and the maximum pore size, respectively, while the γ_l is the liquid surface tension. It can be seen from the equation that for the membrane to have a high wetting resistance, the membrane needs to have a high contact angle and a small pore size. Usually, the membrane for MD has a pore size below 1μm, yet, too small of the pore size would hinder the mass transfer, therefore reducing flux (22). For MD application, an optimization of the membrane parameters like pore size, hydrophobicity, thickness porosity, etc. is needed. On the other hand, the surface tension of the feed and permeate solution would also affect the wettability of the membrane. For instance, if the feed solution contains low surface tension solvents or surfactants, the membrane would be more prone to wetting (21, 23).

$$LEP = \frac{-B\gamma_l cos\theta}{r_{max}} \qquad 2-5$$

In an MD system, the feed side is usually in contact with the membrane surface, yet, the method of condensation on the permeate side can be varied. There are four main configurations of the MD system depending on the configuration of the permeate, namely, direct contact membrane distillation (DCMD), vacuum membrane distillation (VMD), air gap membrane distillation (AGMD), and sweeping gas membrane distillation (SGMD) (Figure 2-3) (19):

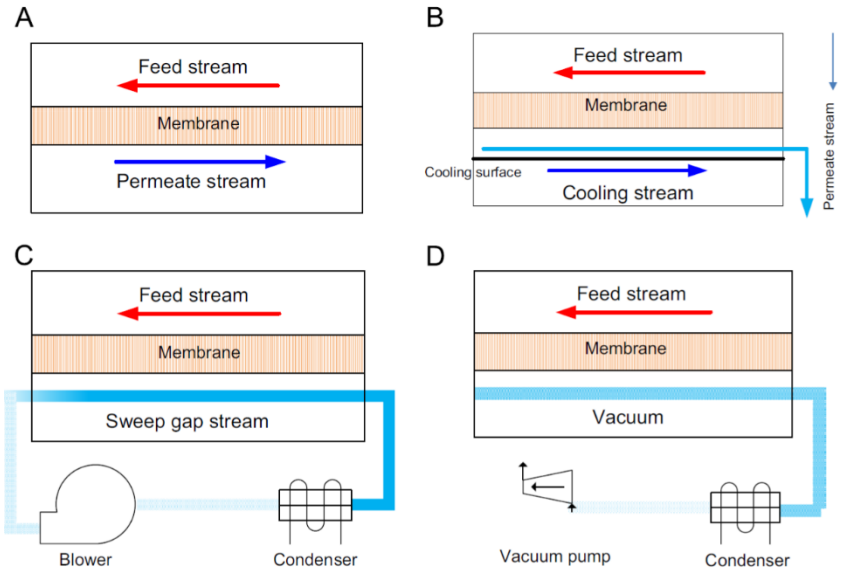

Figure 2-3: Schematic of the four main configurations of the MD systems: (A) DCMD, (B) AGMD, (C) SGMD, and (D) VMD (19)

i) The DCMD (Figure 2-3, A) is one of the most common MD systems due to its simple configuration, both feed and the permeate solution are in contact with the membrane and circuit on each side of the membrane in a counter-current fashion (24,25).

ii) In AGMD (Figure 2-3, B), an air gap is presented on the permeate side between the membrane surface and the cold condensing surface. There is a lower chance of wetting in this configuration since the permeate solution is not directly in contact with the membrane surface. Additionally, due to the low thermal conductivity of the air gap, the heat loss through the membrane can also be minimized. Yet, the air gap will also increase the vapor transportation pass, therefore, resulting in a lower flux (26,27).

iii) Similar to AGMD, SGMD (Figure 2-3, C) has no liquid directly contacting the permeate side of the membrane. A cold sweeping gas was applied and carried the vapor into a cold trap. In this method, the system also has a high wetting resistance and can have higher flux due to the sweeping gas. However, the system is also having a high degree of complexity, which makes it unfavorable among all MD configurations (28).

iv) For VMD (Figure 2-3, D), the water vapor is been drawn by a vacuum pump on the permeate side and condensed by a cold trap. In this case, the driving force is the combination of the vapor pressure and the vacuum, hence, a higher flux can be

obtained compared to the other MD configurations. However, due to the additional pump and condenser, the complexity of the system also increases (29,30).

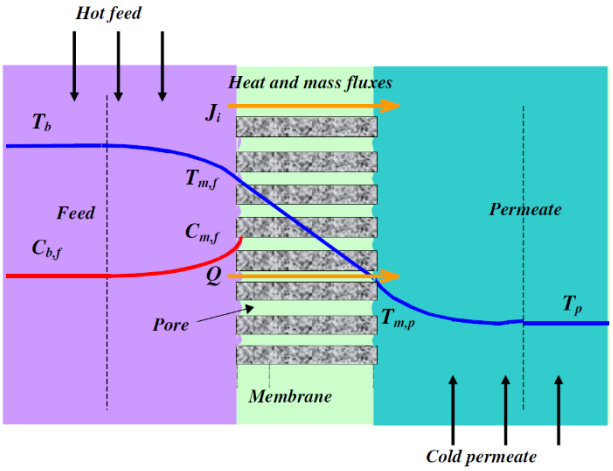

Figure 2-4: Schematic diagram of the heat and mass transfer in a DCMD system.(31)

The mass transportation mechanism of the MD system is largely depending on the applied configurations. For the sake of concision, the discussion of the mass transfer mechanism will mainly focus on DCMD (Figure 2-4). The flux (J) of a DCMD system can generally be described as Equation 2-6, where C_m is a coefficient of the membrane and P_f and P_p are the vapor pressure of the feed and permeate solution respectively, which can be expressed as the function with temperature, where $T_{f,m}$ and $T_{p,m}$ are the temperatures at the membrane surface of the feed and permeate side, respectively (32). Hence, Equation 2-6 can be rearranged as Equation 2-7.

$$J = C_m[P_f - P_p] \qquad 2-6$$

$$J = C_m \frac{dP}{dT}(T_{f,m} - T_{p,m}) \qquad 2-7$$

In most cases, the MD system is dealing with a feed solution with a high concentration of solute, Schofied et al. proposed an extension of Equation 2-7 by taking the effect of the osmotic pressure into consideration (Equation 2-8) (33). Then ΔT_{th} represent the threshold temperature and the χ_m is the solute mole fraction in membrane pores.

$$J = C_m \frac{dP}{dT}[(T_{f,m} - T_{p,m}) - \Delta T_{th}](1 - \chi_m) \qquad 2-8$$

The mass transfer of the MD can be affected by the structure of the membrane and the air present within the membrane. When the air trapped inside of the membrane is not

considered, the mass transfer can be explained by the Knudsen diffusion or the Poiseuille flow model, when the air inside of the membrane is considered, the mass transfer can be distributed by the molecular diffusion model (31, 32). The ratio between the transported molecules mean free path (λ) and membrane pore diameter (d_p) can be used to determine which models are having a dominant effect on the mass transfer of the DCMD.

$$K_n = \frac{\lambda}{d_p} \qquad 2-9$$

When $K_n > 1$, the vapor molecules will have a higher chance of colliding with the membrane pore wall than with itself, therefore, the mass transfer can be explained by the Knudsen diffusion (31, 34):

$$C_{Kn} = \frac{2\pi}{3}\frac{1}{RT}\left(\frac{8RT}{\pi M_W}\right)^{1/2}\frac{r^3}{\tau\delta} \qquad 2-10$$

In the equation, r, τ, and δ are the membrane pore size, tortuosity, and thickness, respectively. Where M_W is the molecular weight of water and R is the gas constant.

If $K_n < 0.01$, the transportation mechanism can be explained by molecular diffusion (equation 2-11). It describes the diffusion of the water vapor in the continuum air phase that is trapped inside the membrane pores (31, 34).

$$C_D = \frac{\pi}{RT}\frac{PD}{P_{air}}\frac{r^2}{\tau\delta} \qquad 2-11$$

In the model, D represents the diffusion coefficient, where P and P_{air} are the total pressure within the pores, and the air pressure that is inside of the membrane.

However, in the transition region, where $0.01 < K_n < 1$, the transportation mechanism can be a combination of both Knudsen diffusion and ordinary diffusion (31, 34). The water molecules will interact with both themselves and the air molecules when traveling through the membrane. Therefore Equation 2-12 can be obtained.

$$C_C = \frac{\pi}{RT}\frac{1}{\tau\delta}\left[\left(\frac{2}{3}\left(\frac{8RT}{\pi M_W}\right)^{1/2} r^3\right)^{-1} + \left(\frac{PD}{P_{air}} r^2\right)^{-1}\right]^{-1} \qquad 2-12$$

2.3 Membrane materials and fabrication methods

As stated in the previous section, an ideal membrane would have a combination of high permeability and selectivity. Other than the membrane structure, the membrane materials play an important role in terms of the membrane performance and strongly conditionate the strategies for designing and fabricating a membrane. At present, polymeric materials, such as polysulfone, polyvinylidene fluoride, polyacrylonitrile, etc., are some of the most common materials for membrane applications (35). On the other hand, as mentioned in the introduction of this thesis, inorganic materials have received more attention over the passing years, in reason of their chemical, thermal, and mechanical robustness (36–38). The state-of-the-art art of membrane materials commercially used for NF and MD applications is briefly discussed in this chapter.

2.3.1 Polymeric membranes

The selectivity of the polymeric NF membranes towards dissolved molecules and ions largely depends on the pores that are formed in the polymer matrix by various synthesis methods, which include interfacial polymerization, phase inversion, and post-treatment of the polymer substrate, etc (13,39,40). Phase inversion is the most wildly applied approach for the fabrication of polymer NF membranes since it is a simple and versatile strategy. The general procedure for phase inversion is to cast a polymer solution onto a substrate and then submerge the cast into a non-solvent of the polymer (typically water), as shown in Figure 2-5 (13). During the process, the homogenous polymer solution is separated into a polymer-rich phase and a polymer-poor phase due to solvent exchange. The polymer-rich phase will form the solid membrane matrix, and the polymer-poor phase will create the pores in the polymer matrix (13).

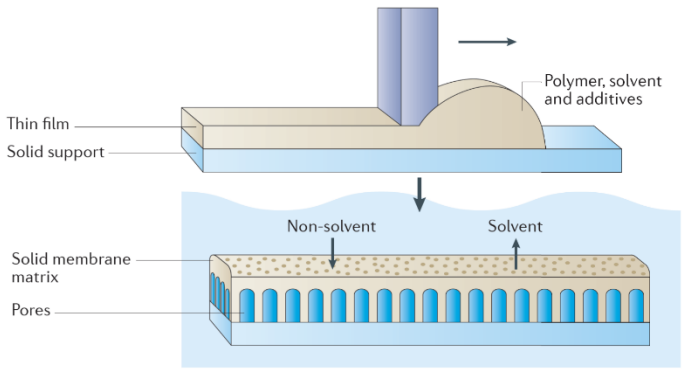

Figure 2-5: The schematic diagram of the non-solvent-induced phase inversion for MF and UF membrane fabrication(13).

Several methods can be used to induce the phase separation of the polymer solution, therefore yielding different pore sizes and membrane structures. Most NF membranes have an asymmetrical structure, meaning the membrane is constructed with a thin and denser top layer to provide selectivity, and a porous support layer to ensure mechanical integrity (41). In the phase inversion process, a solvent with high volatility can be used for the polymer solution. During the casting of the solution, the evaporation of the solvent will create a higher polymer concentration at the liquid-air interface (42). With the subsequent solvent exchange, an asymmetrical membrane that has a top layer with NF range pore size can be formed.

Another important fabrication method for NF membranes is interfacial polymerization. A vast majority of commercial polymer NF and RO membranes are fabricated by interfacial polymerization (40). A typical interfacial polymerization process involves two immiscible solutions each containing the active monomers or monomers and catalysts. When the solutions are contacting with each other, the polymerization can take place at the interfaces of the two phases (40, 44). In this case, a very thin membrane layer at about 50nm can be created, hence, a high permeability can be obtained. One of the common examples of interfacial polymerization reaction for membrane material synthesis is the reaction between piperazine (PIP) and trimethyl chloride (TMC) (Figure 2-6), ultra-thin polyamide NF membrane can be obtained.

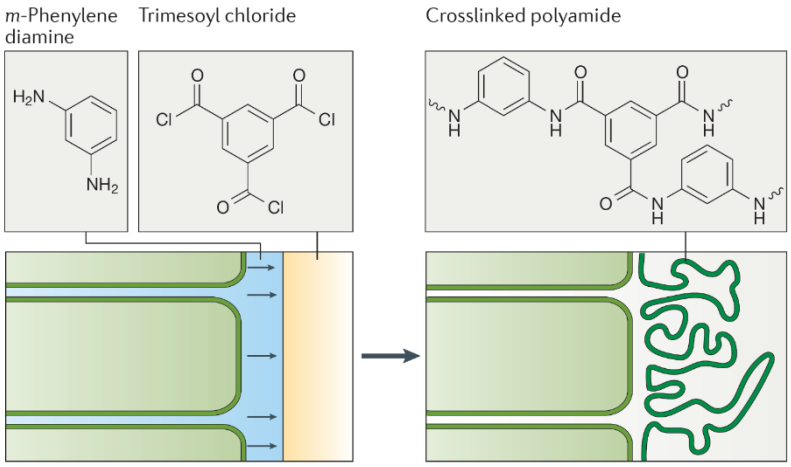

Figure 2-6: The schematic diagram of the interfacial polymerization of the piperazine (PIP) and trimethyl chloride (TMC) for NF membrane fabrication(13).

The current approach for the MD membranes is to apply commercial hydrophobic MF membranes. Hydrophobicity is required for the MD membrane materials, therefore, polymers with low surface energy such as polypropylene (PP), polyvinylidene fluoride (PVDF), and polytetrafluoroethylene (PTFE) are commonly applied for the

fabrication of the MD membranes (44–46). Depending on the properties of the membrane materials and the desired structure of the membrane, different methods such as phase inversion, electro-spinning, sintering, melt exclusion, etc, can be used for MD membrane fabrication (46, 47). For membrane materials that can be dissolved by a solvent, like PVDF, phase inversion can be used for the MD membrane fabrication, similar to NF membranes (48–50). Additionally, electro-spinning can be used for the fabrication of fibrous MD membranes. An electro-spinning system usually has a high-voltage power supply, a syringe, and a fiber collector as shown in Figure 2-7 (51). The polymer solution contained in the syringe is fed by a syringe pump, while the high voltage is applied between the needle and the collector (usually between 1 to 30 kV) (51). The polymer solution pendent droplet from the needle is electrified. Once the electrostatic forces exceed the surface tension of the polymer solution, a liquid jet can be ejected from the nozzle of the syringe. Therefore, the polymer fiber can be obtained when the liquid jet is deposited on the collected, and over time non-woven membrane can be formed from the collector (51).

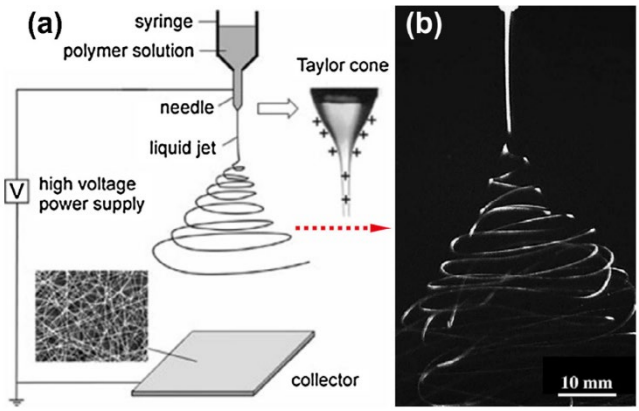

Figure 2-7: (a) The schematic diagram of the electro-spinning process for fibrous membrane fabrication, and (b)the image of the polymer solution liquid jet forming during the electro-spinning process (51).

For polymeric MD membrane materials that cannot be processed in the form of solutions, such as PTFE and PP, the sintering or melt exclusion method is often applied (19, 47). In the sintering process, fine polymer particles are mixed with petroleum-based lubricant, and the mixture is then subject to pressing and extrusion into the desired geometry (flat sheet, hollow fiber, etc.) (19). After heat treatment, the lubricant is evaporated, and the microporous membranes can be formed.

2.3.2 Inorganic membranes

Inorganic materials have been studied extensively over the past years. Inorganic materials can offer higher mechanical, chemical, and thermal stability than their polymeric counterparts. The most applied method for the fabrication of inorganic NF membranes is sol-gel synthesis. The mechanism of the sol-gel process will be elaborated in detail in the following section, but in general, the sol-gel method can synthesize nanoparticles in a solution. When coating the solution onto a porous substrate, a film with nanopores can be formed (52, 53). Sol-gel-derived metal oxides, such as Al_2O_3, ZrO_2, and TiO_2, are some of the common materials for membrane applications (52).

To date, the commercial application of the inorganic NF membrane is rarely reported. One of the most common ceramic materials that are applied to the membrane application is alumina (Al_2O_3) (54). The crystal phase of the alumina has a large impact on the pore size of the final membrane, and the phases of alumina depend on the synthesis and the heat treatment procedures. Alumina has seven common polymorphs, namely, α, γ, χ, κ, δ, θ, and η (Figure 2-7). Among them, α- and γ-alumina have been frequently applied for membrane fabrication(55). α-Alumina can be obtained at a heat treatment temperature above 1000°C, it is the most stable form of alumina that can withstand extreme pH and thermal conditions (56). Nevertheless, the application range of the α-alumina is mostly MF, in reason of the large pores formed by the rapid crystal growth during the heat treatment (57). On the other hand, smaller pore sizes (2-5nm) can be obtained for membranes made of γ-alumina. Such membranes can be potentially used for NF applications, but their stability is lower compared to those made of α-alumina. The γ-alumina membranes are obtained by dip-coating pre-existing support (e.g. α-alumina) in boehmite sols, followed by heat treatment at the temperature range between 600-800°C (56).

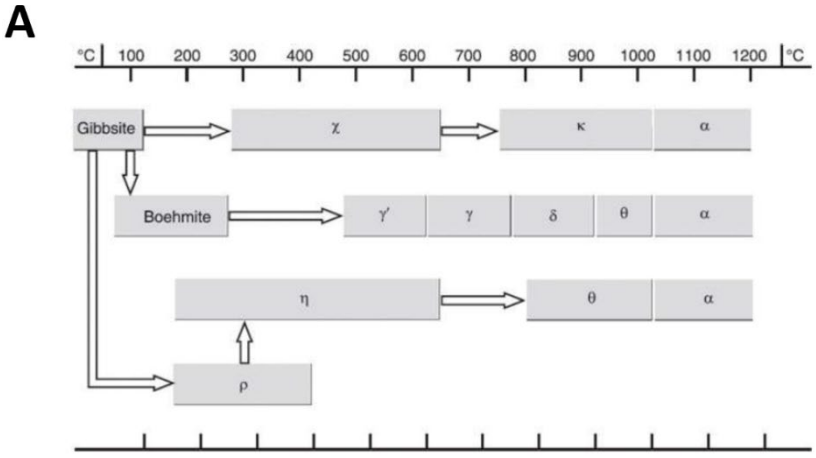

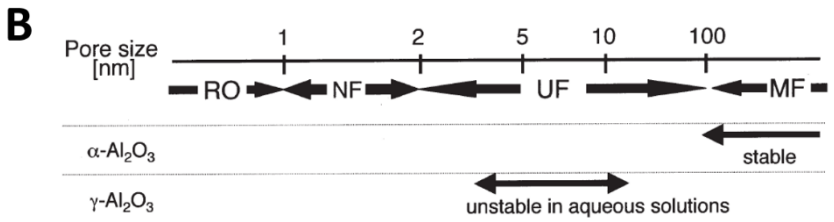

Figure 2-8: (A) The forming of the crystal phases of Al_2O_3 based on the starting materials and heat treatment temperatures, and (B) the application range of α-alumina and γ-alumina for membrane synthesis(56, 58)

Other common inorganic materials that can be used for membrane applications include zirconia, titania, and silica. For zirconia, the application as a membrane material can range from MF to NF. There are three main crystal phases, namely, monoclinic, tetragonal, and cubic. With increasing the heat treatment temperature, the zirconia will transit from the monoclinic phase to the tetragonal, and cubic phases (20). Similar to alumina, zirconia can provide high mechanical chemical and thermal stability as a membrane material. Additionally, zirconia has shown higher hydrophilicity compared with other ceramic membrane materials (59-61). Therefore, a higher flux and lower fouling tendency can be observed from zirconia membranes (59). As for titania, it can be used for UF and NF applications. Generally, titania has three phases rutile, anatase, and brookite (20). Except for the high stability, the titania membrane also has photocatalytic properties (61). Studies have shown by using titania as membrane material, under UV irradiation, the membrane can have anti-bacterial and antifouling properties (62–64).

2.3.3 The sol-gel method

Powder sintering is one of the most applied methods for the synthesis of inorganic/ceramic membranes. When the green body is sintered under a high temperature, the pores of the membranes are originated from the interspaces between the particles (65). Nevertheless, the same strategy cannot be used for NF membranes since nanoparticles are needed to create the desired nano-sized pores. The nanoparticles are not only difficult to obtain with physical milling but also easy to agglomerate to create a large and uneven pore size distribution in the consolidated material. On the contrary, the sol-gel method has been proven to be the most appropriate for the fabrication of nano porous NF membranes, since it can synthesize nanoparticles directly from a solution. The suspension of the nanoparticles is defined as the sol, over time, a rigid network can be developed from the particles and lead to a viscous gel (66). The mixtures for sol-gel syntheses generally consist of four

components: the alkoxide precursor, solvent, water, and acid or alkaline compound as a catalyst (52). The formation of the nanoparticles is achieved via hydrolysis and condensation reactions (52). For silica-based nanoparticles, tetraethyl orthosilicate (TEOS) is the most common precursor.

In the hydrolysis reaction, water reacts with the alkoxide groups of TEOS, replacing them with hydroxides, and producing ethanol as a side product. Then, two hydrolyzed precursor molecules can react to form a Si-O-Si bonding (i.e., condensation reaction) and produce a water molecule as a side-product (Figure 2-9) (67). With the progression of the reaction, the development of the silica network leads to the formation of the SiO_2 nanoparticles in the solution. The resulting silica materials from the sol-gel process are intrinsically porous, the pores are the voids within the silica network (usually below 10nm) (68). For the NF membrane synthesis, pore-forming agents can be added during the sol-gel process to create the desired pore size. Therefore, the permeability and selectivity of the sol-gel-derived membranes can be tuned by the concentration and species of pore-forming agents such as surfactants in the sol-gel system (67).

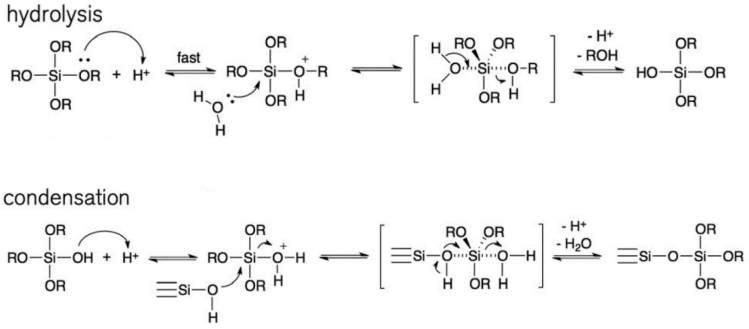

Figure 2-9: The mechanism of hydrolysis and condensation reaction of TEOS in a sol-gel reaction (67).

Membranes are obtained by coating the sol that contains nanoparticles onto a porous substrate. One of the most widely applied methods for membrane fabrication from the sol-gel process is dip coating. As shown in Figure 2-10, in the dip coating process, the substrate is usually withdrawn from the coating sol solution at a constant speed, while a thin film can be formed onto the surface of the substrate. Parameters such as the viscosity, rate of evaporation, particle size, and withdrawal speed of the coating sol during the dip coating process. Can largely determine the structure and defect formation of the membrane (70).

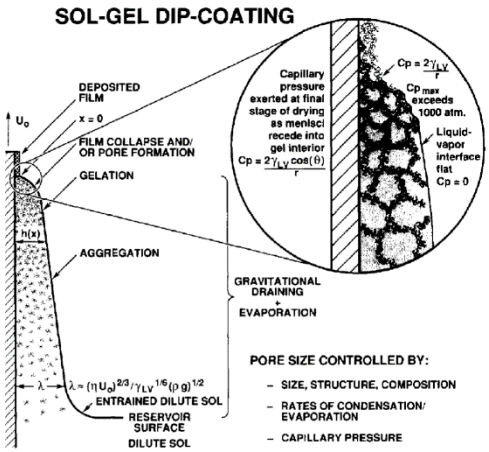

Figure 2-10: A Schematic diagram of the dip coating process. Reprinted after modification from ref. (70).

One of the major challenges of pure silica membranes development for filtration application is hydrothermal instability (71). The high surface energy nanoporous silica structure will constantly undergo the hydrolysis and condensation reaction when exposed to hydrothermal conditions, the reactions will give the silica network a degree of mobility and shift the structure towards lower surface energy, gradually, losing permeability and selectivity (71). Some of the common approaches to stabilizing the silica network include introducing organic motifs into the silica network, applying carbon as the pore template, or doping metal oxide into the silica structure (72).

Metal oxide doping is one of the most common methods to improve the stability of the silica membrane. The metal oxide doping can be achieved by introducing additional metal alkoxide during the sol-gel synthesis, and the metal oxide can be integrated into the silica network due to the hydrolysis and condensation reaction. Several studies have proved that the doping of metal oxides can improve the performance and stability of silica membranes (69,73,74). However, one of the challenges for metal oxide doping in sol-gel synthesis is the reactivity difference between the metal alkoxide and TEOS. Generally, metal alkoxides have higher reactivity than TEOS, therefore, the metal alkoxides tend to react with themselves more than with TEOS (75). This would result in an inhomogeneous membrane material in chemical composition which could greatly jeopardize the membrane performance.

Surfactants are often added in the sol-gel synthesis as a pore-forming agent, studies have also found that the addition of surfactants can reduce the reaction rate for hydrolysis and condensation reaction of alkoxides species in a sol-gel system (76,77). The surfactant molecules can be absorbed onto the sol particles, usually, the hydrophilic head of the surfactants is absorbed on the surface of the particles while

the hydrophobic tail points outward. This shielding of the surfactant molecules prevents the nucleophiles of the water, and the condensation reaction between the particles, hence, the reactivity of the alkoxides is reduced (78). In terms of the membrane synthesis with multiple components by the sol-gel method, a more homogenous membrane material can be the addition of surfactant.

In Paper I, 5mol% of Al_2O_3 was doped into the silica membrane to improve the hydrothermal stability via the sol-gel method. While a surfactant, CTAB, was applied as both the pore-forming agent and a stabilizer for the reactive alumina precursor. The optimal ratio between the surfactant and oxides for NF application has been found. The groundwater desalination performance of the alumina-doped silica membrane was compared with the commercial polyamide NF membrane in Paper II.

CHAPTER 3. NANOFILTRATION FOR GROUNDWATER DESALINATION

Groundwater has always been an important part of freshwater resources, about 30% of the total freshwater supply is contributed from groundwater (79). However, pollution caused by anthropogenic or natural processes can jeopardize the quality of groundwater (80). In the Puglia Region, Italy, groundwater suffers from: i) high salinity due to seawater infiltration, and ii) potential pollution from the discharge of pesticides and pharmaceuticals (81,82). In this project, the potential of NF membranes in desalting and depolluting groundwater from Lecce (Puglia, Italy) was investigated. The conductivity of the groundwater samples that we received was about 4.6 mS cm^{-1}, which prevents its possible use for human consumption or irrigation. The main benefit of applying NF instead of RO is that the porous structure of the NF membrane allows for higher permeabilities and water recovery factors while requiring a lower energy consumption. Moreover, NF can fully retain water pollutants and partially retain dissolved ions (83). Therefore, NF can reduce the water salinity to a level that is suitable for human consumption without making it necessary to partially repristinate salinity before human consumption, as in the case of RO. This chapter offers an overview of SiO_2-based NF membranes by the sol-gel method and their optimization in terms of water permeability, desalination, and detoxification when filtering model solutions and real groundwater samples. Moreover, a comparison with a commercial polyamide NF membrane is given.

3.1 Fabrication and optimization of SiO_2-Al_2O_3 membranes

In this study, 5mol% Al_2O_3 doped silica membrane was synthesized as one of the candidates for groundwater desalination. The Al_2O_3 was doped into the silica sol-gel system in the form of aluminum isopropoxide (AIP) to stabilize the silica network. However, the AIP is a highly reactive alkoxide, the direct doping to the sol-gel system will result in phase separation, which will jeopardize the performance of the membrane (75). Therefore, the surfactant was applied as a bifunctional agent, to reduce the reactivity of the AIP and performance as a pore-forming template (84, 85). The detailed synthesis of the two SiO_2-Al_2O_3 membranes was described in Paper I (86). In brief, TEOS and AIP were used as the precursor of SiO_2 and Al_2O_3 in the sol-gel system, and a final concentration of 5mol% Al_2O_3 was achieved in the membrane material. Cetrimonium bromide (CTAB), a cationic quaternary surfactant, was added during the sol-gel synthesis. the concentration of the CTAB in the coating sol is relative to the concentration of the oxide. To investigate the optimal CTAB concentration for membrane performance, the membranes with a molar ratio between CTAB and (SiO_2 + Al_2O_3) of 0.25, 0.5, 1.0, 2.0, and 4.0 was synthesized (the

surfactant and oxides ratios are labeled as S/O=X). Subsequently, the sol with different CTAB concentrations was dip-coated onto α-alumina tubular support (250mm × 7mm) with a γ-alumina intermedia layer, after drying and heat treatment, the 5mol% Al_2O_3 doped silica membranes are obtained (Figure 3-1) (86, 87).

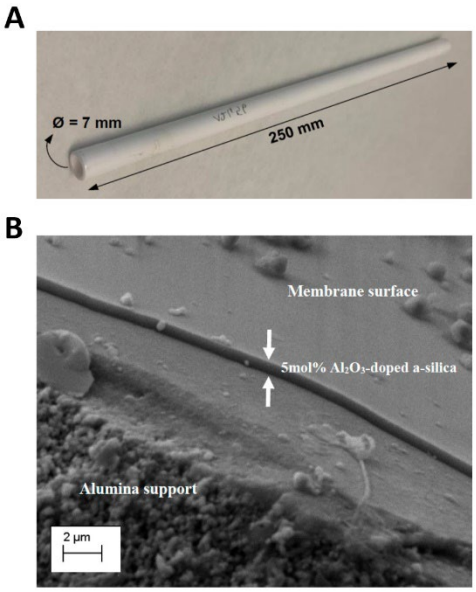

Figure 3-1: (A) The tubular α-alumina support with γ-alumina intermedia layer and a selective layer of the 5mol% Al_2O_3 doped silica membrane, and (B) the SEM image of the % Al_2O_3 doped silica selective layer (86, 87).

Figure 3-2 (a) shows the effect of CTAB concentration on membrane permeability and selectivity (86). It can be seen that the permeabilities first increase and then decrease with the increase of the CTAB concentration. The lowest permeability can be observed for the membrane with a S/O of 0.25 at about 0.68 LMH bar^{-1}. When the S/O increase to 2, the membrane permeability also increases to around 2.3 LMH bar^{-1}, the increase of the permeability can be coursed by the increase of the pore interconnectivity with the concentration of CTAB. Further increasing the CTAB concentration, the membrane permeability decreased to 1.9 LMH bar^{-1} (S/O=4). This could result from the collapsing of the membrane pores during the heat treatment at a high concentration of CTAB (86).

The selectivity of the membranes synthesized with different CTAB concentrations is shown in Figure 3-1(B) (86). The membrane rejection was tested by using NaCl, $MgSO_4$, and Na_2SO_4 solutions with 0.01 M of ionic strength, and 10 ppm of caffeine solution as feed. The membranes have shown a high rejection for $MgSO_4$, Na_2SO_4, and caffeine. For those salts and the organic pollutant, the rejection also increased and then decreased with increases in the CTAB concentration. The highest rejection for

$MgSO_4$, Na_2SO_4, and caffeine can be achieved, at about 95%, 98%, and 98%, respectively, for the membrane that is S/O=0.5. On the other hand, all the membranes have shown a relatively low rejection for NaCl. This is common since NF membranes generally can only partially reject monovalent ions like Na^+ and Cl^- but have a high rejection for divalent ions and organic pollutants. With the increase of the CTAB concentration from S/O=0.25 to 4, the NaCl rejection decreased from 81% to 59% (86). From this study, we can conclude that the membrane of S/O=2 has the highest permeability among all tested membranes while the membrane S/O=0.5 has the highest rejection for divalent ions and caffeine, therefore, the two optimized membranes were selected for the desalination of real groundwater samples (87).

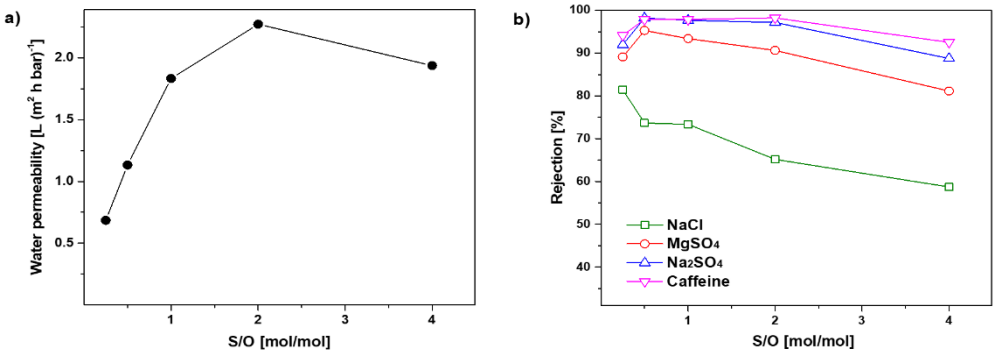

Figure 3-2: The water permeability (a) and membrane rejection for different salts and caffeine (b) of the SiO_2-Al_2O_3 membranes that were synthesized by the CTAB concentration from S/O=0.25 to S/O=4. (86).

3.2 Groundwater desalination by SiO_2-Al_2O_3 membranes

In this study, the performance of the two selected SiO_2-Al_2O_3 membranes, S/O=0.5 and S/O=2, were tested with the crossflow NF system with a transmembrane pressure of 5bar. 2L of groundwater collected from Acquedotto Pugliese s.p.a. (Puglia, Italy) was used as the feed of the system (87). The flux and the water recovery factor of the two SiO_2-Al_2O_3 membranes are shown in Figure 3-3 (87). Both membranes have shown a reduction in water flux with the increase of the water recovery factor. When both membranes were at 1% of the water recovery factor, the fluxes of S/O=2 and S/O=0.5 were at about 28 and 17LMH, respectively. At 50% of the water recovery factor, the fluxes of S/O=2 and S/O=0.5 are reduced to 19 and 3 LMH, respectively. The reduction of the flux could be ascribed to two possible factors: i) the occurrence of fouling and scaling during the filtration process and ii) the increase of the osmotic pressure coursed by the up concentrating of the feed solution (87). Compare with the S/O=0.5, the higher flux of the S/O=2 membrane is resulting from the higher concentration of pore-forming template in the coating sol. The final water recovery factor of the S/O=0.5 and S/O=2 membranes can reach around 55% and 65%,

respectively (87). The water recovery rate for the membrane also decreases over time, because of the decreasing water permeation rate.

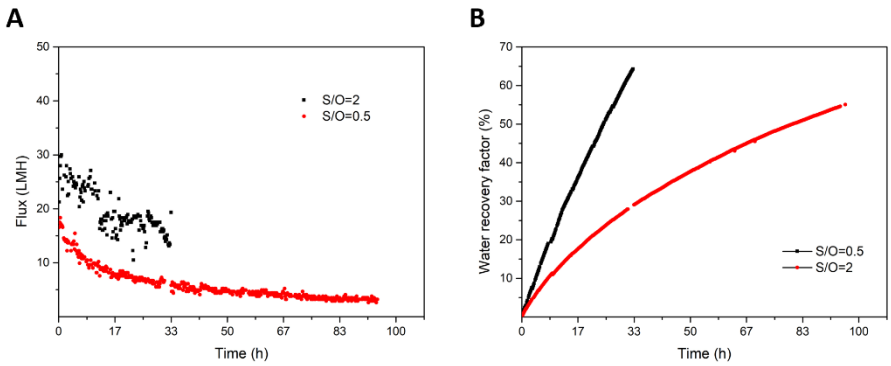

Figure 3-3: (A) The water flux and (B) the water recovery factor of membrane S/O=2.0 and S/O=0.5 at 5bar of transmembrane pressure (87).

The salt rejection of the S/O=0.5 and S/O=2 membranes was determined by inductively coupled plasma spectroscopy (ICP). Four major cationic concentrations of the feed and permeate samples have been identified, namely, Na^{+}, K^{+}, Mg^{2+}, and Ca^{2+}, the change in the rejections of the ions of the S/O=2 and S/O=0.5 over time are demonstrated in Figure 3-4 (87). It can be seen that the majority of the salts present in the groundwater are sodium salts. Generally, there is a slightly increasing trend for the cation concentration of the feed solution during the filtration experiment, while the permeate cation concentrations remain relatively constant, therefore the ion rejection of the two tested membranes was increased over time. The possible explanation for this phenomenon can be that the deposition of the fouling/scaling layer on the membrane surface promotes the selectivity of the membrane (88,89). The S/O=0.5 shows a higher ion rejection than S/O=2. For S/O=0.5, the final Mg^{2+} and Ca^{2+} rejection are about 67% and 57%, respectively, but only about 28% and 23% for S/O=2 (87). The difference in ion rejections of the two membranes can result from the specific volume and connectivity of the pores, created by the different concentrations of surfactant in the coating solution.

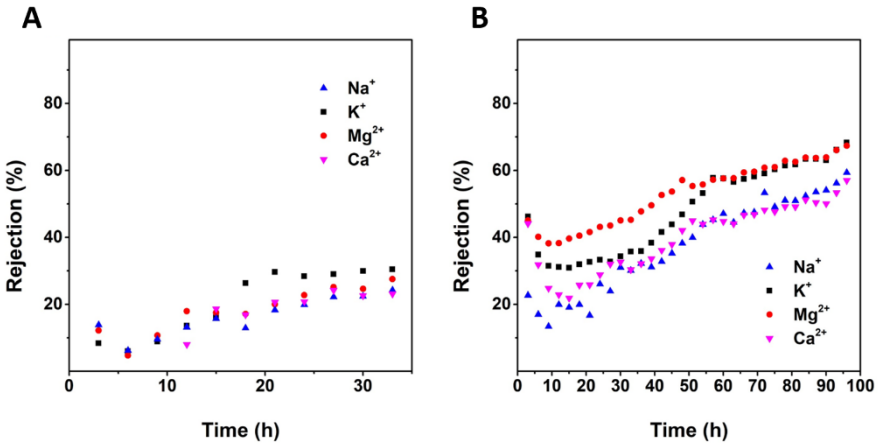

Figure 3-4: Rejection of cations for (A) S/O=2.0 and (B) S/O=0.5 NF membranes while filtering a groundwater sample (87).

The change of conductivity of the permeate solution from both membranes over water recovery factors is illustrated in Figure 3-5. It can be seen that the conductivity is relatively stable through the filtration experiment for both membranes, indicating a stable performance of the SiO_2-Al_2O_3 membranes (87). Compared to the conductivity of the groundwater (4.6 mS cm^{-1}), the conductivity of the permeate solution for both membranes has shown a large reduction. The permeate of the S/O=2 has shown a higher conductivity (3.8 mS cm^{-1}) than S/O=0.5(2.4 mS cm^{-1}) (87). This number is consistent with the ions rejection in Figure 3-5. the conductivity of the permeate for S/O=0.5 is at the upper limit for drinking water (2.5 mS cm^{-1}). In reality, there could be fluctuations in the groundwater salinity, resulting in the permeate exceeding this limation. On the other hand, the permeate conductivity of the S/O=2 has largely exceeded the limation for drinking water, therefore, cannot be used for consumption (87).

To investigate the membranes at rejecting potential organic pollutants in the local range such as pesticides, three model micropollutants, namely acetamiprid (ACE, 98%, Sigma Aldrich), imidacloprid (IMI, 98%, Sigma Aldrich), and thiacloprid (THI, 98%, Sigma Aldrich), were added into the groundwater samples with a concentration of 10ppm. The rejections of these micropollutants are shown in Figure 3-6. For S/O=0.5, the rejections of the ACE, THI, and IMI were at about 35%, 8%, and, 10%, respectively, while the S/O=2 membrane has a rejection of around 6%, 15%, and 14% for the ACE, THI, and IMI, respectively (87).

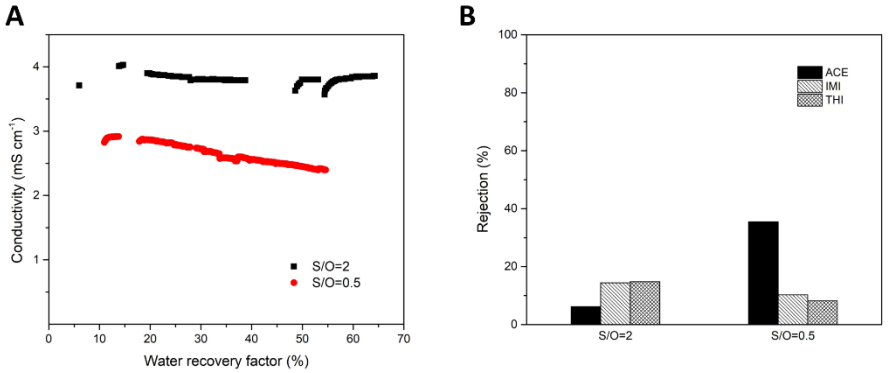

Figure 3-5: (A) The permeate conductivity of membranes S/O=2.0 and S/O=0.5 over water recovery factor and (B) the micropollutant rejections of membranes S/O=2.0 and S/O=0.5 (87).

3.3 Groundwater desalination by polymeric NF membrane

On the other hand, a commercial polyamine NF membrane (FilmTec™ membranes, Dow Chem.) was also tested for the desalination of the groundwater under the same conduction as the SiO_2-Al_2O_3 membranes. The water flux and water recovery factor of the membrane have shown in Figure 3-6. Similar to the SiO_2-Al_2O_3 membranes, the water flux reduced from 25 LMH to 11 LMH when the recovery factor increases from 1% to 50% (87). The decrease in the flux can also be explained by the increase in the osmotic pressure of the feed solution and the formation of the fouling and scaling. After the filtration experiment, a layer of deposition is visible on the membrane surface (87).

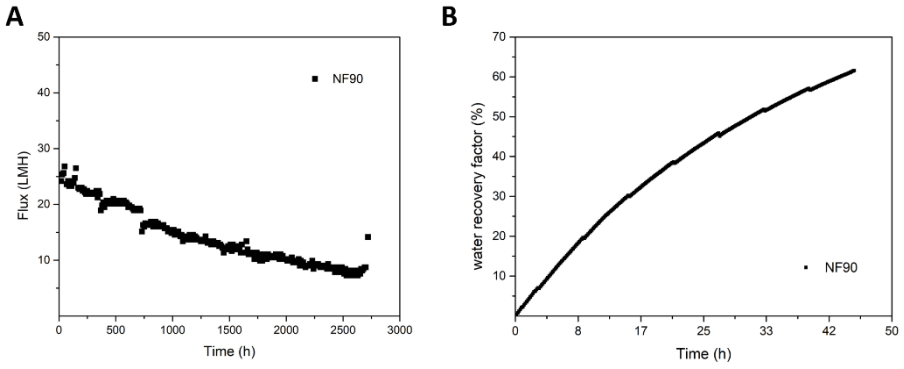

Figure 3-6: (A) The water flux and (B) the water recovery factor of NF90 at 5bar of transmembrane pressure (87).

Overall, the NF90 has a higher rejection than the SiO_2-Al_2O_3 membranes. The ion concentration of the feed and permeate solution and the ion rejections as a function of time have shown in Figure 3-7. The NF90 has shown a slightly higher rejection towards monovalent ions (Na^+, K^+) than the divalent ions (Mg^{2+}, Ca^{2+}) since the rejection mechanism of the ions includes both size exclusion and Donna exclusion (90). The final rejection for the Ca^{2+} and Mg^{2+} can reach about 90%, and around 80% of rejection can be achieved for Na^+ and K^+ (87).

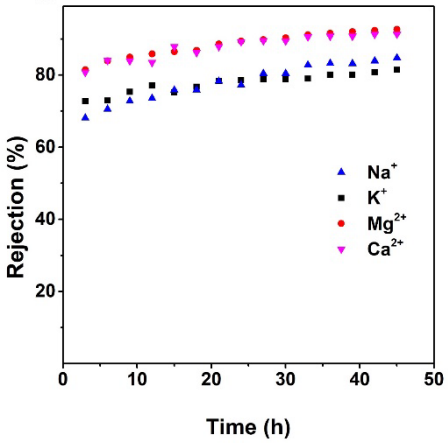

Figure 3-7: Cation rejection of NF90 while filtering a groundwater sample (87).

The NF90 has also shown a stable performance during the filtration experiment, indicated by the constant value of the permeate conductivity. Due to the high ion rejection, the permeate of the NF90 has obtained the lowest conductivity (about 1.3 mS cm^{-1}) among all membranes. This level of conductivity is below the limit (2.5 mS cm^{-1}) of the local authority (91). Therefore, the permeate of the NF90 could be used for consumption. On the other hand, the NF90 has also shown high retention of micropollutants. With the groundwater samples that are doped with 10ppm of ACE, THI, and IMI, the NF90 can achieve a rejection of 56%, 85%, and 59%, respectively. The high rejection of the micropollutants is mainly contributed by the size exclusion of the nano-sized pores from the membrane.

3.4 Economic consideration and upscaling

The Lab-scale filtration tests allowed to estimate the specific energy consumption (SEC, kWh m^{-3}) while filtering samples of groundwater on each of the membranes by applying Eq. 3-1, where Q_f and Q_p represent the feed and permeate volumetric flow rates, and ΔP is the pressure drop (N m^{-2}) along the membrane module at the feed side.

$$SEC = 2.778 \cdot 10^{-7} \frac{\Delta P \cdot Q_f}{Q_p} \qquad 3-1$$

The SEC values of the three membranes in lab-scale tests are reported in Figure 3-8a. It is estimated that the 3 membranes need between 0.12 and 0.17 kWh to produce 1 m^3 of permeate, with the SiO_2-Al_2O_3 membranes requiring less energy than the polymeric one.

Despite these promising results, the technology of SiO_2-Al_2O_3 NF membrane requires further maturation before real-scale applications. Indeed, this type of membrane showed lower selectivity than the commercial polymeric NF90, whose real-scale modules can be acquired on the market at prices around 50 € m^{-2} of effective filtering area, while the fabrication of SiO_2-Al_2O_3 NF membrane in our lab is now costing > 1000 € m^{-2}. For this reason, NF90 was here considered for pilot tests. Therefore, groundwater desalination was tested on the pilot plan in Figure 3-8b carrying an NF90-4040 module with an effective filtering area of 7.6 m^2. The selectivity of the membrane was similar to that observed during batch tests performed to observe the change in membrane permeability and SEC at different recovery factors. As shown in Figure 3-8c, the permeate flow drops at recovery factors higher than 80%. This can be ascribed to the increased osmotic pressure difference across the membrane and the scaling of precipitated salts on the membrane surface. The change in permeability corresponds to an increase in SEC (Figure 3-8d). Nevertheless, the maximum value measured in our tests was 0.656 kWh m^{-3} at a concentration factor of 97%. Considering a cost of 0.20 € kWh^{-1} for the electrical energy, the membrane is potentially able to generate a permeate at a cost of about 0.13 € m^{-3}, which is compatible with a commercial prise for the freshwater of about 1.5 € m^{-3}, as in the Puglia region. At present, a demonstrative plan carrying four NF90 membrane modules with a total area of 30.4 m^2 is functioning in desalting water of the historical well Cozza-Guardati, in Lecce, Italy.

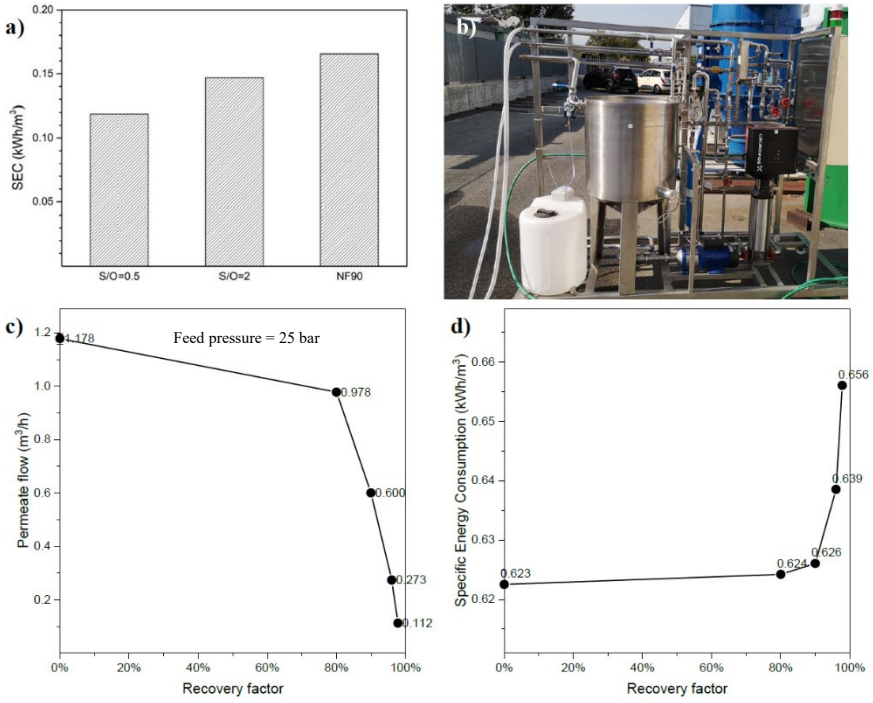

Figure 3-8: (a) Specific energy consumption of ceramic (S/O=0.5 and S/O=2) and polymeric (NF90) as calculated from laboratory tests (87)*; (b) pilot plan for testing NF90 (membrane area 7.6 m²); (c) Permeate flow vs recovery factor while filtering the groundwater in the NF pilot; (d) Specific energy consumption as measured while filtering in groundwater in the NF pilot.*

3.5 Summary

In this study, sol-gel methods were used for the thesis of the 5 mol% Al_2O_3-doped silica NF membranes, the membranes were optimized by changing the surfactant concentration in the coating sol. Two SiO_2-Al_2O_3 membranes, S/O=0.5 and S/O=2, were obtained from this study with optimal selectivity and permeability, respectively.

Subsequently, two optimized SiO_2-Al_2O_3 membranes together with a commercial polymeric membrane, NF90, were tested for groundwater desalination application in the Puglia Region, Italy. From the filtration test, polymeric membrane NF90 has shown the highest selectivity, the rejection for divalent ions is in the range of 80% to 90% rejection, while about 56% to 85% of rejection for organic micropollutants can be achieved. About 62% of water recovery factors can be obtained by NF90. On the other hand, the SiO_2-Al_2O_3 membranes have shown a lower salt rejection, the

permeate conductivity of S/O=2 was at about 3.8 mS cm^{-1} while S/O=0.5 was at 2.4 mS cm^{-1}. However, the membrane S/O=0.5 have shown the lowest energy consumption which can have an equivalent specific water cost of about €0.02 m^{-3}. Therefore, NF90 was selected for the desalination demonstrative site in Lecce, Italy. Furthermore, in an extended study, the SiO_2-Al_2O_3 membranes have been combined with the thermocatalytic perovskite, cerium-doped strontium ferrate, for the removal of micropollutants (92). The stability of the SiO_2-Al_2O_3 membranes has provided an opportunity of the apply thermocatalytic perovskite without the risk of damaging the membrane layers.

CHAPTER 4. MEMBRANE DISTILLATION-UVC/VUV FOR THE TREATMENT OF A SEAWATER AQUACULTURE EFFLUENT

In recent years, membrane distillation has been considered to be more suitable for the treatment of wastewater with high salinity than traditional pressure-driven membrane technologies, due to its high rejection and high recovery factor (45). One of the projects that have been conducted in the Ph.D. is the desalination of the seawater aquaculture effluent by MD. The increasing demand for fish products has driven aquaculture to become one of the fastest-growing sections of the food industry (93). The effluent of seawater aquaculture not only contains a high concentration of organic pollutants but also a high salinity. The MD is efficient at retaining the salt ions, yet, it has a poor ability at retaining volatile pollutants (45). One of the volatile pollutants that used as have been frequently added to the aquaculture system is formaldehyde, it has been extensively applied as an antifungal and antiparasitic agent (94). On the other hand, advanced oxidation processes (AOP) have attracted much attention for the abatement of organic pollutants. Generally, the mechanism of AOP is rely on the generation of hydroxyl radicals (•OH) and the degradation of the organic pollutant into water and CO_2 (95). Recent studies have shown that VUV/UVC can effectively remove organic pollutants without the input of chemicals (96). In this section, the desalination and detoxification of the seawater aquaculture effluent by using formaldehyde as the model pollutant was conducted by a combination of MD with commercial polyproline hollow fiber membrane and VUV/UVC.

4.1 The MD performance

The effluent sample of the seawater aquaculture was collected from the National Center for Mariculture, Israel. The inlet of the fish farm is coming from the red sea area, meaning that the effluent has a salinity above average seawater, the salinity post a challenge for the recycling/reuse of the water at a later stage. Therefore, MD was tested as a desalination solution for the affluent. The detailed experiment procedure is described in Paper IV. In brief, 2L of pre-filtered effluent water sample was used as the feed solution. In addition, 20ppm of formaldehyde was doped into the feed as the volatile model pollutants. The membrane for the MD system was the hollow fiber PP membrane that has a pore size of 0.2 μm and a filtration area of 0.1m^2. Three temperatures (40℃, 55℃, and 70℃) were selected for the heating bath of the feed, while the 0.7L of DI water was cycling on the permeate side, with a cooling bath kept at 15 ℃. The water flux of the membrane under three different temperatures can be seen in Figure 4-1(A). Generally, the membrane can produce a stable flux under all the testing temperatures. It can be seen that the flux increased with the temperature,

when the heating temperatures of the feed were at about 40℃, 55℃, and 70℃, the flux was at around 0.6, 1.5, and 2.6 LMH, respectively. The increase of the flux results from the increase of the driven force, vapor pressure difference, with the temperature. Compare with the osmotic pressure, the vapor pressure is a dominating driven force, therefore, unlike the pressure-driven membrane technologies, there is no obvious reduction of the flux over time. On the other hand, a high water recovery factor can be obtained by the MD process. The water recovery factories increased linearly over time, and the rate of water recovery also increases with the temperature. By the end of the MD process, the water recovery factories are in the range of about 80% to 90% throughout all testing temperatures (Figure 4-1(B)). For each testing temperature, the salt crystals precipitation can be observed at the later stage of the MD process.

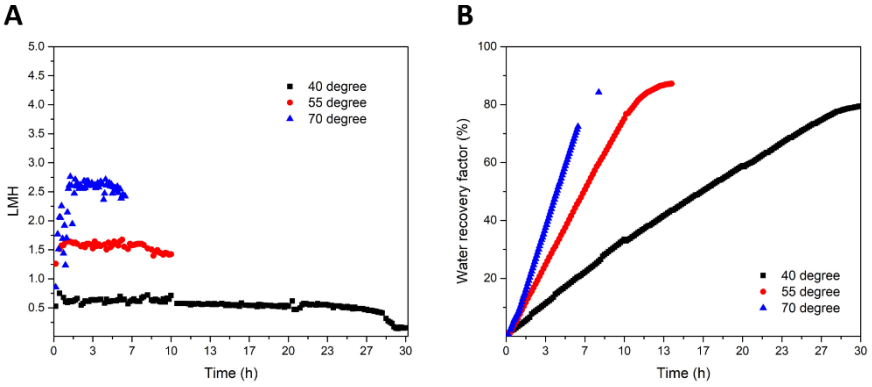

Figure 4-1: The development of flux (A) and water recovery factor (B) of the MD process over time, when the feed operating temperatures were 40 ℃, 55 ℃, and 70 ℃ (Paper IV).

The MD process has also shown a high desalination ability. The conductivity was measured to indicate the salinity of the feed and permeate solution. Before the MD process, the conductivity of the feed is about 42000μs cm^{-1}. During the MD process, the conductivity of permeate solution at all of the tested temperatures does not exceed 115μs cm^{-1}, which indicated an almost 100% salt rejection was achieved. The high selectivity is resulting from the high wetting resistance of the membrane, meaning during the MD process, the membrane function as an effective barrier between the feed and permeate. However, the conductivity of the permeates under all tested temperatures had a trend of increasing first and then decreasing during the MD process as shown in Figure 4-2. The park of the conductivity for each permeate has shown a slightly increasing trend over the temperature. The peak of the conductivity can be observed at around 100μs cm^{-1}, 107μs cm^{-1}, and 113 μs cm^{-1} for the heating temperature of 40℃, 55℃, and 70℃, respectively. The rise of the conductivity of the permeate could be coursed by the permeation of the conductive volatile species like NH_3 from the feed. The increase in the temperature results in an increase in the vapor pressure for the volatile species, therefore, a higher concentration of the volatile

species in the permeate. At a later stage, when the water evaporation rate exceeds the volatile species, the dilution of the volatile species course a decrease in the conductivity.

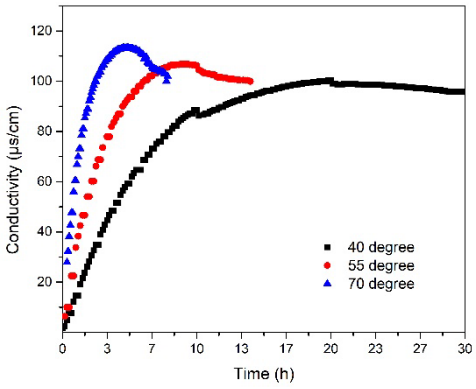

Figure 4-2: The change of permeate conductivity over time for the feed operating temperatures of 40 ℃, 55 ℃, and 70 ℃ (Paper IV).

Despite the high salt rejection, the MD membrane has shown a low rejection of formaldehyde. It can be seen from Figure 4-3(A) that the formaldehyde concentrations in the permeates solution increased linearly over time for all testing temperatures, and finally reached about 7.1, 15.8, and 10.9 ppm for 40℃, 55℃, and 70℃, respectively. This indicates that the formaldehyde has a relatively stable evaporation rate through the MD process. To have an intuitive presentation of the formaldehyde concentration development from the permeate, the net formaldehyde concentration in the transported flux was also calculated (Figure 4-3(B)), by excluding the initial dilution of the 0.7l DI water of the permeate. Generally, the net formaldehyde concentration of the flux increase with the heating temperature. The average concentration rises from 8.3 to 16.2 ppm when the temperature increases from 40℃ to 70℃. Similar to the increasing trend of the permeate conductivity with the temperature, the coursed of the increasing net formaldehyde concentration could be increasing the formaldehyde vapor pressure with the temperature. It is worth noticing that the concentration of formaldehyde from the permeate is lower than the initial 20ppm formaldehyde from the feed. This could be resulting from the lower evaporation rate of formaldehyde compared with water. It is reasonable to assume that most of the formaldehyde that did not permeate through the membrane is retained in the feed.

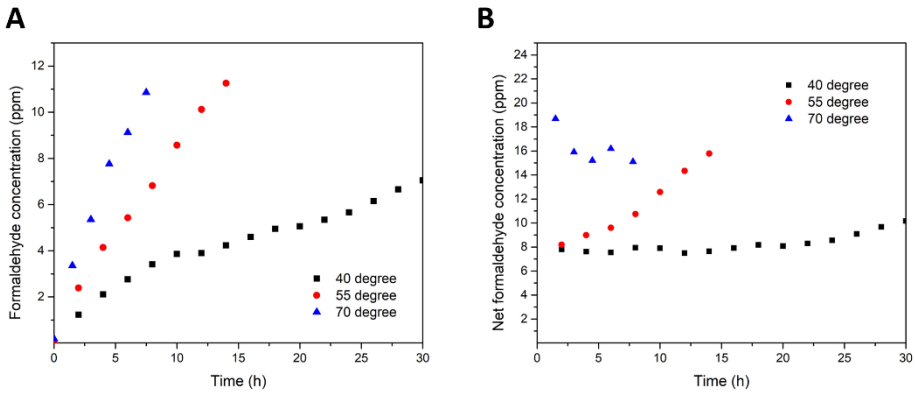

Figure 4-3: The change of the formaldehyde concentration (A) and net formaldehyde concentration (B) over time for the feed operating temperatures of 40 ℃, 55 ℃, and 70 ℃ (Paper IV).

4.2 The crystal formation

The MD can not only recover fresh water. During the MD process, when the concentration of the feed solution exceeded the saturation point, solutes can also start to precipitate and recovered. In terms of the MD process of the seawater aquaculture effluent, the precipitation of the salt crystals can be observed. Crystal formation during the MD can have a huge impact in terms of membrane scaling, wetting, and mineral recovery. Therefore, the process of crystal formation from the feed solution is discussed in this study.

The process of crystal growth when feed is heated at 70°C is observed via the optical microscope (Figure 4-4), the pictures were taken every 15min after the precipitation was observed. The salt crystals firstly appeared when the MD process have been running for about 6.5h, at which point the water recovery factor is above 72%. It can be seen from the picture that there is the formation of two types of crystals. From 6.5h to 7h, the growth and agglomeration of the first type of salt particles are visible. At this stage, the salts do not have a clearly defined geometry under the microscope, and the precipitation is suspected to be some of the solutes with a low solubility such as Ca and Mg salts. After 7h, a large number of cubic crystals start to appear in the feed solution. With the typical geometry, it is safe to assume that the forming crystals are mainly NaCl. At the temperature of 70°C, the solubility of the NaCl is about 375g L^{-1}, therefore, the concentration of the feed should exceed this threshold.

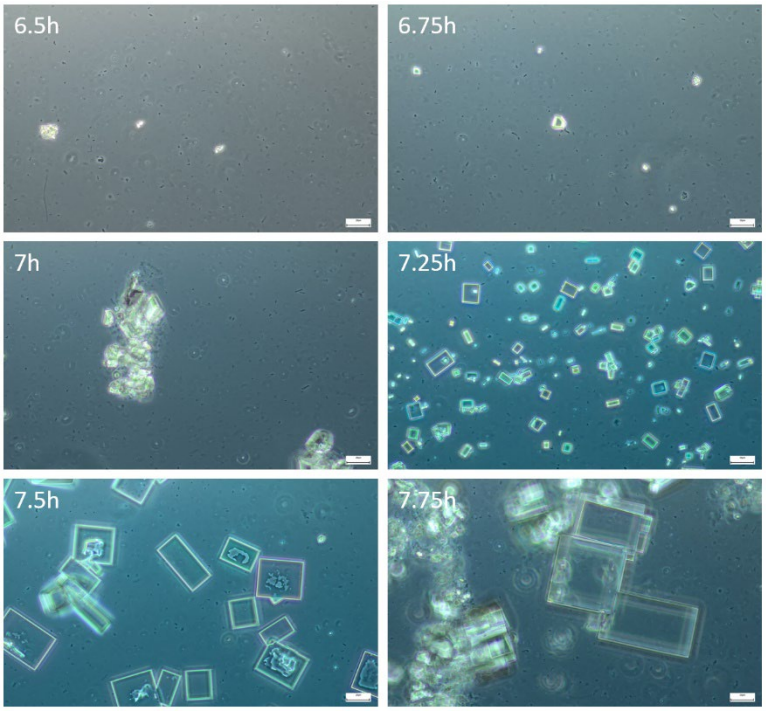

Figure 4-4: The microscope image of the salt crystals formation at the 70℃ of the feed operating temperature between 6.5h to 7.75h (Paper IV).

To further investigate the salt crystals from the feed of all tested temperatures by centrifugation at 1500rpm and subsequently dried at room temperature. The composition of the salts is analyzed by re-dissolving the salts in DI water to reach a final concentration of 1g L^{-1} and measured by inductively coupled plasma spectrometry (ICP). The crystal structure of the obtained salts is also analyzed by X-ray diffraction analysis (XRD).

Table 4-1: The cation weight percentage of the precipitated salts solution obtained for the feed testing temperature of 40 ℃, 55 ℃, and 70 ℃ based on the ICP measurement (Paper IV).

Feed temperatures(℃)	**Na^+ (wt%)**	**K^+ (wt%)**	**Ca^{2+} (wt%)**	**Mg^{2+} (wt%)**	**P (wt%)**
40	5.78	0.40	15.34	0.61	0.02
55	21.77	0.81	7.09	1.32	0.01
70	21.03	0.76	7.16	1.21	

It can be seen from the ICP analysis (Table 4-1) that the main composition of the salt ions in the precipitation is Na^+, K^+, Ca^{2+}, and Mg^{2+}, and the presents of heavy metal ions are not been detected. By the order of the concentrations, Ca^{2+} has the highest concentration in the salts obtained from feed that is operated at 40℃, than are Na^+, Mg^{2+}, and K^+. While Na^+ has the highest concentration in the salts that are obtained from both operating temperatures of 55℃ and 70℃, followed by Ca^{2+}, Mg^{2+}, and K^+. The composition of the salts obtained from 55℃ and 70℃ are relatively similar, however, the salts from 40℃ have a signification higher concentration of Ca^{2+} and a much lower concentration of Na^+. The concentration difference could be resulting from the water recovery factor difference at the different operating temperatures. The water recovery factors for 40℃, 55℃, and 70℃ are 79%, 87%, and 84%, respectively. This indicates that the majority of Na salts precipitate after the water recovery factor reaches 79%, before that is mainly the formation of the insoluble Ca salts. Another possible explanation for the high concentration of Ca salts in lower temperatures could be the increase of the Ca salts solubility with the increase of the solution temperature. The small amount of P in the salts can be coursed by the residue of organic matter in the feed solutions.

The XRD analysis of the salts obtained from all tested temperatures is shown in Figure 4-5. The XRD results of the salt samples are compared with the pure NaCl sample. It can be seen that most of the peak positions for the salts from the operating temperatures 55℃, and 70℃ are matching with the XRD of NaCl, confirming most of the salts present in the precipitation from the two temperatures are NaCl. On the other hand, the characteristic peaks of NaCl for the salt sample derived from the 40℃ have a much lower intensity, combined with results from ICP, it is safe to assume that the salts that have been obtained are low soluble Ca salts.

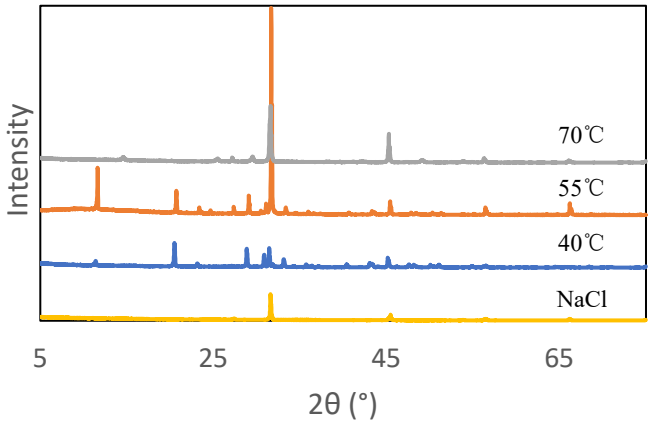

Figure 4-5: The XRD measurement of the precipitated salt crystals obtained from the feed testing temperature of 40 ℃, 55 ℃, and 70 ℃.

4.3 The VUV-UVC degradation

The previous results have shown that permeate solution still contains a relatively high concentration of formaldehyde. In this study, to remove the remaining formaldehyde, the permeate solutions obtained from all temperatures have been diluted with DI water to 3.5 L, and fed into a VUV/UVC photolysis reactor, as shown in Figure 4-6 (97). The detailed experimental description of the VUV-UVC degradation process has presented in Paper IV. In brief, the photo reactor consists of a stainless-steel cylinder that contained an amalgam VUV/UVC lamp (1050mm*19mm). During the degradation experiment, the 3.5L of the permeate solution from the MD process was fed into the reactor recycling via a centrifugal pump with a flow speed of about 2L min^{-1}, while a cooler is operated at 10℃ to prevent the heating from the lamp. The equipped lamp can emit simultaneously UVC and VUV with a 4:1 ratio that can produce 56 W and 14 W of radiation flux, respectively. The total irradiation time for all permeate water samples was 64min, to test the degradation performance of the reactor, water samples were taken throughout the experiment to determine the formaldehyde, also, the pH of the permeate solution is monitored during the experiment.

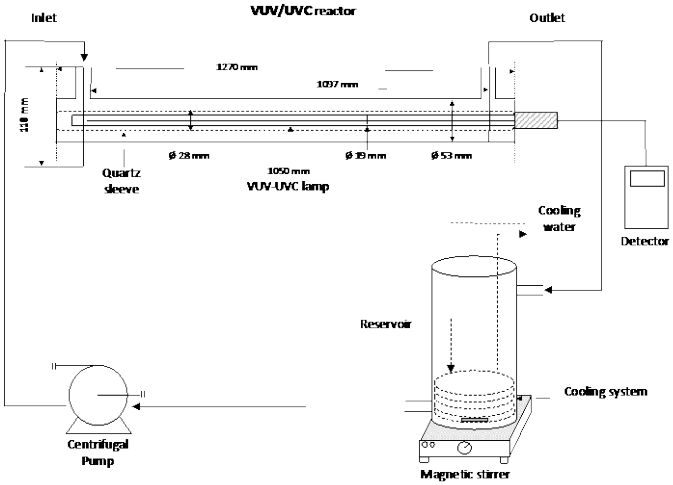

Figure 4-6: The schematic diagram of the VUV/UVC photolysis reactor for the formaldehyde degradation experiments (97).

A previous study has shown that the VUV/UVC reactor is effective at degrading clotrimazole within the initial 8 min (97). A similar performance can be observed in this study. Figure 4-7(A) have shown the development of formaldehyde concentration over time. The initial formaldehyde concentrations for the permeate samples obtained from the feed temperature of 40℃, 55℃, and 70℃ are 4.0ppm, 8.0ppm, and 7.3 ppm, respectively. The exponential decrease of the formaldehyde concentration can be

observed. A 97% of formaldehyde reduction has been achieved for the sample from 40℃ after 8min. And for the permeate samples from 55℃, and 70℃, the concentration of formaldehyde dropped below the detection limit after 16min, which indicates almost complete removal of the formaldehyde. A faster degradation rate can be seen for the permeate obtained from 40℃ due to the lower initial concentration compared with permeate sample obtained from 55℃, and 70℃. The general degradation of the formaldehyde is coursed by the generation of hydroxyl radicals from VUV/UVC irradiation of the water. The free radical can be formed directly by the homolysis of water (Equation 4-1) and oxygen molecules (Equation 4-3) (98). Additionally, electrons can also be produced during the photolysis process (Equation 4-2) which can reduce organic micropollutants and metal ions (98).

$$H_2O + hv(\lambda = 185nm) \rightarrow H\cdot + OH\cdot \qquad 4-1$$

$$H_2O + hv(\lambda = 185nm) \rightarrow H^+ + OH\cdot + e^- \qquad 4-2$$

$$O_2 + hv(\lambda = 185nm) \rightarrow 2O\cdot \qquad 4-3$$

A similar trend can be observed for the development of pH of all permeate samples during the VUV/UVC degradation process Figure 4-7(B). All the permeate samples have a natural pH in the range between 7.3 and 7.6 before the degradation experiments. During the degradation experiments, a noticeable reduction in pH can be observed. The pH decreased slightly within the first 10 min of the experiment and kept relatively constant at the range of 6.5-6.6 for the rest of the experiments. The development of the pH corresponding to the change of formaldehyde concentrations over time could indicate that the formaldehyde has been degraded into formic acid, the reduction of the pH can also be contributed by the generation of H^+ as shown in Equation 4-2 (98).

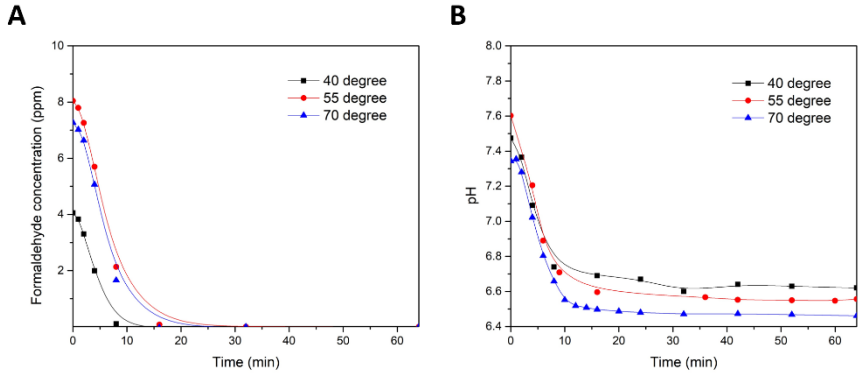

Figure 4-7: The development of the formaldehyde concentration (A) and pH (B) of the permeate solution during the VUV/UVC photolysis process.

4.4 Summary

This study has provided a new strategy for the desalination and detoxification of seawater aquaculture effluent with maximum recovery of resources and minimum environmental impact. By coupling the MD with the VUV/UVC photolysis reactor, the salinity can be almost completely removed by MD while the photolysis from the VUV/UVC can effectively degrade the formaldehyde down to a level below the detection limit. To test the MD performance of the hollow fiber PP membranes, three operation temperatures were applied. The flux of the MD increases with the increase of the temperature, at the end of the MD process, a water recovery factor between 80 to 90% can be obtained, and almost 100% of salt rejection can be achieved, due to the feed solution concentrating, salt can be precipitated. Yet, the membrane has shown poor retention for formaldehyde. Therefore, a VUV/UVC photolysis reactor has applied the removal of the formaldehyde. The VUV/UVC photolysis process was able to completely remove the formaldehyde within 20min.

CHAPTER 5. INORGANIC MD MEMBRANE

To date, there are very few membranes on the market that is designed for the MD process. The membranes that are applied for MD are mostly hydrophobic polymeric microfiltration membranes (45). Although such type of membrane can deliver a relatively reasonable performance as shown in the previous chapter, yet, they usually have a high cost and are not been optimized based on the unique condition of MD processes, including the high operating temperatures and high concentration of dissolved chemical species in the feed. The lack of suitable membranes is one of the biggest obstacles to MD implementation. In fact, the cost of the membrane in an MD system is estimated to be about 50% of the total investment costs for MD systems (99). In this study, an MD membrane that has a high performance with low thermal conductivity and high chemical/thermal stability based on a low-cost industrial inorganic material is developed. As of the date of writing, the newly developed inorganic MD membrane is undergoing a patenting process, therefore, the detailed synthesis material, method, and performance of the membrane will not be discussed in this thesis. Instead, the general strategy for the fabrication of inorganic MD membranes will be elaborated in this section from the perspective of chemical modification and membrane structure.

5.1 The membrane material and hydrophobic modification

As mentioned many times in this thesis, inorganic membranes present higher chemical and thermal stability than polymeric membranes (20). Despite this advantage, inorganic membrane materials have several challenges in terms of MD application. Firstly, most inorganic materials are intrinsically hydrophilic, therefore they cannot prevent the permeation of liquid water through the membrane pores. Secondly, inorganic materials have much higher thermal conductivity compared to polymeric materials. The high thermal conductivity favors heat transfer along the membrane module, causing a drop in temperature gradient across the membrane, thus making the process less efficient (20). Additionally, the fabrication of inorganic materials, such as ceramic, can be very costly, due to expensive raw materials and the energy-intensive heat treatment processes. this Ph.D. study primarily addresses these disadvantages, focusing on the development of novel inorganic MD membranes with superior performance and high energy efficiency.

For ceramic membranes, surface hydrophobicity can be altered by chemical modification. In general, the hydrophobicity of the membrane surface is determined by the surface roughness and chemical composition (20). Surface grafting can be achieved via the sol-gel method, immersion, and CVD (100). In many studies, the hydrophobic modification is done by the sol-gel coating of the fluoroalkyl silane

(FAS) compounds. There is a wide range of silane compounds that can be used for the modification as shown in Figure 5-1 (100). The hydrophobicity is given by the low surface energy fluorocarbon functional group of the silane. In a sol-gel reaction, the FAS compounds will first be hydrolyzed and then condensed to the hydroxide groups on the ceramic membrane surface via heat treatment. Hence, the hydrophobic functional group can be grafted onto the membrane surface (Figure 5-1).

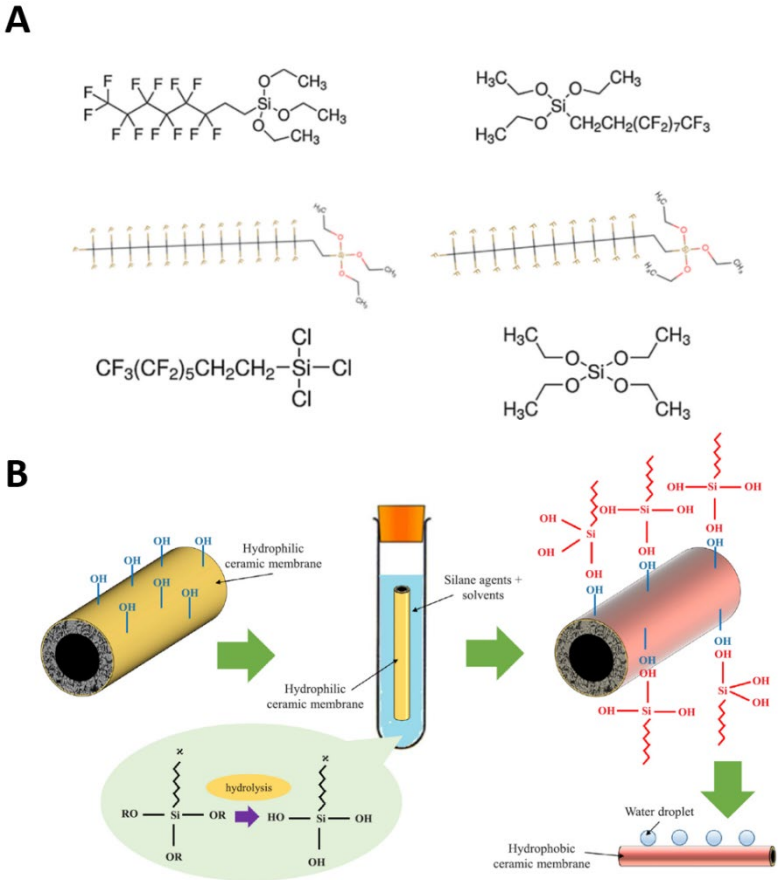

Figure 5-1: The chemical structures of FAS that can be used for hydrophobic modification (A) and the grafting of the hydrophobic functional group via immersion method (B) (100)

In a previous study, the hydrophobic modification was applied to a SiC membrane for the MD application (101). The modification were done by 1H,1H,2H,2H-Perfluorodecyl triethoxysilane (PFDS), and 1H,1H,2H,2H-perfluorooctyl trichlorosilane (PFCS) (101). Figure 5-2 have shown the SiC membrane surface contact angle before and after the hydrophobic modification. Before the modification,

the membrane surface has a contact angle of about 31.5°, and after the modification, the contact angle can reach about 143.2° (101). The MD performance of the SiC membrane was also tested with 5wt% of NaCl solution as the feed. The salt rejection of the membrane can reach about 98% during the 8h of the MD process (101). However, the membrane has shown permeate flux not higher than 0.13 LMH, which is almost 10 times lower when compared to the commercial polymeric membranes discussed in Chapter 4, under similar operational conditions. The low flux could result from the thick membrane layer and the high thermal conductivity. Indeed, an increase in the membrane thickness would increase the vapor transportation path, which leads to a decrease in the permeate flux. More importantly, SiC, as a ceramic material, has a much higher thermal conductivity (>200 W m^{-1} K^{-1}) than polymeric materials (about 0.1-0.5 W m^{-1} K^{-1}) (102, 103). Therefore, during the MD process, the conductive heat loss through the membrane material will lead to a temperature polarization between the temperatures at the bulk solution and the membrane surface. This temperature polarization will cause a decrease in the temperature difference across the membrane and, therefore, reduce the permeate flux.

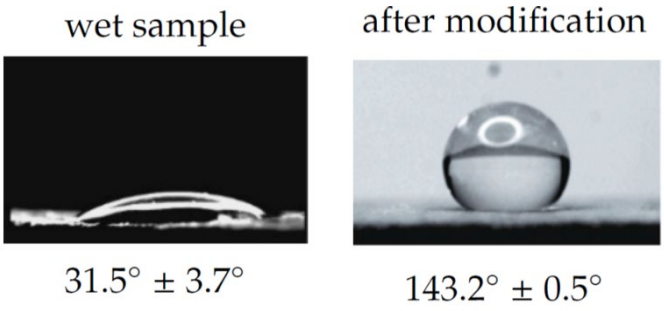

Figure 5-2: The SiC membrane surface contact angle before (left)and after (right) the hydrophobic modification (101).

5.2 The membrane structures

The hydrophobicity and thermal conductivity are not only determined by the chemical composition of the membrane, but also by the structure and the morphology of the membranes. For example, the control of both surface chemistry and surface roughness is needed for achieving a superhydrophobic membrane surface (i.e., a surface with a contact angle higher than 145°). Indeed, a superhydrophobic membrane surface usually has a micro/nano texture. When the membrane surface contacts a liquid, the air pocket set in the crevices of the microstructure reduces the liquid-solid interface, thus improving the anti-wetting properties. The relation between hydrophobicity and surface roughness of a membrane surface can be illustrated by the Kao diagram as shown in Figure 5-3 (20). The contact angle of the rough surface is represented as θ_r,

while the contact angle is derived from Young's equation (θ_s), in the equation, the surface is assumed to be smooth and flat. When plotting the cosine value of the contact angle between the rough and smooth surfaces, the Kao diagram can be obtained (20). The hydrophilic membrane surface can be found in the first quadrant of the diagram, where the liquid is fully soaked into the membrane surface. With the increase in hydrophobicity, the contact angle of the flat surface reaches about 120° which is the highest possible hydrophobicity of a flat and smooth surface, the surface is categorized in the Wenzel region. When the high hydrophobicity combined with the micro/nano textures is created on the surface, the θ_r is increased significantly and can be considered as the Cassie-Baxter region (20). In this quadrant, the hydrophobicity of the surface can exceed the one achieved by simple chemical modification and the membrane becomes super-hydrophobic, achieving excellent anti-wetting and anti-fouling properties (104).

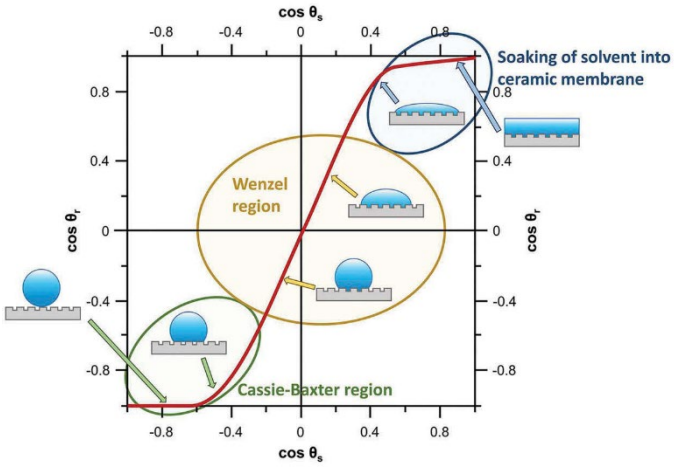

Figure 5-3: The illustration of the Kao diagram (20).

On the other hand, the thermal conductivity materials have a huge impact on the MD process. A low thermal conductivity is needed when designing the membrane materials for MD application, it can prevent heat loss through the membrane area. Therefore, the intrinsically high thermal conductivity of the inorganic materials is challenging for the development of MD membranes. The thermal conductivity of a membrane can be contributed by the conductive and convective heat transfer. Yet, it is proven to be difficult to investigate the thermal transfer coursed by convection due to the thin and fragile nature of the membrane selective layer (105). Nevertheless, the conductivity heat transfer of a membrane in an MD process can be contributed by the conductivity of the solid membrane matrix and the conductivity of the water vapor, as shown in Equation 5-9 (106)

$$k_m = (1 - \varepsilon)k_s + \varepsilon k_g \qquad 5 - 9$$

In the equation, k_m, k_s, and k_g is the overall thermal conductivity of the membrane, the thermal conductivity of the solid membrane matrix, and the thermal conductivity of the gas (or water vapor) present in the membrane pores, respectively. While ε the membrane porosity. Some studies have attempted to address this challenge by developing inorganic membrane materials with low thermal conductivity (107, 108). Nevertheless, the thermal conductivity of the resulting membranes can not be lowered to the same magnitude as the polymeric membranes. This could be resulting from the formation of covalent bond bonding of the particle sintering during the heat treatment (109).

Moreover, Equation 5-9 shows that the membrane thermal conductivity can largely be influenced by the porosity of the membrane materials. In terms of the MD membrane design, the thermal conductivity of the inorganic membranes can be reduced by increasing the membrane porosity to minimize the temperature polarization coursed by conductive heat loss, and subsequently improving the thermal efficiency and flux. On the other hand, the increase of the flux would also promote the endothermic and exothermic processes on the feed and permeate membrane surfaces, respectively, course by the water evaporation and condensation (110), and consequently, reduction of the permeation driving force. Therefore the porosity, MD configurations, and the shape of the membrane unit should be optimized, depending on the specific operational conditions.

5.3 summary

In this section, the general synthesis strategy for a high-performance inorganic MD membrane has been elaborated. Some of the major obstacles to the development of the inorganic membrane include low hydrophobicity and high thermal conductivity. The challenges can be addressed from the aspect of chemical and structural. The hydrophobicity of the membrane surface can be improved by the combination of the grafting of the hydrophobic functional group and the construction of the micro/nano structure on the membrane surface. Furthermore, the thermal conductivity of the inorganic membrane material can be reduced by increasing the membrane porosity. At present, the novel inorganic MD membrane has been obtained by following the strategy have shown a superior MD performance to the commercial PP hollow fiber membranes. Since the membrane is derived from a low-cost industrial material, future investigation will be focusing on the potential of the commercialization of the novel inorganic MD membrane.

CHAPTER 6. CONCLUSIONS

This Ph.D. project has investigated the potential of porous membranes, namely NF and MD, for the desalination of real water systems. It is known that the inorganic membranes present a higher chemical, mechanical, and thermal stability than their polymeric counterparts. Nevertheless, the technology for the fabrication of inorganic membranes lies at an earlier maturation stage compared to commercial polymeric membranes. Therefore, this Ph.D. thesis focused on membrane development by applying inorganic materials, while the performance of the commercial membrane was investigated as a reference. Three studies have been conducted during this thesis aiming to provide a suitable solution for two demonstrative sites in the Project Ô.

Highly stable 5mol% Al_2O_3-doped silica membranes were developed in the first study. The active layer material was optimized by varying the pore-forming agent (i.e., the cationic surfactant CTAB) concentration in the coating solution. The study has shown that when the molar ratio of the oxide and the surfactant are 0.5 and 2, the membrane was shown the optimal selectivity and permeability, respectively. Therefore, the two 5mol% Al_2O_3 doped silica membranes together with a commercial polyamide NF membrane were selected for groundwater desalination in Puglia, Italy. In general, the commercial polymeric membrane has shown the most promising desalination performance. Around 80-90% of divalent ions and 56-85% of organic micropollutants can be rejected. The 5mol% Al_2O_3 doped silica membranes have shown a lower rejection, the divalent ions rejection is in the range of 67% to 57% and 28% to 23% for the membrane S/O=0.5 and S/O=2, respectively.

In the second, the MD was applied for the effluent desalination of the inland mariculture site in Eliat, Israel. The water sample was sparked with 20ppm of formaldehyde to simulate the potential pollution during the fish farming process. A commercial PP hollow fiber membrane was applied for the MD. During the MD process can reach a high water recovery factor at a range of 80% to 90% at an operation temperature between 40℃ to 70℃ while keeping an also complete salt rejection. In fact, the formation of salt crystals can be observed at the final stage of the MD process. With ICP and XRD measurement, the precipitated salts are identified as mostly Na and Ca salts. Despite the high salt rejection, the MD process has shown a low rejection for formaldehyde, the concentration of the formaldehyde in the permeate after the MD process is in the range of 7 to 11 ppm. Therefore, the UVC/VUV photolysis process was coupled with the MD to remove the pollutants from the permeate. The photolysis process can complete degrading the formaldehyde within 20min due to the generation of the hydroxide free radicals.

As an extension of the second study, an inorganic MD membrane that has high thermal and chemical stability with enhanced MD performance has been developed. Due to the undergoing patenting process, the material, method, and performance of the

inorganic MD membrane are not been shared in this thesis. Instead, the general strategy to overcome some of the major challenges, such as the low hydrophobicity and high thermal conductivity for inorganic MD membrane development is elaborate. The author believes that the challenges can be resolved from the aspect of membrane chemical composition and membrane structure. By grafting low surface energy functional groups can transform the membrane surface from hydrophilic to hydrophobic. More importantly, by increasing the surface roughness, a superhydrophobic membrane can be achieved. On the other hand, the high thermal conductivity of the inorganic membrane materials can not only be addressed by the development of the low thermal conductivity materials but also by increasing the membrane porosity.

The future perspective of this Ph.D. project will be focusing on converting the data and the membranes that have been obtained from the studies regarding NF and MD desalination to the construction of the demo sites of Project Ô. A patent will be obtained based on the novel inorganic MD membrane, and the potential for commercialization of the membrane will be further investigated in the future.

BIBLIOGRAPHY

1. Baron J. Issues in Ecology: Water in a changing world. Bull Ecol Soc Am. 2008;89(4):341–3.

2. Lee A, Elam JW, Darling SB. Membrane materials for water purification: Design, development, and application. Environ Sci Water Res Technol. 2016;2(1):17–42.

3. Sridhar S, Smitha B, Aminabhavi TM. Separation of carbon dioxide from natural gas mixtures through polymeric membranes - A review. Sep Purif Rev. 2007;36(2):113–74.

4. Lalia BS, Kochkodan V, Hashaikeh R, Hilal N. A review on membrane fabrication: Structure, properties and performance relationship. Desalination. 2013;326:77–95.

5. Greenlee LF, Lawler DF, Freeman BD, Marrot B, Moulin P. Reverse osmosis desalination: Water sources, technology, and today's challenges. Water Res. 2009;43(9):2317–48.

6. Lonsdale HK, Merten U, Riley RL. Transport properties of cellulose acetate osmotic membranes. J Appl Polym Sci. 1965;9(4):1341–62.

7. Paul DR. Reformulation of the solution-diffusion theory of reverse osmosis. J Memb Sci. 2004;241(2):371–86.

8. Bartels C, Franks R, Rybar S, Schierach M, Wilf M. The effect of feed ionic strength on salt passage through reverse osmosis membranes. Desalination. 2005;184(1–3):185–95.

9. Wilf M, Bartels C. Optimization of seawater RO systems design. Desalination. 2005;173(1):1–12.

10. Morillo J, Usero J, Rosado D, El Bakouri H, Riaza A, Bernaola FJ. Comparative study of brine management technologies for desalination plants. Desalination. 2014;336(1):32–49.

11. Mohammad AW, Teow YH, Ang WL, Chung YT, Oatley-Radcliffe DL, Hilal N. Nanofiltration membranes review : Recent advances and future prospects. DES. 2015;356:226–54.

12. Farsi A, Malvache C, Bartolis O De, Magnacca G, Kjær P, Lykkegaard M, et al. Design and fabrication of silica-based nanofiltration membranes for water desalination and detoxification. Microporous and Mesoporous Materials. 2017;237:117–26.

13. Werber J, Osuji C, Elimelech M. Materials for next-generation desalination and water purification membranes. Nat Rev Mater. 2016; 1: 16018.

14. Bowen WR, Welfoot JS. Modeling the performance of membrane nanofiltration: critical assessment and model development. Chem Eng Sci. 2002;57:1121–37.

15. Farsi A, Boffa V, Qureshi HF, Nijmeijer A, Winnubst L, Lykkegaard M. Modeling water flux and salt rejection of mesoporous γ-alumina and microporous organosilica membranes. J Memb Sci. 2014;470:307–15.

16. Roy Y, Sharqawy MH, Lienhard JH. Modeling of flat-sheet and spiral-wound nanofiltration configurations and its application in seawater nanofiltration. J Memb Sci. 2015;493:360–72.

17. Roy Y, Warsinger DM, V JHL. Effect of temperature on ion transport in nanofiltration membranes : Diffusion, convection, and electromigration. 2017;420:241–57.

18. Geraldes V, Brites Alves AM. Computer program for simulation of mass transport in nanofiltration membranes. J Memb Sci. 2008;321(2):172–82.

19. Wang P, Chung TS. Recent advances in membrane distillation processes: Membrane development, configuration design, and application exploring. J Memb Sci. 2015;474:39–56.

20. Tai ZS, Abd Aziz MH, Othman MHD, Mohamed Dzahir MIH, Hashim NA, Koo KN, et al. Ceramic Membrane Distillation for Desalination. Sep Purif Rev. 2020;49(4):317–56.

21. Franken ACM, Nolten JAM, Mulder MHV, Bargeman D, Smolders CA. Wetting criteria for the applicability of membrane distillation. J Memb Sci. 1987;33(3):315–28.

22. Cabassud C, Wirth D. Membrane distillation for water desalination: How to choose an appropriate membrane? Desalination. 2003;157(1–3):307–14.

23. Lin PJ, Yang MC, Li YL, Chen JH. Prevention of surfactant wetting with agarose hydrogel layer for direct contact membrane distillation used in dyeing

wastewater treatment. J Memb Sci. 2015;475:511–20.

24. Lawson KW, Lloyd DR. Membrane distillation. J Memb Sci. 1997;124(1):1–25.

25. Song L, Ma Z, Liao X, Kosaraju PB, Irish JR, Sirkar KK. Pilot plant studies of novel membranes and devices for direct contact membrane distillation-based desalination. J Memb Sci. 2008;323(2):257–70.

26. Thiruvenkatachari R, Manickam M, Ouk Kwon T, Shik Moon I, Woo Kim J. Separation of water and nitric acid with porous hydrophobic membrane by air gap membrane distillation (AGMD). Sep Sci Technol. 2006;41(14):3187–99.

27. Guillén-Burrieza E, Blanco J, Zaragoza G, Alarcón DC, Palenzuela P, Ibarra M, et al. Experimental analysis of an air gap membrane distillation solar desalination pilot system. J Memb Sci. 2011;379(1–2):386–96.

28. Xie Z, Duong T, Hoang M, Nguyen C, Bolto B. Ammonia removal by sweep gas membrane distillation. Water Res. 2009;43(6):1693–9.

29. Al-Asheh S, Banat F, Qtaishat M, El-Khateeb MY. Concentration of sucrose solutions via vacuum membrane distillation. Desalination. 2006;195(1–3):60–8.

30. Mengual JI, Khayet M, Godino MP. Heat and mass transfer in vacuum membrane distillation. Int J Heat Mass Transf. 2004;47(4):865–75.

31. Khayet M. Membranes and theoretical modeling of membrane distillation: A review. Advances in Colloid and Interface Science. 2011.

32. Alkhudhiri A, Darwish N, Hilal N. Membrane distillation: A comprehensive review. Desalination. 2012;287:2–18.

33. Schofield RW, Fane AG, Fell CJD. Heat and mass transfer in membrane distillation. J Memb Sci. 1987;33(3):299–313.

34. Mengual JI. Modeling mass transport through a porous partition : Effect of pore size distribution. 2004;29(3):279–99.

35. Jhaveri JH, Murthy ZVP. A comprehensive review on anti-fouling nanocomposite membranes for pressure-driven membrane separation processes. DES. 2016;379:137–54.

36. Wang Z, Wu A. Recent Advances in Nanoporous Membranes for Water

Purification. Nanomaterials. 2018. 8(2):65.

37. Peyki A, Rahimpour A, Jahanshahi M. Preparation and characterization of thin film composite reverse osmosis membranes incorporated with hydrophilic SiO_2 nanoparticles. DES. 2015;368:152–8.

38. Mohmood I, Lopes CB, Lopes I. Nanoscale materials and their use in water contaminants removal - a review. Environ Sci Pollut Res. 2013; 20: 1239–1260.

39. Agnieszka K. Hołda,Ivo F.J. Vankelecom. Understanding and guiding the phase inversion process for synthesis of solvent resistant nanofiltration membranes. J Appl Polym Sci. 2015;42130:1–17.

40. Lu X. Interfacial polymerization : history, current efforts, and future directions. Chem Soc Rev. 2021;6290–307.

41. Radovanovic P, Thiel SW, Hwang S. Formation of asymmetric polysulfone membranes by immersion precipitation. Part I . Modelling mass transport during gelation. J Memb Sci. 1992;65:213–29.

42. Trong Q, Tahiri O, Yang H, Mbareck C. Dry-cast process for synthetic microporous membranes : Physico-chemical analyses through morphological studies. J Memb Sci. 2010;358(1–2):13–25.

43. Zhang F, Fan J, Wang S. Interfacial Polymerization : From Chemistry to Functional Materials. Angewandte. 2020;21840–56.

44. Zhang J, Li J De, Gray S. Effect of applied pressure on performance of PTFE membrane in DCMD. J Memb Sci. 2011;369(1–2):514–25.

45. Camacho LM, Dumée L, Zhang J, Li J de, Duke M, Gomez J, et al. Advances in membrane distillation for water desalination and purification applications. Water. 2013;5(1):94–196.

46. Prince JA, Singh G, Rana D, Matsuura T, Anbharasi V, Shanmugasundaram TS. Preparation and characterization of highly hydrophobic poly(vinylidene fluoride) - Clay nanocomposite nanofiber membranes (PVDF-clay NNMs) for desalination using direct contact membrane distillation. J Memb Sci. 2012;397–398:80–6.

47. Gryta M. Influence of polypropylene membrane surface porosity on the performance of membrane distillation process. J Memb Sci. 2007;287(1):67–78.

48. García-Payo MC, Essalhi M, Khayet M. Effects of PVDF-HFP concentration on membrane distillation performance and structural morphology of hollow fiber membranes. J Memb Sci. 2010;347(1–2):209–19.

49. Wang P, Tai-Shung Chung. Exploring the Spinning and Operations of Multibore Hollow Fiber Membranes for Vacuum Membrane Distillation. AIChE J. 2012;59(4):215–28.

50. Tomaszewska M. Preparation and properties of flat-sheet membranes from poly(vinylidene fluoride) for membrane distillation. Desalination. 1996;104(1–2):1–11.

51. Li D, Xia Y. Electrospinning of nanofibers: Reinventing the wheel? Adv Mater. 2004;16(14):1151–70.

52. Brinker CJ, Scherer GW. Sol-gel science, the physics and chemistry of sol–gel processing. Academic Press, Inc; 1990.

53. Wang Z, Wei Y, Xu Z, Cao Y, Dong Z, Shi X. Preparation, characterization and solvent resistance of γ-Al_2O_3/α-Al_2O_3 inorganic hollow fiber nanofiltration membrane. J Memb Sci. 2016;503:69–80.

54. He Z, Lyu Z, Gu Q, Zhang L, Wang J. Ceramic-based membranes for water and wastewater treatment. Colloids Surfaces A. 2019;578:123513.

55. Zou D, Qiu M, Chen X, Fan Y. One-step preparation of high-performance bilayer α -alumina ultrafiltration membranes via co-sintering process. J Memb Sci. 2017;524:141–50.

56. Younssi, S. A., Breida, M., Achiou, B. . Alumina Membranes for Desalination and Water Treatment. In: Eyvaz, M. , Yüksel, E. , editors. Desalination and Water Treatment. London: IntechOpen; 2018.

57. Zou D, Chen X, Qiu M, Drioli E, Fan Y. Flux-enhanced α-alumina tight ultrafiltration membranes for effective treatment of dye/salt wastewater at high temperatures. Sep Purif Technol. 2019;215:143–54.

58. Tsuru T. Inorganic porous membranes for liquid phase separation. Sep Purif Methods. 2001; 30:2, 191–220.

59. Hofs B, Ogier J, Vries D, Beerendonk EF, Cornelissen ER. Comparison of ceramic and polymeric membrane permeability and fouling using surface water. Sep Purif Technol. 2011;79(3):365–74.

60. Da X, Chen X, Sun B, Wen J, Qiu M, Fan Y. Preparation of zirconia nanofiltration membranes through an aqueous sol-gel process modified by glycerol for the treatment of wastewater with high salinity. J Memb Sci. 2016;504:29–39.

61. Zhang BX, Zhang T, Ng J, Sun DD. High-performance multifunctional TiO_2 nanowire ultrafiltration membrane with a hierarchical layer structure for water treatment. Adv Funct Mater. 2009;3731–6.

62. Athanasekou CP, Romanos GE, Katsaros FK, Kordatos K, Likodimos V, Falaras P. Very efficient composite titania membranes in hybrid ultrafiltration/photocatalysis water treatment processes. J Memb Sci. 2012;392-393:192-203.

63. Eduardo F, Coelho B, Deemter D, Candelario VM, Boffa V, Malato S, et al. Development of a photocatalytic zirconia-titania ultrafiltration membrane with anti-fouling and self-cleaning properties. J Environ Chem Eng. 2021;9(6):106671.

64. Zhang L, Chiang T, Ng A, Liu X, Gu Q, Pang Y, et al. Applied Catalysis B : Environmental Hydrogenated TiO_2 membrane with photo catalytically enhanced anti- fouling for ultrafiltration of surface water. Appl Catal B Environ. 2020;264:118528.

65. Keskin Avci S, Erucar I. Porous Materials. Vols. 2–5, Comprehensive Energy Systems. 2018. 182–203 p.

66. Brinker CJ, Scherer GW. Sol-Gel Science: The Physics and Chemistry of Sol-Gel Processing. Sol-Gel Science: The Physics and Chemistry of Sol-Gel Processing. 2013.

67. Lofgreen JE, Ozin GA. Controlling morphology and porosity to improve performance of molecularly imprinted sol-gel silica. Chem Soc Rev. 2014;43(3):911–33.

68. Hench LL, West JK. The Sol-Gel Process. Chem Rev. 1990;90(1):33–72.

69. Lin CXC, Ding LP, Smart S, Diniz da Costa JC. Cobalt oxide silica membranes for desalination. J Colloid Interface Sci. 2012;368(1):70–6.

70. Brinker CJ, Frye GC, Hurd AJ, Ashley CS. Fundamentals of sol-gel dip coating. Thin Solid Films. 1991;201(1):97–108.

71. Fotou GP, Lin YS, Pratsinis SE. Hydrothermal stability of pure and modified

microporous silica membranes. J Mater Sci. 1995;30(11):2803–8.

72. Elma M, Yacou C, Wang DK, Smart S, Diniz da Costa JC. Microporous silica-based membranes for desalination. Water. 2012;4(3):629–49.

73. Boffa V, Magnacca G, Jørgensen LB, Wehner A, Dörnhöfer A, Yue Y. Toward the effective design of steam-stable silica-based membranes. Microporous Mesoporous Mater. 2013;179:242–9.

74. Boffa V, Parmeggiani L, Nielsen AH, Magnacca G. Hydrophilicity and surface heterogeneity of TiO_2-doped silica materials for membrane applications. Microporous Mesoporous Mater. 2016;221:81–90.

75. Wen J, Wilkes GL. Organic/inorganic hybrid network materials by the sol-gel approach. Vol. 8, Chemistry of Materials. 1996. p. 1667–81.

76. Julbe A, Balzer C, Barthez JM, Guizard C, Larbot A, Cot L. Effect of non-ionic surface active agents on TEOS-derived sols, gels and materials. J Sol-Gel Sci Technol. 1995;4(2):89–97.

77. Mege S, Vereist M, Lecante P, Perez E, Ansart F, Savariault JM. Surfactant effects in vanadium alkoxide derived gels. J Non Cryst Solids. 1998;238(1–2):37–44.

78. Kumar B, Ghosh KK, Dafonte PR. Comparative Study of the Cationic Surfactants and Their Influence on the Alkaline Hydrolysis of Acetylsalicylic Acid. Int. J. Chem. Kinet. 2010;43:1–8.

79. Shiklomanov IA, Peter G. World freshwater resources, in Water in Crisis: A Guide to the World's Fresh Water Resources. Oxford Univ Press, N. Y. 1993;13–24.

80. Zwahlen F, COST Action 620. Vulnerability and Risk Mapping for the Protection of Carbonate (Karst) Aquifers.Commission E. 2003;115–96.

81. Lugoli F, Leopizzi M.I, Bagordo F, Grassi T, Guido M, De Donno A. Widespread microbiological groundwater contamination in the South-eastern Salento (Puglia-Italy). J. Environ. Monit. 2011;13:192–200.

82. Meffe R, de Bustamante I. Emerging organic contaminants in surface water and groundwater: A first overview of the situation in Italy. Sci. Total Environ. 2014;481:280–295.

83. Farsi A, Boffa V, Qureshi HF, Nijmeijer A, Winnubst L, Christensen ML.

Modeling water flux and salt rejection of mesoporous γ-alumina and microporous organosilica membranes. J Memb Sci. 2014;470:307–15.

84. Samiey B, Cheng CH, Wu J. Effects of surfactants on the rate of chemical reactions. J. Chem. 2014; 2014:2090–9063.

85. Wijaya S, Duke MC, Diniz da Costa JC. Carbonized template silica membranes for desalination. Desalination. 2009;236(1–3):291–8.

86. Ma X, Janowska K, Fabbri D, Magnacca G, Calza P, Yue Y, et al. Surfactant-assisted fabrication of alumina-doped silica nanofiltration membranes with enhanced water purification performances. Nanomaterials. 2019;9:1368.

87. Ma X, Quist-Jensen CA, Ali A, Boffa V. Desalination of groundwater from a well in Puglia region (Italy) by Al_2O_3-doped silica and polymeric nanofiltration membranes. Nanomaterials. 2020;10(9):1–12.

88. Hilal N, Al-Zoubi H, Mohammad AW, Darwish NA. Nanofiltration of highly concentrated salt solutions up to seawater salinity. Desalination. 2005;184(1–3):315–26.

89. Kaya C, Sert G, Kabay N, Arda M, Yüksel M, Egemen Ö. Pre-treatment with nanofiltration (NF) in seawater desalination-Preliminary integrated membrane tests in Urla, Turkey. Desalination. 2015;369:10–7.

90. Llenas L, Martínez-Lladó X, Yaroshchuk A, Rovira M, de Pablo J. Nanofiltration as pretreatment for scale prevention in seawater reverse osmosis desalination. Desalin Water Treat. 2011;36(1–3):310–8.

91. Servizio Studi - Dipartimento ambiente Recepimento della dir. 2006/118/CE sulla protezione dell'acque sotterranee dall'inquinamento e dal deterioramento Schema di D.Lgs. n. 56 (art. 1, L. 34/2008); 2009.

92. Janowska K, Ma X, Boffa V, Jørgensen MK, Candelario VM. Combined nanofiltration and thermocatalysis for the simultaneous degradation of micropollutants, fouling mitigation and water purification. Membranes. 2021;11(8).

93. Lu S, Wang Q, Gao M, Zhao C, She Z, Zhao Y, et al. Effect of aerobic/anoxic duration on the performance, microbial activity and microbial community of sequencing batch biofilm reactor treating synthetic mariculture wastewater. Bioresour Technol. 2021;333:125198.

94. Jung SH, Kim JW, Jeon IG, Lee YH. Formaldehyde residues in formalin-

treated olive flounder (Paralichthys olivaceus), black rockfish (Sebastes schlegeli), and seawater. Aquaculture. 2001;194(3–4):253–62.

95. Leong S, Razmjou A, Wang K, Hapgood K, Zhang X, Wang H. TiO_2 based photocatalytic membranes: A review. J Memb Sci. 2014;472:167–84.

96. Del Puerto O, Gonçalves NPF, Medana C, Prevot AB, Roslev P. Attenuation of toxicity and occurrence of degradation products of the fungicide tebuconazole after combined vacuum UV and UVC treatment of drinking water. Environ Sci Pollut Res. 2022;58312–25.

97. Gonçalves NPF, del Puerto O, Medana C, Calza P, Roslev P. Degradation of the antifungal pharmaceutical clotrimazole by UVC and vacuum-UV irradiation: Kinetics, transformation products and attenuation of toxicity. J Environ Chem Eng. 2021;9(5):106275.

98. Abbaszadeh Haddad F, Moussavi G, Moradi M. Advanced oxidation of formaldehyde in aqueous solution using the chemical-less UVC/VUV process: Kinetics and mechanism evaluation. J Water Process Eng. 2019;27:120–5.

99. Al-Obaidani S, Curcio E, Macedonio F, Di Profio G, Al-Hinai H, Drioli E. Potential of membrane distillation in seawater desalination: Thermal efficiency, sensitivity study and cost estimation. J Memb Sci. 2008;

100. Hubadillah SK, Tai ZS, Othman MHD, Harun Z, Jamalludin MR, Rahman MA, et al. Hydrophobic ceramic membrane for membrane distillation: A mini-review on preparation, characterization, and applications. Sep Purif Technol. 2019;217:71–84.

101. Boffa V, Lunghi C, Quist-Jensen CA, Magnacca G, Calza P. Fabrication and surface interactions of super-hydrophobic silicon carbide for membrane distillation. Nanomaterials. 2019;9(8).

102. Nakano H, Watari K, Kinemuchi Y, Ishizaki K, Urabe K. Microstructural characterization of high-thermal-conductivity SiC ceramics. J Eur Ceram Soc. 2004;24(14):3685–90.

103. Huang C, Qian X, Yang R. Thermal conductivity of polymers and polymer nanocomposites. Mater Sci Eng R Reports. 2018;132:1–22.

104. Liao Y, Zheng G, Huang JJ, Tian M, Wang R. Development of robust and superhydrophobic membranes to mitigate membrane scaling and fouling in membrane distillation. J Memb Sci. 2020;601:117962.

105. Vanneste J, Bush JA, Hickenbottom KL, Marks CA, Jassby D, Turchi CS, et al. Novel thermal efficiency-based model for determination of thermal conductivity of membrane distillation membranes. J Memb Sci. 2018;548:298–308.

106. Ismail MS, Mohamed AM, Poggio D, Pourkashanian M. Direct contact membrane distillation: A sensitivity analysis and an outlook on membrane effective thermal conductivity. J Memb Sci. 2021;624:119035.

107. Wang JW, Li L, Zhang JW, Xu X, Chen CS. β-Sialon ceramic hollow fiber membranes with high strength and low thermal conductivity for membrane distillation. J Eur Ceram Soc. 2016;36:59–65.

108. Yang MY, Wang JW, Li L, Dong B Bin, Xin X, Agathopoulos S. Fabrication of low thermal conductivity yttrium silicate ceramic flat membrane for membrane distillation. J Eur Ceram Soc. 2019;39(2–3):442–8.

109. Østergaard MB, Petersen RR, König J, Johra H, Yue Y. Influence of foaming agents on solid thermal conductivity of foam glasses prepared from CRT panel glass. J Non Cryst Solids. 2017;465:59–64.

110. Zhu Z, Wang W, Zhang Q, Chen X. Insight into the feed/permeate flow velocity on the trade-off of water flux and scaling resistance of superhydrophobic and welding-pore fibrous membrane in membrane distillation. J Memb Sci. 2021;620:118883.

LIST OF PUBLICATIONS

Publications in peer-reviewed journals

Ma X, Janowska K, Boffa V, Fabbri D, Magnacca G, Calza P, et al. Surfactant-assisted fabrication of alumina-doped amorphous silica nanofiltration membranes with enhanced water purification performances. *Nanomaterials*. **2019**;9(10):1–12.

Ma X, Quist-Jensen CA, Ali A, Boffa V. Desalination of groundwater from a well in Puglia region (Italy) by Al_2O_3-doped silica and polymeric nanofiltration membranes. *Nanomaterials*. **2020**;10(9):1–12.

Janowska K, **Ma X**, Boffa V, Jørgensen MK, Candelario VM. Combined nanofiltration and thermocatalysis for the simultaneous degradation of micropollutants, fouling mitigation, and water purification. *Membranes*. **2021**;11(8).

Altin I, **Ma X**, Boffa V, Bacaksız E, Magnacca G. Hydrothermal preparation of B–TiO2-graphene oxide ternary nanocomposite, characterization and photocatalytic degradation of bisphenol A under simulated solar irradiation. *Mater Sci Semicond Process*. 2021;123:105591.

Bortot Coelho FE, Nurisso F, Boffa V, **Ma X**, Rasse-Suriani FAO, Roslev P, et al. A thermocatalytic perovskite-graphene oxide nanofiltration membrane for water depollution. *J Water Process Eng*. **2022**;49:102941.

Ma X, Flanjak L, Chen X, Quist-Jensen CA, Ali A, Roslev P, Boffa V, VUV-UVC Coupled Membrane Distillation for Recirculating of inland Mariculture Effluents (*to be submitted*)

Chen X, **Ma X**, Boffa V, and Yue Y, Recent Advances in Oxide Membranes for Water Desalination (*to be submitted*).

Oral and poster presentations at conferences

Contribute as the main presenter

'Graphene Oxide for Oil and Gas Technologies' *International Conference on Chemical Energy and Semiconductor Photochemical*, Trabzon, Turkey, 2019

'Case Studies of Nanofiltration and Membrane Distillation Membranes for Desalination Applications' *Euromembrane*, Copenhagen, Denmark, 2021.

‘Hydrophobic modified ceramic membrane for membrane distillation’ *16th International Conference on Inorganic Membranes*, Taipei, 2022

Paper I

nanomaterials

MDPI

Article

Surfactant-Assisted Fabrication of Alumina-Doped Amorphous Silica Nanofiltration Membranes with Enhanced Water Purification Performances

Xianzheng Ma [1], Katarzyna Janowska [1], Vittorio Boffa [1,*], Debora Fabbri [2], Giuliana Magnacca [2,3], Paola Calza [2] and Yuanzheng Yue [1]

[1] Department of Chemistry and Bioscience, Aalborg University, Fredrik Bajers vej 7H, 9220 Aalborg, Denmark; xm@bio.aau.dk (X.M.); kaj@bio.aau.dk (K.J.); yy@bio.aau.dk (Y.Y.)
[2] Department of Chemistry, University of Turin, Via P. Giuria 5/7, 10125 Torino, Italy; debora.fabbri@unito.it (D.F.); giuliana.magnacca@unito.it (G.M.); paola.calza@unito.it (P.C.)
[3] NIS Interdepartmental Center, Universitá di Torino, Via P. Giuria 7, 10125 Torino, Italy
* Correspondence: vb@bio.aau.dk; Tel.: +45-9940-3579

Received: 31 August 2019; Accepted: 20 September 2019; Published: 24 September 2019

Abstract: Surfactant-templated 5 mol% Al_2O_3-doped silica membranes nanofiltration membranes were synthesized via the sol-gel method, and afterward, were optimized, and tested with respect to the permeability and rejection rate. The disordered silica network was stabilized by doping 5 mol% alumina. Tetraethyl orthosilicate and aluminum isopropoxide were used as the silica and alumina precursors, respectively. Cetyltrimethylammonium bromide (CTAB) was used not only as a pore-forming agent, but also to control the reaction rate of the aluminum isopropoxide, thus obtaining highly homogeneous materials. The results about filtration of model solutions showed that the optimized membranes are featured by both a relatively high water permeability (1.1–2.3 $L{\cdot}m^{-2}{\cdot}h^{-1}{\cdot}bar^{-1}$) and a high rejection for salts (74% for NaCl, and >95% for $MgSO_4$ and Na_2SO_4) and organic pollutants (e.g., about 98% for caffeine). High rejection of divalent ions and organic molecules was also observed when a real wastewater effluent was filtered. The influence of the synthesis conditions on the membrane performance is discussed.

Keywords: sol-gel; wastewater; depollution; desalination; selectivity

1. Introduction

Water scarcity is one of the most pressing challenges for the human population. Moreover, the growing demand for clean water and the limited access to water resources for a large part of the global population urgently require sustainable approaches to address this problem, without compromising water access for the future generations [1,2]. Various approaches have been developed to address water depollution in an energy-efficient manner, including adsorption, filtration, electrochemistry, and photocatalysis [3]. In this context, pressure-driven membrane filtration systems, such as nanofiltration (NF), have become increasingly popular since they do not require any chemical treatment or thermal input to the treated water. NF membranes have a pore size ranging between 1 and 2 nm. Therefore, such membranes are efficient for removing multivalent salt ions and small organic pollutants [2,4,5]. Hence, NF membranes might represent one of the possible solutions to the issues of water scarcity and water pollution. Currently, polymeric membranes dominate the NF market, because they can offer a good compromise between selectivity and water permeability. Indeed, commercial polyamide NF membranes can achieve a rejection of about 97% for divalent ion salts ($MgSO_4$) while maintaining a good permeability (i.e., 6.7–10.9 $L{\cdot}m^{-2}{\cdot}h^{-1}{\cdot}bar^{-1}$) [6–8]. However, polymer membranes have a low tolerance for harsh mechanical and chemical conditions. Membrane fouling requires frequent chemical cleaning, which limits their usage and lifespan [9,10]. On the other hand, inorganic NF membranes

show great potential for water desalination and detoxification, because they are easy to be cleaned and have a long service life [11,12]. Nevertheless, inorganic NF modules have low water permeability and filtering area density compared to the polymer membranes, preventing them from practical application in water filtration [13].

Surfactant-templated amorphous (i.e., non-crystalline) silica represents ideal membrane materials, due to their high pore volume and narrow pore size distribution in a range suitable for NF. Surfactants are applied as sacrificial templates to create nanopores during material consolidation and calcination, thus tailoring the porosity of the final membrane material [14]. However, amorphous silica (*a*-silica) membranes are unstable in basic solutions [15], and in the hydrothermal environment [16,17]. Hence, this limits the perm/selectivity and the field of usage of *a*-silica membranes. The stability of the *a*-silica framework can be enhanced by doping with metal oxides. Moreover, doping can alter interfacial properties, morphology, hydrophilicity, and surface charge of the membranes [13,14,18], and therefore, improve membrane performances, such as ion rejection and fouling resistance [3,18].

The stability of several metal oxide–silica compositions, such as cobalt oxide–silica, zirconium oxide–silica, and titanium oxide–silica, etc., have been studied [15,19,20]. In particular, the enhanced stability has been observed for the SiO_2-Al_2O_3 film-based membrane [21]. The Al_2O_3-SiO_2 system is often used for the fabrication of zeolite membranes, which are highly stable and can achieve high rejection for ions and micropollutants. However, their crystalline structure makes it difficult to reduce the thickness of the membrane layer to below 1 μm, thus limiting their permeability, which is usually lower than 0.1 $L{\cdot}m^{-2}{\cdot}h^{-1}{\cdot}bar^{-1}$ [22]. On the other hand, surfactant-templated *a*-silica consists of a long-range disordered network with an open structure, which can be synthesized via a simple sol-gel method and deposited as films with the thickness of a few hundred nanometers by dip-coating. Moreover, surfactant-templated silica possesses pores with size ranging from 1.5 to 10 nm, while zeolites have typically pore size of <1 nm. Therefore, surfactant-template silica membranes typically allow for much greater water fluxes than zeolite membranes [23].

When synthesizing the binary silica-alumina films for membranes by the sol-gel method, it might be a challenge to obtain homogeneous colloids, since aluminum alkoxides have a much higher hydrolysis rate than tetraethyl orthosilicate (TEOS) [24]. A two-steps synthesis approach is often applied to obtain homogeneous sol systems when two precursors have different reactivities [13,25,26]. The first step is the pre-hydrolysis of the precursor with the lowest reactivity. The second step is the addition of the precursor with the highest reactivity. Previous studies have shown that surfactant molecules can also reduce the hydrolysis and condensation rate of alkoxide precursors, as they can interact with the metal center in the forming particles and limiting the reactions rates [25,26]. Hence, the surfactant was introduced into the reaction mixture after the pre-hydrolysis of TEOS, but before adding the aluminum alkoxide. Therefore, the surfactant had a dual function: (i) To control the hydrolysis and the condensation rate of precursors during synthesis, and (ii) to control the pore structure, as sacrificial pore-forming agent during material consolidation and calcination. Indeed, precipitation of Al_2O_3 from the sol was always observed when the surfactant was added after the second step. Nevertheless, depending on the synthesis conditions and sol composition, phase separation might occur in the final membrane material when the molar ratio of the alumina reach to 10% [27–29].

In this work, the 5 mol% Al_2O_3-doped silica membranes NF membranes were fabricated by optimizing the concentration of the coating sol and the molar ratio of surfactant/oxide (S/O). The impact of these fabrication parameters on membrane selectivity and permeability was investigated by performing filtration tests with model solutions. Then, the optimized membranes were tested regarding their ability to retain ions and pollutants in a real wastewater sample.

2. Experimental

2.1. Sol-Synthesis and Membrane Fabrication

The fabrication procedure of our 5 mol% Al_2O_3-doped silica membranes is depicted in Figure 1. A two-steps approach was applied for the sol synthesis. The first step of synthesis was the hydrolysis of TEOS, which was achieved by letting to react a mixture of TEOS (98%, Sigma Aldrich, St. Louis, MO, USA), ethanol (99.9%, VWR Chemicals, Radnor, PA, USA), distilled water, and nitric acid (69%, Sigma Aldrich, St. Louis, MO), with a molar ratio of 1:4:2.5:0.04, at 60 °C for 3 h. Then, in the second step of the synthesis, CTAB (99%, Sigma Aldrich, St. Louis, MO, USA) was added to the pre-hydrolyzed TEOS solution to achieve the desired CTAB: (SiO_2 + Al_2O_3) molar ratio. After the complete dissolution of CTAB, aluminum isopropoxide (AIP) (98%, Sigma Aldrich, St. Louis, MO, USA) was directly added to the mixture to obtain a 5 mol% Al_2O_3 concentration in the final consolidated membrane material. The mixture was continuously stirred at 60 °C until all the AIP was dissolved and a transparent yellowish solution was obtained (the reaction times are summarized in Table 1).

Sols were diluted by 1:11, 1:15, and 1:20 volume ratios with ethanol and subsequently filtered with 0.2 μm syringe filter (Minisart RC, 25 mm, Sigma Aldrich, St. Louis, MO, USA) to remove dust particles and impurities before the coating. The membranes were coated on commercial α-alumina tubular support with a γ-alumina intermedia layer (250 × 10 × 7 mm (L × OD × ID), Pervatech B.V., Rijssen, The Netherlands). The membranes were fabricated by dip-coating of the alumina-doped silica sols onto the supporting substrates. Specifically, the inside of the supports was coated vertical by a lab-made device at a dipping/withdrawing rate of <2.5 cm/min. After drying at room temperature for 24 h, the membranes were calcined at 450 °C for 2 h at the heating and cooling rate of 2 °C/min.

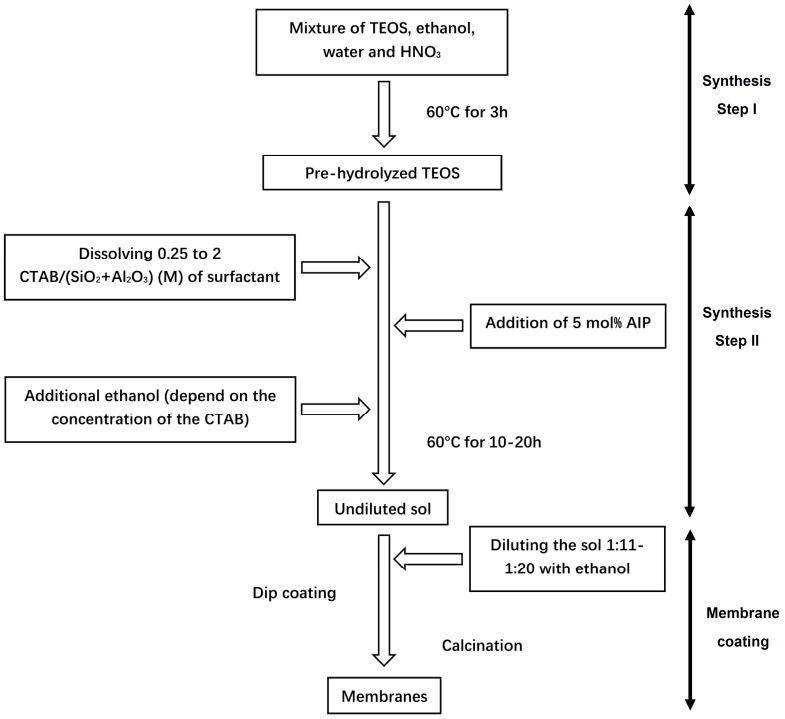

Figure 1. Synthesis process of the membranes with different cetyltrimethylammonium bromide (CTAB) concentration.

The corresponding powdered samples were obtained by filtering the rest of coating sol through a 0.2 μm syringe filter after dilution with ethanol (1:1 V/V) and dried in Petri-dishes. The membrane materials were calcined by following the same temperature ramp of the supported membranes. After the calcination, the membrane materials were crushed in a mortar and kept for further analysis.

Table 1. Fabrication parameters of the membrane samples synthesized in this work.

S/O [#]	Reaction Time (h)	TEOS:Ethanol (mol:mol)	Al_2O_3:SiO_2 (mol%)	Al_2O_3 + SiO_2 Concentration [§] ($g \cdot L^{-1}$)
Membrane samples with different sol dilutions				
0.25	15	1:4	5%	11.8
0.25	15	1:4	5%	8.7
0.25	10	1:4	5%	6.5
Membrane samples with different CTAB concentrations				
0.25	10	1:4	5%	6.5
0.5	10	1:4	5%	6.5
1	10	1:8 *	5%	6.5
2	20	1:12 *	5%	6.5
4	40	1:32 *	5%	6.5

[#] S/O = surfactant/oxide ratio = CTAB/(SiO_2 + Al_2O_3) (mol/mol); * additional ethanol was added to dissolve the CTAB; [§] Sols were diluted before coating to achieve the oxide (SiO_2 + Al_2O_3) concentration reported in this table.

2.2. Membrane Characterization

The pore structure of the membrane materials was investigated by nitrogen adsorption at liquid-nitrogen boiling point on a gas volumetric apparatus ASAP 2020 (Micromeritics, Norcross, GA, USA), after outgassing at 300 °C in the vacuum (residual pressure 10^{-2} mbar) to avoid undesired interferences of gaseous products from materials during the gas-volumetric determinations. Specific surface areas were determined using the Langmuir model. Pore volumes and pore size distributions were calculated by using the density functional theory (DFT) method to examine simultaneously both micro and mesoporosity of the samples [30]. The morphology of the membrane cross-section and surface was investigated by SEM analysis using a EVO 50 XVP microscope (Zeiss, Köln, Germany) with LaB_6 source. The samples were mounted on metallic stubs with double-sided conductive tape and ion coated with a gold layer (thickness ~25 nm) by a sputter coater (Baltec SCD 050, Pfäffikon, Switzerland) for 60 s under vacuum at a current intensity of 60 mA to avoid any charging effect.

2.3. Filtration Tests

The cross-flow setup for the filtration experiment is described in detail elsewhere [31]. Water permeability was measured under four different operating pressure ranges from 5 to 7 bar. The following reagents were dissolved in deionized water to prepare model solutions for the filtration test: NaCl (99.0%, Chemsolute, Roskilde, Denmark), $MgSO_4 \cdot 7H_2O$ (99.0%, Acros Organics, Geel, Belgium), Na_2SO_4, (99.0%, Sigma Aldrich, St. Louis, MO, USA), and caffeine (Sigma Aldrich, St. Louis, MO, USA). Salt solutions with an ionic strength of 0.01 M and a caffeine solution (10 ppm) were prepared as feed for selectivity measurements. The selectivity tests were operated at 7 bar, the salt rejection was determined by measuring the electrical conductivity of the feeding and permeate water by using a conductivity meter Seven Multi (Mettler Toledo, Columbus, OH, USA). Caffeine concentration was determined by HPLC over a Dionex ASI-100 chromatograph with a Phenomenex Luna C18 column, with diameter, length, and pore size of 4.60 mm, 250 mm, and 5 µm, respectively. The mobile phase was deionized water (buffered with 0.025 M KH_2PO_4) and acetonitrile (ACN) with a proportion ACN/buffer of 20/80, delivered at a flow rate of 1.2 $mL \cdot min^{-1}$.

In order to test the performance of membranes towards the inorganic ions and organic pollutants, we analyzed the wastewater effluent and the permeate for the presence of some ions (Cl^-, NO_3^-, SO_4^{2-}, Na^+, K^+, Mg^{2+}, Ca^{2+}) and for the presence of contaminants of emerging concern (in particular imidacloprid (IMI), ciprofloxacin (CPX), carbamazepine (CBZ), 1,2,3-benzotriazole (BZT) 5-methyl-1H-benzotriazole (MBZT). The content of total organic carbon (TOC) and total carbon (TC) was evaluated before and after the filtration step. The concentration of these target parameters was determined according to the procedures, which are described in detail in the Supplementary Materials (MS-MS conditions are reported in Table S1).

3. Results and Discussion

3.1. Impact of CTAB Concentration on Membrane Porosity

The pore structure of the membrane materials with five different CTAB concentrations (S/O = 0.25, 0.5, 1.0, 2.0, and 4.0) was determined by low-temperature N_2 adsorption. Despite the different CTAB concentrations, all the samples have similar adsorption isotherms and pore size distributions, as shown in Figure 2. Most of the adsorption occurs at a nitrogen relative pressure smaller than 0.1 (type I isotherms, according to the IUPAC classification, which is typical of microporous materials [32]). As a consequence, the pore size of the membrane materials ranges from 0.5 to 2.5 nm. This pore size distribution is consistent with the use of CTAB as the pore-forming agent. The relation between the CTAB concentration and specific surface area (SSA) of the membrane materials is plotted in Figure 3. At first, SSA increases with increasing CTAB concentration. SSA reaches a maximum at 732 $m^2 \cdot g^{-1}$ when the surfactant/oxide molar ratio (S/O = CTAB/(SiO_2 + Al_2O_3)) is 1. Any further increase of CTAB concentration results in a reduction of the specific surface area, which may be caused by the collapse of the pore structure when a high amount of surfactant is burned out during calcination.

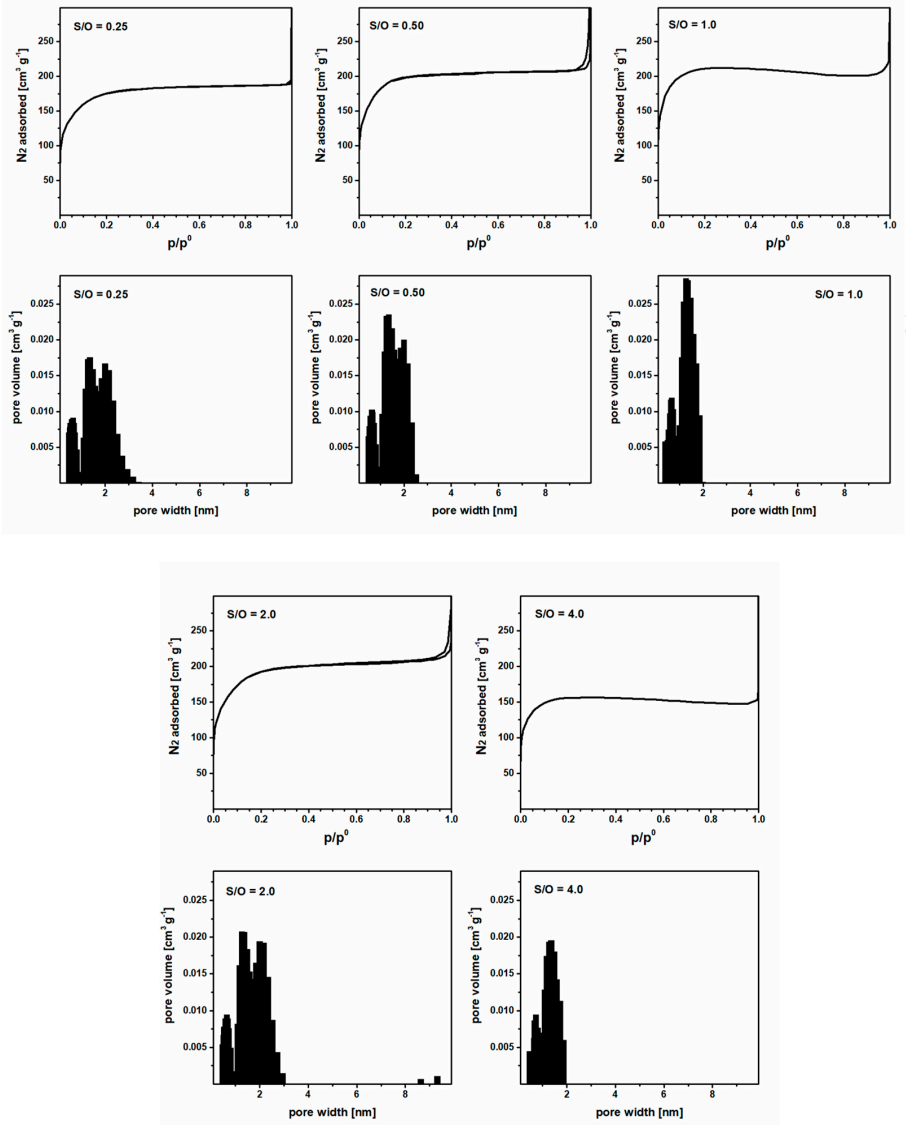

Figure 2. Adsorption isotherms and pore size distributions of the membrane materials (5 mol% Al_2O_3–doped silica) synthesized by the sol-gel method with different surfactant/oxide molar ratio (S/O) in the reaction mixture.

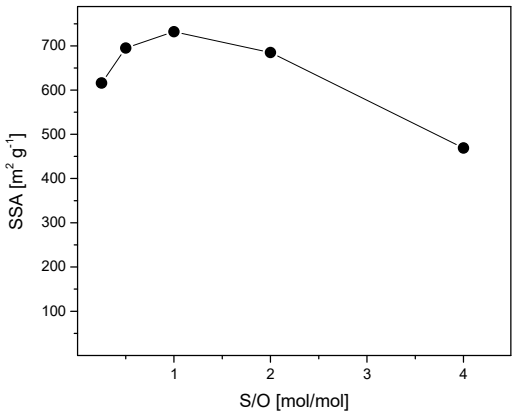

Figure 3. Specific surface area (SSA) of the membrane materials (5% Al_2O_3–doped *a*-silica) as a function of the surfactant/oxide molar ratio (S/O) in the reaction mixture.

3.2. Concentration of the Coating Sol

The membrane materials were deposited on commercial membrane tubes by dip-coating. Different dilutions were used and Table 1 summarizes the oxide (SiO_2 + Al_2O_3) concentrations of the final coating sols. Figure 4 shows the SEM image of a membrane obtained from a sol with S/O = 0.25 and oxides (SiO_2 + Al_2O_3) concentration of 11.8 g·L^{-1}. The micrograph shows a continuous membrane layer covering the multi-layered alumina support. Form the picture, the thickness of the membrane is estimated to be around about 590 nm. Therefore, we attempted to reduce the membrane thickness and increase membrane permeability by dilution of the coating sol. Two new membranes were prepared by reducing the oxide concentration in the sol from 11.8 to 8.7 and 6.5 g·L^{-1} while S/O was kept constant to 0.25.

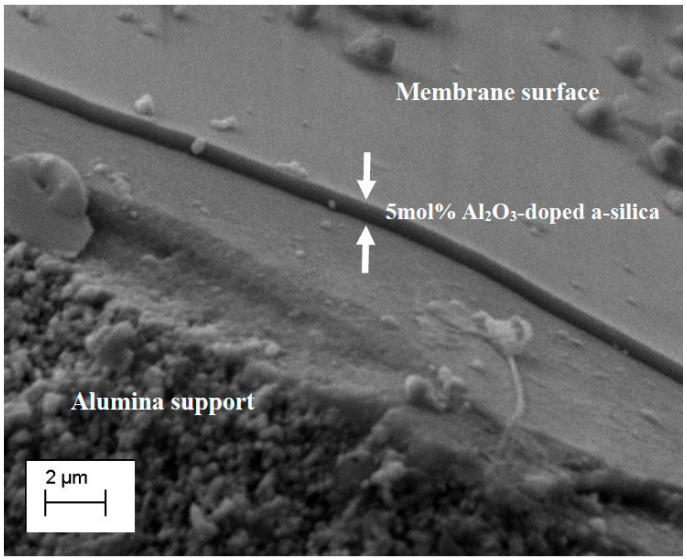

Figure 4. Cross-sectional SEM micrograph of the membrane obtained by coating a 5 mol% Al_2O_3-doped silica sol with a surfactant/oxide ration (S/O) of 0.25 and an oxide (SiO_2 + Al_2O_3) concentration of 11.8 g·L^{-1}. White arrows indicate the 5 mol% Al_2O_3-doped silica layer.

SEM images of the membrane cross-section were taken to compare the thickness of the membranes with different sol concentrations. The relation between the membrane thickness and the sol dilution is reported in Figure 5a. The thickness of the 5 mol% Al_2O_3-doped silica membrane layer decreases by reducing the oxide concentration in the coating sol: From 560 nm to 96 nm when the sol oxide concentration was reduced from 11.8 to 6.5 g·L^{-1}. Surprisingly, the difference in membrane thickness

did not reflect in a large variation of the water permeability of the three membranes, as shown in Figure 5a. Indeed, when the oxide concentration in the sol decreases from 11.8 to 6.5 g·L^{-1} the average water permeability has only changed slightly: From 0.64 to 0.68 L·m^{-2}·h^{-1}·bar^{-1}, that is, the change of the water permeability is negligible when compared to the decrease of the membrane thickness. This may be caused by the infiltration of the sol particles into the porous intermedia layer during the coating, resulting in a much thicker 5 mol% Al_2O_3-doped silica layer than that observed in the SEM images.

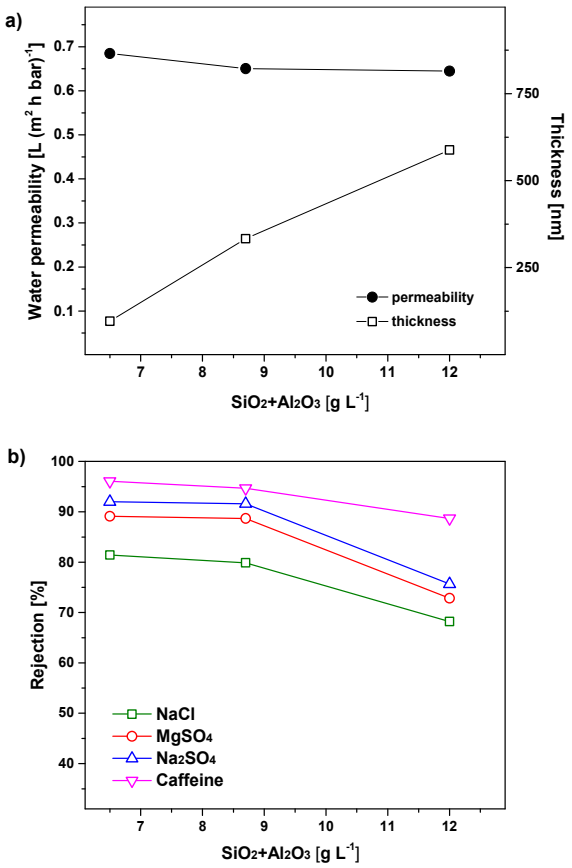

Figure 5. (**a**) Water permeability and thickness of 5 mol% Al_2O_3-doped silica membranes as a function of the SiO_2 + Al_2O_3 concentration in the coating sol. (**b**) Membrane rejection for inorganic salts and caffeine as a function of the SiO_2 + Al_2O_3 concentration in the coating sol.

The rejection of the membranes to inorganic salts and caffeine (as a model micropollutant) is shown in Figure 5b. Rejection values of the three membranes are consistent with NF membrane layers. Indeed, the three membranes show good rejection for salts of monovalent ions (68–81% for NaCl) and high rejection towards salts of divalent ions (73–89% for $MgSO_4$ and 76–92% for Na_2SO_4), and even higher rejection for caffeine (89–96%). In general, the membranes ionic rejection depends on the size and the charge of the hydrated ions. For non-charged species such as caffeine, the rejection mechanism is mainly attributed to the steric exclusion. These results indicate that the three membranes consist of NF layers with a really small or negligible defect density. Counterintuitively, the rejection of ions and caffeine have an increasing trend with the decrease of the membrane thickness. For instance, the rejection for NaCl is increased from 68.2% to 81.4% when the oxide concentration in the coating sol decreases from 11.8 to 6.5 g·L^{-1}. A possible explanation could be that thicker films have a higher chance of defect formation during drying [33], as all the membranes have the same composition and have similar pore structure. This result shows that dilution of the coating sol could improve the selectivity

without sacrificing the membrane permeability. Therefore, we decided to prepare the membranes by using the coating sol with a rather low oxides concentration (6.5 g·L^{-1}) in the rest of the study.

3.3. Optimization of the S/O Ratio

Figure 6a illustrates the relationship between the water permeability of the membranes and the surfactant/oxides ratio (S/O = 0.25, 0.5, 1.0, 2.0, and 4.0). A dramatic increase of the water flux is observed when S/O is increased from 0.25 to 2.0. In this S/O range, the permeability increases rapidly from 0.68 to 2.3 L·m^{-2}·h^{-1}·bar^{-1}. However, a further increase of the surfactant concentration (S/O from 2.0 to 4.0) results in a reduced permeability (1.9 L·m^{-2}·h^{-1}·bar^{-1}). The initial rise of the permeability for increased S/O ratios may arise from increased pore interconnectivity. However, when the concentration of surfactant is fourfold higher than the oxide materials, pore walls might collapse during calcination.

The rejections of these membranes for inorganic salts and caffeine are depicted in Figure 6b. The rejection for NaCl decreases from 81% to 59% when the surfactant concentration (S/O) increases from 0.25 to 4.0. On the contrary, the rejections for $MgSO_4$, Na_2SO_4, and caffeine reach a maximum (95%, 98%, and 98%, respectively) for the membrane prepared from a sol with S/O of 0.50. The increase of membrane rejection with increasing S/O from 0.25 to 0.50 could be due to the fact that surfactant molecules contribute to reduce capillary stresses during the drying of the membrane films, thereby reducing the probability of defect formation [34]. However, when further increasing the surfactant concentrations in the coating sols, the rejection decreases for the tested three types of ions and caffeine. This trend might be ascribed to the formation of some defects in the membrane films due to the high relative mass loss and gas product development during the calcination step.

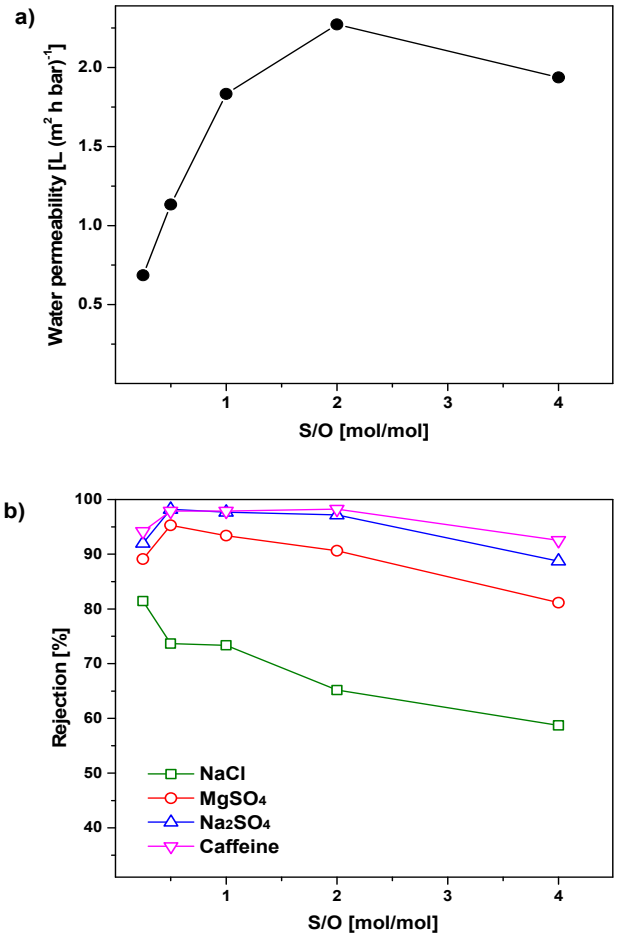

Figure 6. (**a**) Water permeability and (**b**) rejection to salt and caffeine of the 5 mol% Al_2O_3-doped silica membranes as a function of the surfactant/oxides (S/O) ratio in the coating sols.

As expected, the effect of S/O on the membrane rejection is not as strong as what we observed for the membrane permeability. Indeed, as shown in Figures 2 and 3, the surfactant concentration has little effect on the pore size distribution, and thus on the membrane selectivity. However, it has a great impact on the specific surface area of the material, and therefore, on the membrane permeability. In detail, the membrane with S/O = 2.0 has the highest permeability, while the membrane with S/O = 0.5 exhibits the best selectivity. These two membranes present selectivity close to those of zeolite membranes [35], but water permeability at least one order of magnitude higher. Therefore, they were selected as optimized membranes for filtering the effluent of the wastewater treatment plant.

3.4. Filtration of A Wastewater Treatment Plant Effluent

Figure 7 shows the wastewater sample before filtration and the permeates collected after the wastewater was filtered through the membranes with S/O = 0.50 and 2.0. The effluent water presents a slightly yellowish color and some turbidity. On the contrary, the permeate water from both membranes is colorless and clear. This picture shows that the membranes have the ability to remove colloids and colored compounds (as humic substances) in the wastewater. As a result of the accumulation of these substances on the membrane surface, the permeability of the two membranes after 2 h of filtration was reduced to 0.16 and 0.32 $L \cdot m^{-2} \cdot h^{-1} \cdot bar^{-1}$ for the membranes with S/O = 0.50 and S/O = 2.0, respectively.

Figure 7. Samples of wastewater treatment plant effluent (**middle**), permeate of the membrane with surfactant/oxide ratio (S/O) = 0.5 (**left**), and permeate of the membrane with S/O = 2.0 (**right**).

Table 2 lists the concentration of inorganic ions and selected micropollutants in the wastewater sample and in the permeates of the two membranes. In general, the two membranes have a similar selectivity. The specific selectivity for ions and total organic carbon (TOC) of the two membranes is plotted in Figure 8. TOC is also reduced by about 85%. Both membranes present a high rejection of organic pollutants. The concentration of imidacloprid (IMI) and 1,2,3-benzotriazole (BZT) were become undetectable after the filtration, while the concentrations of carbamazepine (CBZ) and 5-methyl-1H-benzotriazole (MBZT) were reduced by more than 95%. The two membranes show a high ability to remove inorganic ions. The highest rejection was observed for divalent ions as Mg^{2+} and Ca^{2+}, SO_4^{2-}, and carbonates, which are likely the most representative species of inorganic carbon (IC) in these samples. In general, the rejection of monovalent ions is lower than the rejection of divalent ions, which is not necessarily a disadvantage, as many applications do not require to remove these ions and the permeation can result in a reduced trans-membrane osmotic pressure.

Table 2. Concentration of ions and micropollutants in the wastewater sample as received and after the filtration over the membranes prepared from sols with S/O = 0.50 (Permeate 0.5) and S/O = 2.0. (Permeate 2). The data for imidacloprid (IMI), carbamazepine (CBZ), 1,2,3-benzotriazole (BZT), and 5-methyl-1H-benzotriazole (MBZT) take into account a preconcentration factor of 200 on solid phase extraction (SPE).

	Wastewater Treatment Plan Effluent (ppm)	Permeate S/O = 0.5 (ppm)	Permeate S/O = 2 (ppm)
Cl^-	92.1	67.5	56.5
NO_3^-	20.2	12.0	14.4
SO_4^{2-}	40.9	15.7	13.0
Na^+	103	16.0	14.4
K^+	27.2	2.95	3.53
Mg^{2+}	7.1	0.11	0.11
Ca^{2+}	92	0.77	0.82
TOC (total organic carbon)	8.51	1.26	1.31
TC (total carbon)	69.0	6.59	6.97
IMI	3×10^{-5}	-	-
CBZ	8.4×10^{-4}	2.3×10^{-5}	3.4×10^{-5}
BZT	1.7×10^{-4}	-	-
MBZT	1.7×10^{-3}	1.5×10^{-5}	2.0×10^{-5}

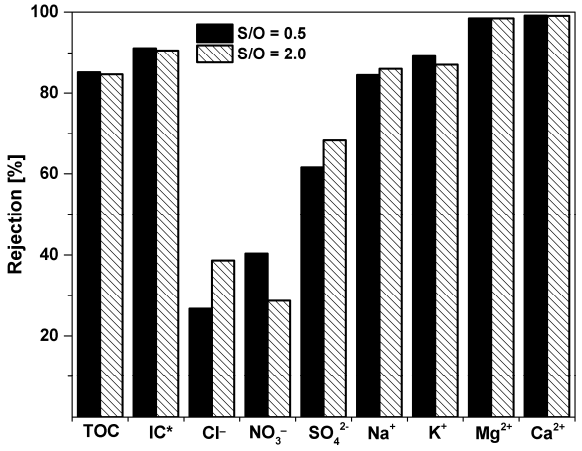

Figure 8. The rejection of the ions, micropollutants, and organic carbon contained in wastewater for the optimized membranes. IC* (inorganic carbon) = TC − TOC.

4. Conclusions

In this study, we presented a simple method for the fabrication of the 5 mol% Al_2O_3-doped silica NF membranes. A surfactant, namely CTAB, was added during the sol-gel synthesis of the membrane material to reduce the hydrolysis and condensation rate of the aluminum alkoxide precursor, thus obtaining a homogeneous amorphous oxide network, and to act as pore-forming agent (template) during the calcination step. NF membranes were obtained by a single coating by dipping commercial alumina support in the Al_2O_3-doped silica sols. This approach may provide good bases for further development and fabrication of other metal oxide-doped silica membranes.

We were able to reduce the thickness of the membranes down to 96 nm. However, membrane thickness, as observed at SEM, had a slight impact on the water permeability of our membranes, probably due to the penetration of the polymeric silica sol into the pores of the membrane support. The increase of the CTAB concentration in the coating sol has little impact on the pore size of the consolidated material, and therefore on the selectivity of the membrane layer. On the contrary, membrane permeability was greatly enhanced by the optimization of the surfactant concentration. During the filtration tests, the highest water permeability (2.3 $L \cdot m^{-2} \cdot h^{-1} \cdot bar^{-1}$) was achieved by the membranes prepared from the sol with S/O = 2.0, while the highest rejection values were obtained for the membrane coated from the sol with S/O = 0.50. All the membranes presented in this work have rather high rejection towards caffeine.

Filtration of an effluent from a wastewater treatment plant indicates that the optimized membranes are capable of removing water-hardness ions such as Mg^{2+} and Ca^{2+}, micropollutants and colored organic matter from real water systems. Thus, the membranes developed in the present study have high potential to be applied in tertiary treatments of wastewater or in the treatment of brackish water.

Supplementary Materials: The following are available online at http://www.mdpi.com/2079-4991/9/10/1368/s1, Table S1: MS-MS conditions of organic pollutants detected in the sample (DP-declustering potential, EP extensions potential, CE collision energy).

Author Contributions: Conceptualization, X.M., V.B. and Y.Y.; methodology, X.M., D.F., G.M. and P.C.; formal analysis, X.M., K.J. and D.F.; investigation X.M. and K.J.; resources, V.B. Y.Y. and P.C.; writing original draft, X.M.; writing—review and editing, V.B. Y.Y. and P.C.; supervision, V.B. Y.Y. and P.C.; funding acquisition, V.B. and P.C.

Funding: This work is part of a project that has received funding from the European Union's Horizon 2020 research and innovation programme under the Marie Skłodowska-Curie Grant Agreement No 765860 (AQUAlity). The authors gratefully acknowledge also financial support from the European Union project "Project Ô" (H2020-CIRC-2017TwoStage, Grant Agreement n. 776816). Moreover, the author wish to thanks Marta Anna Nierychlo for her support with the wastewater sample.

Acknowledgments: The authors wish to thank the European Commission for funding.

Conflicts of Interest: The authors declare no conflict of interest.

References

1. Shrivastava, A.; Rosenberg, S.; Peery, M. Energy efficiency breakdown of reverse osmosis and its implications on future innovation roadmap for desalination. *Desalination* **2015**, *368*, 181–192. [CrossRef]
2. Elimelech, M.; Phillip, W. The future of seawater desalination: Energy, technology, and the environment. *Science* **2011**, *333*, 712–717. [CrossRef] [PubMed]
3. Darling, S.B. Perspective: Interfacial materials at the interface of energy and water. *J. Appl. Phys.* **2018**, *124*, 030901. [CrossRef]
4. Elma, M.; Yacou, C.; Wang, D.K.; Smart, S.; Diniz da Costa, J.C. Microporous silica based membranes for desalination. *Water* **2012**, *4*, 629–649. [CrossRef]
5. Shannon, M.A.; Bohn, P.W.; Elimelech, M.; Georgiadis, J.G.; Marĩas, B.J.; Mayes, A.M. Science and technology for water purification in the coming decades. *Nature* **2008**, *452*, 301–310. [CrossRef] [PubMed]
6. Greenlee, L.F.; Lawler, D.F.; Freeman, B.D.; Marrot, B.; Moulin, P. Reverse osmosis desalination: Water sources, technology, and today's challenges. *Water Res.* **2009**, *43*, 2317–2348. [CrossRef] [PubMed]
7. *Form No. 609-00519-1206, FILMTEC NF270 Nanofiltration Elements for Commercial Systems*; The Dow Chemical Company: Midlan, MI, USA; Available online: https://www.dupont.com/products/filmtecnf2704040.html (accessed on 22 September 2019).
8. *Form No. 609-00379-0503, FILMTEC Membranes, Nanofiltration Produces Sparkling Clean Water for Swedish Resort Community*; The Dow Chemical Company: Midlan, MI, USA; Available online: https://www.dupont.com/content/dam/dupont/amer/us/en/water-solutions/general/documents/609-00379.pdf (accessed on 22 September 2019).
9. Lee, K.P.; Arnot, T.C.; Mattia, D. A review of reverse osmosis membrane materials for desalination-Development to date and future potential. *J. Memb. Sci.* **2011**, *370*, 1–22. [CrossRef]
10. Farahbakhsh, K.; Svrcek, C.; Guest, R.K.; Smith, D.W. A review of the impact of chemical pretreatment on low-pressure water treatment membranes. *J. Environ. Eng. Sci.* **2004**, *4*, 237–253. [CrossRef]
11. Tsuru, T. Inorganic porous membranes for liquid phase separation. *Sep. Purif. Methods.* **2001**, *30*, 191–220. [CrossRef]
12. Lin, Y.S. Microporous and dense inorganic membranes: Current status and prospective. *Sep. Purif. Technol.* **2001**, *25*, 39–55. [CrossRef]
13. Farsi, A.; Malvache, C.; De Bartolis, O.; Magnacca, G.; Kristensen, P.K.; Christensen, M.L.; Boffa, V. Design and fabrication of silica-based nanofiltration membranes for water desalination and detoxification. *Microporous Mesoporous Mater.* **2017**, *237*, 117–126. [CrossRef]
14. Wijaya, S.; Duke, M.C.; Diniz da Costa, J.C. Carbonised template silica membranes for desalination. *Desalination* **2009**, *236*, 291–298. [CrossRef]

15. Boffa, V.; Parmeggiani, L.; Nielsen, A.H.; Magnacca, G. Hydrophilicity and surface heterogeneity of TiO_2-doped silica materials for membrane applications. *Microporous Mesoporous Mater.* **2016**, *221*, 81–90. [CrossRef]
16. Fotou, G.P.; Lin, Y.S.; Pratsinis, S.E. Hydrothermal stability of pure and modified microporous silica membranes. *J. Mater. Sci.* **1995**, *30*, 2803–2808. [CrossRef]
17. Boffa, V.; Blank, D.H.A.; ten Elshof, J.E. Hydrothermal stability of microporous silica and niobia-silica membranes. *J. Memb. Sci.* **2008**, *319*, 256–263. [CrossRef]
18. Waldman, R.Z.; Choudhury, D.; Mandia, D.J.; Elam, J.W.; Nealey, P.F.; Martinson, A.B.F.; Darling, S.B. Sequential Infiltration Synthesis of Al_2O_3 in Polyethersulfone Membranes. *JOM* **2019**, *71*, 212–223. [CrossRef]
19. Lin, C.X.C.; Ding, L.P.; Smart, S.; Diniz da Costa, J.C. Cobalt oxide silica membranes for desalination. *J. Colloid Interface Sci.* **2012**, *368*, 70–76. [CrossRef] [PubMed]
20. Boffa, V.; Magnacca, G.; Jørgensen, L.B.; Wehner, A.; Dörnhöfer, A.; Yue, Y. Toward the effective design of steam-stable silica-based membranes. *Microporous Mesoporous Mater.* **2013**, *179*, 242–249. [CrossRef]
21. Gu, Y.; Hacarlioglu, P.; Oyama, S.T. Hydrothermally stable silica–alumina composite membranes for hydrogen separation. *J. Membr. Sci.* **2008**, *310*, 28–37. [CrossRef]
22. Li, L.; Liu, N.; McPherson, B.; Lee, R. Enhanced water permeation of reverse osmosis through MFI-type zeolite membranes with high aluminum contents. *Ind. Eng. Chem. Res.* **2007**, *46*, 1584–1589. [CrossRef]
23. Goh, P.S.; Ismail, A.F. A review on inorganic membranes for desalination and wastewater treatment. *Desalination* **2017**, *434*, 60–80. [CrossRef]
24. Wen, J.; Wilkes, G.L. Organic/inorganic hybrid network materials by the sol-gel approach. *Chem. Mater.* **1996**, *8*, 1667–1681. [CrossRef]
25. De Lange, R.S.A.; Kumar, K.N.P.; Hekkink, J.H.A.; van de Velde, G.M.H.; Keizer, K.; Burggraaf, A.J.; Dokter, W.H.; van Garderen, H.F.; Beelen, T.P.M. Microporous SiO_2 and SiO_2/MO_x (M=Ti, Zr, Al) for ceramic membrane applications: A microstructural study of the sol-stage and the consolidated state. *J. Sol.-Gel Sci. Technol.* **1994**, *2*, 489–495. [CrossRef]
26. Boffa, V.; Castricum, H.L.; Garcia, R.; Schmuhl, R.; Petukhov, A.V.; Blank, D.H.A.; Ten Elshof, J.E. Structure and growth of polymeric niobia-silica mixed-oxide sols for microporous molecular sieving membranes: A saxs study. *Chem. Mater.* **2009**, *21*, 1822–1828. [CrossRef]
27. Samiey, B.; Cheng, C.H.; Wu, J. Effects of surfactants on the rate of chemical reactions. *J. Chem.* **2014**, *2014*, 564–567. [CrossRef]
28. Mege, S.; Vereist, M.; Lecante, P.; Perez, E.; Ansart, F.; Savariault, J.M. Surfactant effects in vanadium alkoxide derived gels. *J. Non. Cryst. Solids* **1998**, *238*, 37–44. [CrossRef]
29. Liu, S.; Boffa, V.; Yang, D.; Fan, Z.; Meng, F.; Yue, Y. Clarifying the gel-to-glass transformation in Al_2O_3-SiO_2 systems. *J. Non. Cryst. Solids* **2018**, *492*, 77–83. [CrossRef]
30. Olivier, J.P. Modeling physical adsorption on porous and nonporous solids using density functional theory. *J. Porous Mater.* **1995**, *2*, 9–17. [CrossRef]
31. Farsi, A.; Boffa, V.; Qureshi, H.F.; Nijmeijer, A.; Winnubst, L.; Christensen, M.L. Modeling water flux and salt rejection of mesoporous γ-alumina and microporous organosilica membranes. *J. Memb. Sci.* **2014**, *470*, 307–315. [CrossRef]
32. Sing, K.S.W.; Everett, D.H.; Haul, R.A.W.; Moscou, L.; Pierotti, R.S.; Rouquerol, J. Siemieniewska, Reporting physisorption data for gas/solid systems with special reference to the determination of surface area and porosity. *Pure Appl. Chem.* **1985**, *57*, 603–619. [CrossRef]
33. Strawbridge, I.; James, P.F. The factors affecting the thickness of sol-gel derived silica coatings prepared by dipping. *J. Non. Cryst. Solids* **1986**, *86*, 381–393. [CrossRef]
34. Brinker, C.J.; Scherer, G.W. *Sol–Gel Science: The Physics and Chemistry of Sol–Gel Processing*, 2nd ed.; Academic Press: San Diego, CA, USA, 1990; pp. 788–797.
35. Zhu, B.; Myat, D.T.; Shin, J.; Na, Y.; Moon, I.; Connor, G.; Maeda, S.; Morris, G.; Gray, S.; Duke, M. Application of robust MFI-type zeolite membrane for desalination of saline wastewater. *J. Memb. Sci.* **2015**, *475*, 167–174. [CrossRef]

Paper II

nanomaterials

MDPI

Article

Desalination of Groundwater from a Well in Puglia Region (Italy) by Al_2O_3-Doped Silica and Polymeric Nanofiltration Membranes

Xianzheng Ma, Cejna Anna Quist-Jensen, Aamer Ali and Vittorio Boffa *

Center for Membrane Technology, Department of Chemistry and Bioscience, Aalborg University, Fredrik Bajers vej 7H, 9220 Aalborg, Denmark; xm@bio.aau.dk (X.M.); cejna@bio.aau.dk (C.A.Q.-J.); aa@bio.aau.dk (A.A.)

* Correspondence: vb@bio.aau.dk; Tel.: +45-99-403579

Received: 30 June 2020; Accepted: 27 August 2020; Published: 1 September 2020

Abstract: Some of the groundwater aquifers in the Puglia Region, Italy, suffer from high salinity and potential micropollutant contamination due to seawater infiltration and chemical discharge. The objective of this study is twofold: to evaluate the performance of the recently reported alumina-doped silica nanofiltration membranes for water potabilization, and to provide a possible solution to improve the groundwater quality in the Puglia Region while maintaining a low energy-footprint. Two lab-made alumina-doped silica membranes with different pore structures, namely S/O = 0.5 and S/O = 2, were tested with real groundwater samples and their performances were compared with those of a commercial polymeric membrane (Dow NF90). Moreover, groundwater samples were sparked with acetamiprid, imidacloprid, and thiacloprid to test the membrane performance in the presence of potential contamination by pesticides. At a trans-membrane pressure of 5 bar, NF90 could reduce the groundwater conductivity from 4.6 to around 1.3 $mS{\cdot}cm^{-1}$ and reject 56–85% of the model pesticides, with a permeate flux of 14.2 $L{\cdot}m^{-2}{\cdot}h^{-1}$. The two inorganic membranes S/O = 2 and S/O = 0.5 reduced the permeate conductivity to 3.8 and 2.4 $mS{\cdot}cm^{-1}$, respectively. The specific energy consumption for all three membranes was below 0.2 $kWh{\cdot}m^{-3}$ which indicates that the potabilization of this groundwater by nanofiltration is commercially feasible.

Keywords: membrane materials; surfactant templated-silica; drinking water; pesticides

1. Introduction

The shortage of clean water is one of the most pressing issues for humanity. Groundwater has always been an extremely valuable water resource, nowadays it contributes to around 30% of the total freshwater supply in the world [1]. However, minerals or organic pollutants might infiltrate aquifers, thus compromising the quality of groundwater. Indeed, a large amount of clean water supply in Europe comes from karst aquifers, which can be contaminated by natural or anthropogenic processes [2]. Over the years, there have been two emerging challenges for the groundwater in the Puglia Region, Italy. On the one hand, some of the aquifers have high salinity, due to the infiltration of seawater, which makes the groundwater unsuitable for human consumption [3]. On the other hand, the groundwater in the Puglia Region could be subjected to potential micropollutants contamination due to the excessive discharge of pesticides and pharmaceuticals [4]. Therefore, desalination and detoxification of the groundwater are vital for local water supplies.

Pressure-driven membrane processes such as reverse osmosis (RO) or nanofiltration (NF) can be applied to reduce the salinity. NF and RO membranes are commercially available and have proven to be effective for partial or full desalination treatments [3–6]. In RO membranes, the active layer consists of a dense polymer, through which water transport occurs via a solution-diffusion mechanism.

In reason of their dense structure, these membranes can reach rejection for monovalent ions higher than 99% [7,8] but the RO membranes require high pressure for the operation (generally, about 15–30 bar for brackish water and 55–70 bar for seawater [9]), which implies high investment costs and high energy consumption during operation. On the contrary, the active layer of NF membranes is porous. In general, the pore size if NF membranes in the range 0.5–2 nm (around 0.5–2 kDa for the molecular weight cut-off) [10]. Therefore, NF membranes allow for higher flux compared to RO membranes. Rejection in NF membranes depends on three mechanisms: the steric exclusion of the nano-sized pores, the Donnan exclusion due to the ionization of the surface functional group, and the dielectric exclusion caused by the energy barrier when ions move from the bulk solution to the confined pores [11,12]. NF membranes can only partially reject monovalent ions, but they operate at a much lower pressure than RO systems and show high retention for the divalent ions, heavy metal ions, and organic pollutants. In reason of these features, NF membranes are more economically favorable than RO for those applications, which complete desalination is not required [13]. To date, most of the NF systems rely on polymeric membranes. However, the lifespan of the polymeric membranes might be compromised by mechanical damage and repetitive chemically cleaning [7,14]. In recent years, an increasing interest has emerged towards inorganic membranes since they are, in principle, more robust and durable than their polymeric counterpart [15–17]. Yet, the cost for the inorganic membranes could be much higher compare to the polymer membrane, but the high manufacturing cost could be compensated by its long lifespan [18]. Inorganic membranes such as silica membranes have shown great potential for filtration applications. Yet, pure silica membranes suffer from hydrothermal instability, meaning the membrane selectivity and permeability would deteriorating rapidly during filtration. Studies have shown the doping of the metal oxides, including alumina, could stabilize the silica membrane [19–21]. In a previous study, we reported new silica membranes doped with 5 mol% alumina, whose permeability and selectivity can be tuned by the concentration of a surfactant that acts as a pore-forming agent in the synthesis mixture [22]. Optimization of such membranes allowed to achieve water permeability higher than 2 $L \cdot (m^2 \cdot h \cdot bar)^{-1}$, rejection of around 95% for Mg^{2+} when tested with a model solution of $MgSO_4$ (ionic strength = 0.01 M) and almost complete rejection for 10 ppm of caffeine [22]. Therefore, Al_2O_3-doped silica membranes have shown potential for water purification and detoxication, but their filtration performance in a real-life application has not been investigated yet.

In this context, the objective of this study is twofold. Firstly, the study aims to test the performances of the new Al_2O_3-doped silica membranes in comparison with a state-of-the-art commercial polymeric NF reference in a relevant case-study, namely the desalination and detoxification of the groundwater. Among the commercially available polymeric membranes, the NF series from Dow Filmtec has been widely studied [10–12]. NF90, in particular, shows a high rejection of salt ions, e.g., about 94–99% for Mg^{2+} [23–25]. Thus, here we selected this membrane as a commercial reference. Al_2O_3-doped silica membranes and NF90 were compared for their filtration performances and their specific energy consumption. Secondly, this study wishes to provide a possible desalination technology for a well owned by Acquedotto Pugliese S.P.A. (Puglia Region, Italy). The well is located near the river Galeso, at less than 3 km from the city of Taranto. This geographical area is characterized by water stress, due to a combination of moderate rainfall supply (<500 mm/year), high density of population (~200,000 inhabitants over an area of 250 km^2), and an industrial district that includes the largest steel factory in Italy. The groundwater in this specific site has a pH of 7.5, and the concentration of pathogens or heavy metals are below the limits to be harmful for humans. However, the conductivity of the water is at 4.6 $mS \cdot cm^{-1}$, which needs to be reduced to 2.5 $mS \cdot cm^{-1}$ in order to be suitable for human consumption according to the Italian authorities [26]. The contamination of water resources by organic micropollutants has been reported in the region. Therefore, NF membranes performances were also tested with water samples spiked with model pollutants.

2. Materials and Methods

2.1. Fabrication and Characterization of Al_2O_3-Doped Silica Membranes

In this study, two 5 mol% Al_2O_3-doped silica membranes with different pore structure were fabricated via the sol-gel method, the detailed synthesized procedure was described in the previous study [22]. In brief, a two-steps sol-gel synthesis was applied. At first, tetraethyl orthosilicate (TEOS, 98%, Sigma Aldrich, St. Louis, MO, USA), ethanol (99.9%, VWR Chemicals, Radnor, PA, USA), distilled water, and nitric acid (69%, Sigma Aldrich, St. Louis, MO) were mixed with a molar ratio of 1:4:2.5:0.04. The mixture was reacted at 60 °C for 3 h to obtain a per-hydrolyzed TEOS solution. Then, cetyltrimethylammonium bromide (CTAB, 99%, Sigma Aldrich, St. Louis, MO, USA) was dissolved into the per-hydrolyzed TEOS solution to achieve CTAB:(SiO_2 + Al_2O_3) molar ratios of 0.5 and 2, thus obtaining two membranes with different porosity. In the second step, aluminum isopropoxide (AIP, 98%, Sigma Aldrich, St. Louis, MO, USA) was added into the mixture, to achieve 5 mol% of alumina doping. After the AIP fully dissolved, the sol was dip-coated on to a commercial (Pervatech B.V. Rijssen, The Netherlands) α-alumina tubular support (250 × 7 mm) with a γ-alumina intermedia layer (Figure 1a). The membranes were then calcinated at 450 °C for 2 h with heating/cooling rates of about 2 °C/min. The two membranes were labeled as S/O = 2 and S/O = 0.5 according to their CTAB:(SiO_2 + Al_2O_3) molar ratios. We learned from the previous study that, in the range of CTAB:(SiO_2 + Al_2O_3) = 0.5 to 4, the S/O = 2 silica-alumina membrane has the optimum permeability, while the S/O = 0.5 exhibit the optimum selectivity [22]. Membrane cross-section was observed over a scanning electron microscope (SEM) EVO 50 XVP microscope (Zeiss, Köln, Germany). The samples were coated with a gold layer (thickness ~25 nm) by a sputter coater (Baltec SCD 050, Pfäffikon, Switzerland) to avoid any charging effect.

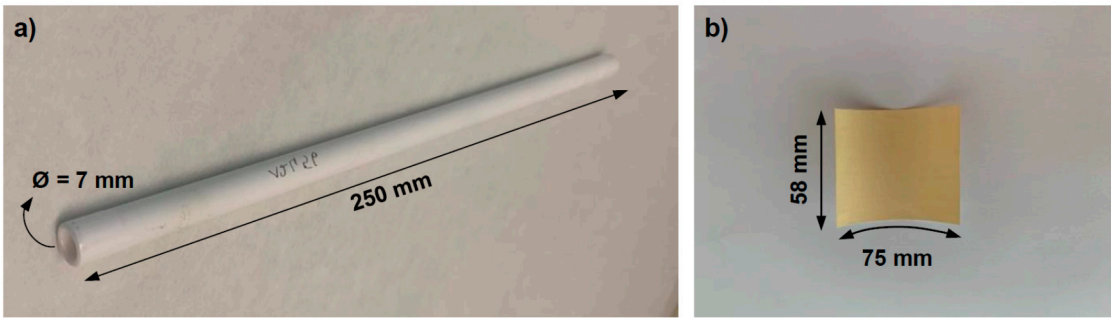

Figure 1. (**a**) Ceramic tube used as support for the Al_2O_3-doped silica nanofiltration (NF) membranes; (**b**) flat-sheet sample of the polymeric NF90 (FilmTec™) used in this study.

2.2. Filtration Experiments

Filtration experiments were conducted on S/O = 2, S/O = 0.5, and on the reference NF90 in Figure 1b (FilmTec™ membranes, Dow Chem., filtration area 75 × 58 mm). The three membranes were placed in different housings according to their geometries and tested in a cross-flow nanofiltration apparatus, which is described elsewhere [13]. In brief, the setup consists of an NF module connected with a high-pressure pump which circulates the feed into the system. Two pressure transmitters (Danfoss, MBS 4010, Nordborg Denmark) are present at the module inlet and outlet to measure the corresponding pressures. The permeate is collected into a container placed on a balance to measure its weight. The apparatus was operated at a transmembrane pressure difference of 5.0 bar, with a pumped water flux of around 4×10^{-6} m^3 s^{-1}. The membrane permeability was measured by a balance placed below the permeate tank. In each filtration test, the apparatus was fed with 2.0 L of groundwater collected from a well, which is the property of Acquedotto Pugliese S.P.A. (Puglia, Italy). This water sample will be hereinafter referred to simply as "the groundwater". The membranes were flushed bydemineralized water for 2 h before each filtration experiment. To test the ability of

the membrane to retain potential organic contaminants, groundwater samples were sparked with 10 ppm of three model pesticides, namely acetamiprid (ACE, 98%, Sigma Aldrich St. Louis, MO, USA), imidacloprid (IMI, 98%, Sigma Aldrich, St. Louis, MO, USA), and thiacloprid (THI, 98%, Sigma Aldrich, St. Louis, MO, USA).

The specific energy consumption (SEC, kWh·m^{-3}), i.e., the energy required to produce each m^3 of freshwater, was estimated by applying Equation (1) to the filtration parameters.

$$SEC = 2.778 \cdot 10^{-7} \frac{\Delta P \cdot Q_f}{Q_p} \quad (1)$$

where ΔP (here expressed in N m^{-2}) is the pressure drop of the feed after passing the membrane module, 2.778×10^{-7} is the conversion factor from joule to kilowatt-hour and Q_f and Q_p are volumetric flow rates of feed and permeate streams, respectively. Q_f for all the tested membranes was the same and was equal to 3.83×10^{-6} m^3/s.

2.3. Characterization of the Water Sample

The permeate conductivity was measured with a MeterLab (CDM210). The measurements of the permeate mass and conductivity were automatically registered via a MatLab 9.7 (MathWorks, Natick, MA, USA). The concentration of relevant cations was measured by inductively coupled plasma spectroscopy (ICP) (PerkinElmer® Optima 8000 Optical Emission Spectrometer, Waltham, MA, USA) after calibration with standards from PlasmaCAL Q.C. No 4 (SCP Science, Clark, QC, Canada). The concentration of organic pollutants was investigated over a high-performance liquid chromatography (HPLC) apparatus equipped with a Dionex ASI-100 (Phenomenex, Torrance, CA, USA) and a Luna 5 U C18 column (Phenomenex, Torrance, CA, USA). The mobile phase consisted of a water/acetonitrile mixture with ratios of 60/40, 70/30, and 60/40 for acetamiprid, imidacloprid, thiacloprid respectively. The elution rate was set at 1 mL min^{-1}. The rejection of the ions and micropollutants was defined according to Equation (2). To evaluate the sodium hazard of the permeate water for irrigation purposes, sodium adsorption ratio (SAR) was applied as Equation (3), where the concentration of the Na^+, Ca^{2+}, Mg^{2+} were expressed as mEq^{-1}.

$$Rejection(\%) = \left(1 - \frac{C_{permeate}}{C_{Feed}}\right) \cdot 100 \quad (2)$$

$$SAR = \frac{Na^+}{\sqrt{\frac{Ca^{2+} + Mg^{2+}}{2}}} \quad (3)$$

3. Results

3.1. Membrane Structure

The two Al_2O_3-doped silica membranes reported in this study, namely S/O = 0.5 and S/O = 2, were coated from sols with the same Al_2O_3 + SiO_2 loading (6.5 g L^{-1}), but a different surfactant/oxide (S/O) molar ratio. From the previous study we found that among the Al_2O_3 doped silica membranes with different surfactant concentrations, the S/O = 0.5 has the highest selectivity while the S/O = 2 has the highest permeability [22]. It is not surprising that their final consolidated NF layers have similar structures, but different porosity. Indeed, the Al_2O_3-doped silica membranes have an asymmetric architecture (Figure 2a,b), which resemble that of the commercial polymeric NF90 (Figure 2c). The thickness of the Al_2O_3-doped silica selective layers is about 0.8 µm, but due to the different concentrations of the surfactant, the pores of S/O = 2 are more interconnected than S/O = 0.5. Nevertheless, according to the low-temperature N_2 adsorption experiment from the former study, the pore size of the two membranes is similar at around 1−2 nm, and the specific surface area was

at 695 and 685 m^2/g for the S/O = 0.5 and S/O = 0.5, respectively [22]. On the other hand, NF90 has a smaller pore size (around 0.55 nm) and the thickness of the active layer at around 0.29 µm.

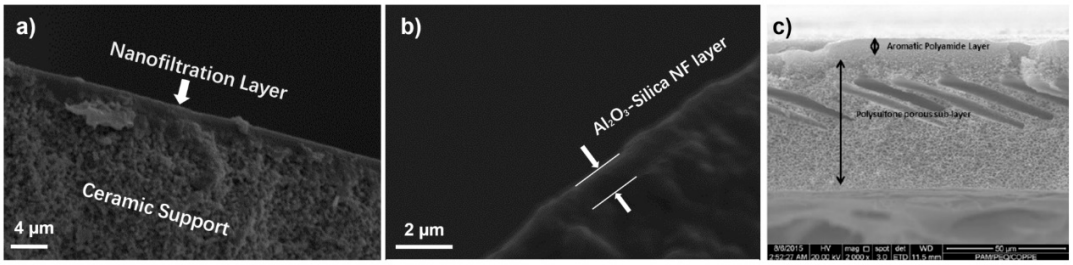

Figure 2. SEM micrographs at (**a**) low and (**b**) high magnification of the cross-section of S/O = 2, and (**c**) cross-section of NF90 (image reprinted from Ref [27] with permission from Elsevier, 2018).

3.2. Water Permeability

Figure 3 shows permeate fluxes and recovery factors of the NF90 and the two Al_2O_3-doped silica membranes, namely S/O = 0.5 and S/O = 2 when filtering the groundwater (initial volume 2.0 L) at 5 bar of transmembrane pressure. At 1% of water recovery, the permeates fluxes for S/O = 2, NF90, and S/O = 0.5 were at 28, 25, and 17 LMH (i.e., $L \cdot m^{-2} \cdot h^{-1}$), respectively. However, when the recovery factor reaches 50% (i.e., after collecting 1.0 L of permeate), the flux reduces to 19, 11, and 3 LMH for S/O = 2, NF90, and S/O = 0.5, respectively. For S/O = 0.5, the flux becomes relatively stable after 50 h, which corresponds to a recovery factor of 38%. The decreasing trend of the flux for all three membranes could be attributed to two factors: the increase of osmotic pressure caused by the increasing feed concentration during the filtration; and the formation of the fouling/scaling layer on the surface of the membrane (Figure 3). We assume the anions present in the feed water were HCO_3^-, Cl^- and SO_4^{2-}. Base on charge balance, a rough estimation of the osmotic pressure of the initial feed and after treatment can maximum account for a flux reduction of 30% for the NF90 membrane, whereas the experimental data shows a flux reduction of around 64%. Therefore, fouling and/or scaling are expected to play a more prominent role in the flux decline during filtration. This was confirmed by visually inspecting the surface of the membranes after the filtration tests. Indeed, as shown for NF90 in Figure 4, where a layer of deposits is clearly visible at the membrane surface.

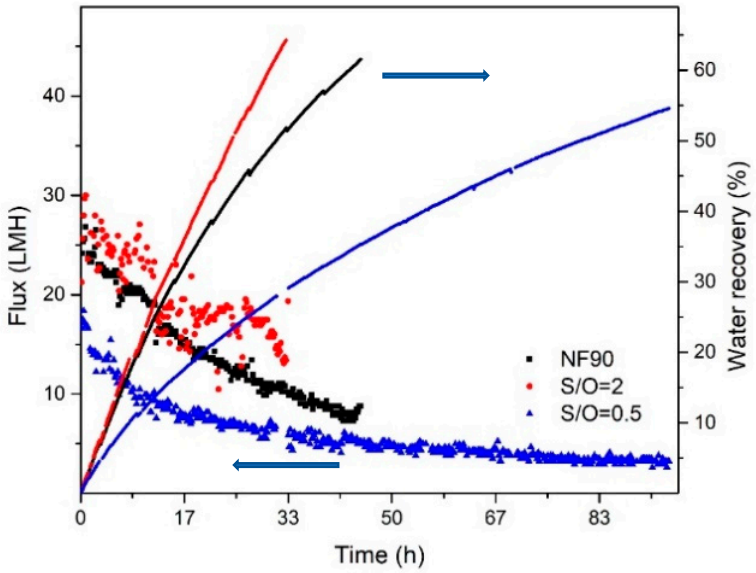

Figure 3. Comparison of the fluxes and water recovery factor as a function of the time for the polymeric commercial NF90 and the lab-made Al_2O_3-doped silica membranes S/O = 2 and S/O = 0.5, when filtering 2.0 L of groundwater.

Figure 4. The surface of NF90 after filtering groundwater (final recovery factor = 60%).

Overall, the S/O = 2 membrane has the highest flux. This can be the result of the high pore density of the membrane when a large amount of surfactant was added into the coating-sol during the membrane synthesis. The three membranes were operated to reach a final water recovery factor of about 60%, which could be easily achieved in our nanofiltration apparatus. Slightly different recovery factors (55–65%) for each membrane were observed in the study, this could due to the different operating times with the three membranes (Figure 3). Similar to the fluxes, the recovery rate was decreasing overtime for all three membranes.

3.3. Ionic Selectivity

The ion selectivities of the membranes were confirmed by the ICP measurement. Figures 5–7 show the variation of the concentrations of the major cationic components of the groundwater (i.e., Na^+, K^+, Ca^{2+}, and Mg^{2+}) in the feed and permeate as a function of the time and ion rejections calculated by using Equation (2). Counterintuitively, for all membranes, the cation concentration of the feed was increasing over time while the ion concentration of the permeate kept constant or decreasing during the filtration. This leads to an increasing rejection over time (Figures 5–7). The increasing of the NF membrane selectivity during filtration have been reported by several studies, the explanation could be the formation fouling/scaling layer from the deposition of multivalent cation compounds or organic matters on the membrane surface has an enhancement to the selectivity [28,29].

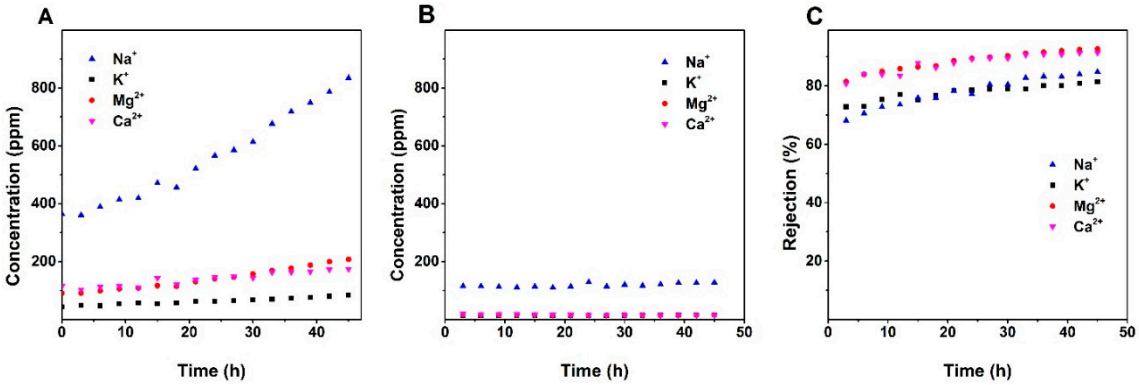

Figure 5. (**a**) Change of cations concentration of the feed and permeate (**b**) over time; (**c**) the change of ions rejection for the polymeric membrane NF90 over time.

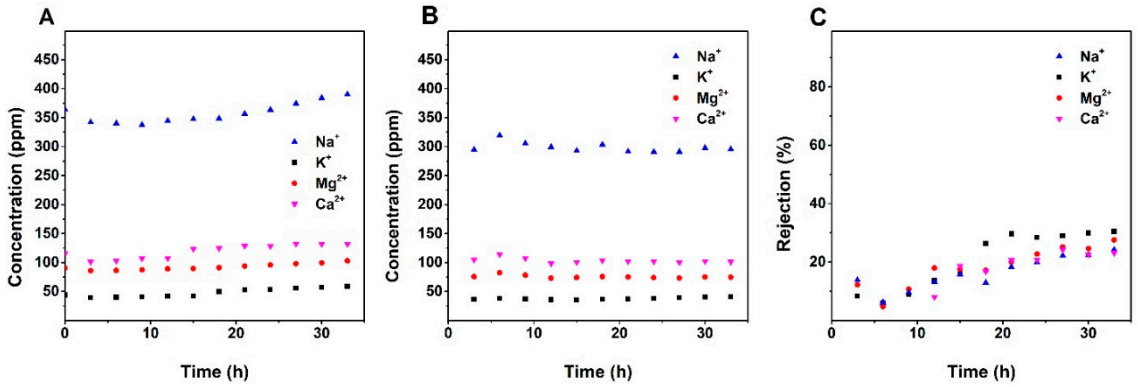

Figure 6. (**a**) Change of cations concentration of the feed and permeate (**b**) over time; (**c**) the change of ions rejection for the S/O = 2 over time.

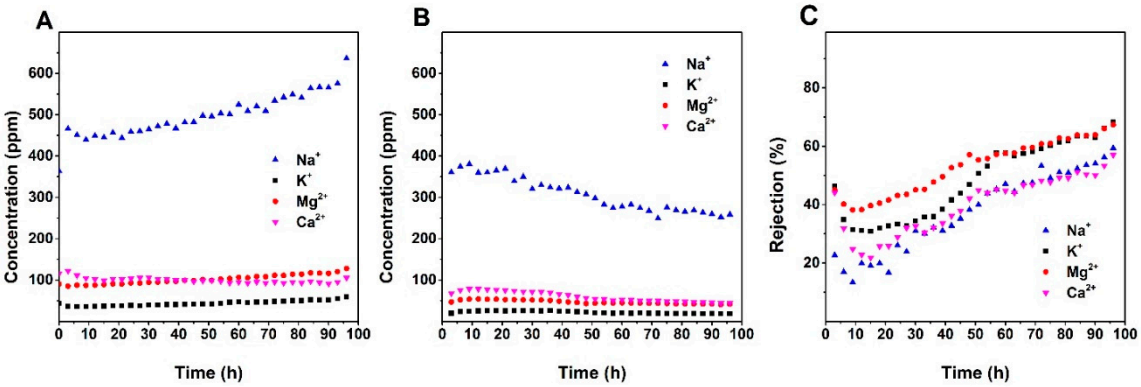

Figure 7. (**a**) Change of cations concentration of the feed and permeate (**b**) over time; (**c**) the change of ions rejection for S/O = 0.5 over time.

A comparison of data provided in Figures 5–7 shows that NF90 has the highest ion rejection among all tested membranes. After 45 h of filtration, the rejection for Mg^{2+} and Ca^{2+} was up to around 90%. NF90 has shown a slightly higher rejection for divalent ion than monovalent ions, this is typical for the polymer NF membranes since the membrane is more efficient at retaining hydrated ions with bigger diameter and higher charge, due to the size exclusion and electrostatic force [30]. The inorganic membranes showed a lower rejection compare to the NF90. By the end of the filtration, the rejection of Mg^{2+} and Ca^{2+} were at around 67% and 57% for S/O = 0.5, and at around 28% and 23% for S/O = 2. This number is much lower compare to the data obtained from the previous study, where the highest rejection for the divalent ions was above 90% [22]. The possible explanation for the relatively low rejection could be the high ion concentration in the groundwater compare to the model solutions tested in the previous study.

3.4. Water Potabilization

The permeate conductivity for each membrane is reported as a function of the water recovery factor in Figure 8. Despite the increase of the ion concentration in the feed over the water recovery factor, the conductivity kept relatively constant for all the membranes. This indicates that a stable performance can be obtained for all three membranes throughout the filtration experiment. When the water recovery factor reaches 50%, the permeates conductivity for S/O = 2 and S/O = 0.5 was observed at around 3.8 $mS{\cdot}cm^{-1}$ and 2.4 $mS{\cdot}cm^{-1}$ respectively. At the same water recovery factor, the lowest permeate conductivity was obtained by NF90 at around 1.3 $mS{\cdot}cm^{-1}$, which is significantly lower than the conductivity of the groundwater sample (4.6 $mS{\cdot}cm^{-1}$). The permeate conductivity for the membranes was consistent with the ICP measurements that showed in Figures 5–7. The conductivity level of the NF 90 permeate has reduced to almost half of the conductive limit (2.5 $mS{\cdot}cm^{-1}$) according to

the Italian standard [26], thus, it is safe to assume the NF90 permeate suitable for human consumption. In principle, S/O = 0.5 can also produce drinking water from the groundwater sample treated in this study. Nevertheless, fluctuations in the feed salinity might results in a permeate with conductivity higher than 2.5 mS·cm^{-1} and therefore not suitable for human consumption. As for the S/O = 2, the permeate has a conductivity largely above the limitation, therefore it is not recommended for consumption as well.

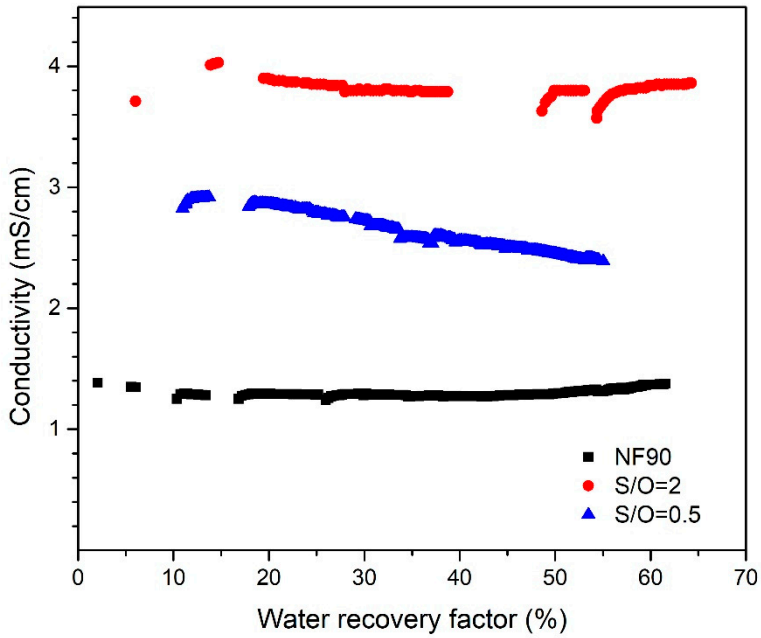

Figure 8. The conductivity of the permeates for the polymeric Dow 90 NF and the inorganic membranes S/O = 2 and S/O = 0.5 as a function of the water recovery factor.

On the other hand, the permeate water could also potentially be used for irrigation purposes since two major concerns for irrigation water is the salinity hazard and sodium hazard, which are generally indicated by the water conductivity and SAR (Equation (3)), respectively. For the conductivity, in the range between 0.76–2.0 μS·cm^{-1}, depending on the species of the plants, the permeate water of NF90 could be used for irrigation of plants with a moderate salinity tolerance, such as tomatoes, soybeans, and wheat [31]. Additionally, the permeate water of S/O = 0.5 is in the range between 1.5 to 3.0 mS·cm^{-1}, which could be used for the irrigation of plants with a high salinity tolerance like cotton or wheatgrass [31]. On the other hand, SAR can be used to measure the risk of the irrigation soil subject to sodium hazard, since the presence of Na^+ could be harmful to the plants. The SAR value for the permeate of NF90 and S/O = 2 were in the range of 4.5 to 5.5, whereas the SAR value for the permeate water of S/O = 0.5 was in the range of 6 to 8. According to the Food and Agriculture Organization (FAO), all the permeate has a SAR below 9, therefore the soil for irrigation subject to no or little sodium hazard [32,33]. It is also worth mentioning that minerals such as calcium, potassium, and magnesium, are fertilizers for plants and their controlled inclusion in water can have a beneficiary effect upon the crops and vegetable production. Thus, the water produced through NF in the current study, can also partially fulfill the fertilizer needs of the plants.

No harmful concentration of organic micropollutants was found in the groundwater sample. Nevertheless, we sparked a groundwater sample with three model pesticides (10 ppm of ACE, IMI, and THI) to mimic a case in which the membrane feed is contaminated with micropollutants and thus to fully investigated the potential of the NF membranes in water potabilization. The rejections of the micropollutants for the membranes is depicted in Figure 9. For the ion rejection, among the three membranes NF90 is the one with the highest rejection for ACE, IMI, and THI: 56%, 59%, and 85% respectively. The inorganic membranes showed a lower selectivity. The rejection of the ACE, IMI, and

THI for the S/O = 0.5 was at 35%, 10%, and 8%, respectively, and 6%, 14%, and 15% for S/O = 2. It is clear to see from the data above that the NF90 has a better perm/selectivity among all membranes.

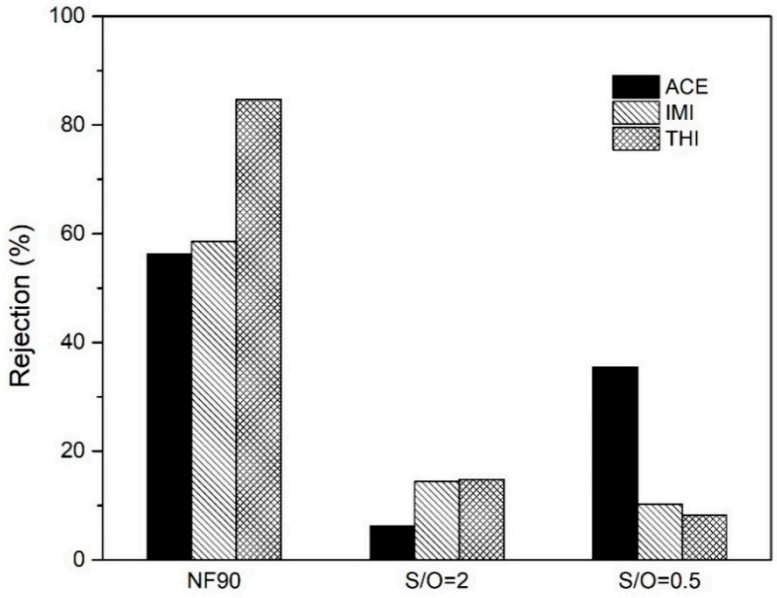

Figure 9. Rejection of acetamiprid (ACE), imidacloprid (IMI), and thiacloprid (THI) for the commercial polymer membrane (NF90) and the Al_2O_3-doped silica membranes (S/O = 2 and S/O = 0.5).

3.5. Specific Energy Consumption

Figure 10 reports the specific energy consumption (SEC) for the three membranes, as calculated from Equation (1). The observed pressure drops for S/O = 2, S/O = 0.5, and NF90 were 0.014, 0.003, and 0.01bar, respectively whereas, the corresponding permeate flow rates, Q_p, were 1.05×10^{-8}, 3.24×10^{-9} and 7.41×10^{-9} m^3/s, respectively. It is evident from the figure that S/O = 0.5 demonstrates the minimum SEC among the tested membranes. Q_p for NF90 and S/O = 0.2 are, respectively, 56 and 69% higher than S/O = 0.5, however, the corresponding pressure drops for these membranes are even higher (70 and 78.5%, respectively). Consequently, S/O = 0.5 demonstrates the minimum SEC. NF90 is the most energy-consuming membrane among all the tested membranes due to its mediocre flux and relatively high pressure drop and demonstrates almost 1.4 times higher SEC than S/O = 0.5. The SEC values observed in the current study are similar or even slightly lower than what has been reported in the literature for similar feed water composition [34,35], thus indicating a good perspective of the applied Al_2O_3-doped silica membranes in desalination through NF. State-of-the-art polymeric nanofiltration membranes are in flat sheet configuration and require the use of spacers to support the membranes as well as to alleviate the concentration polarization within the module. The presence of spacers, however, causes additional pressure drop within the membrane module. Tube-shaped Al_2O_3-doped silica membranes used in the current study do not require any spacers and therefore, pressure drop within the module channels remains low. Relatively lower energy consumptions for ceramic membranes observed in the current study can be attributed to lower pressure drop compared to traditional flat sheet polymeric membranes where the applied spacers contribute significantly in total observed pressure drop [36].

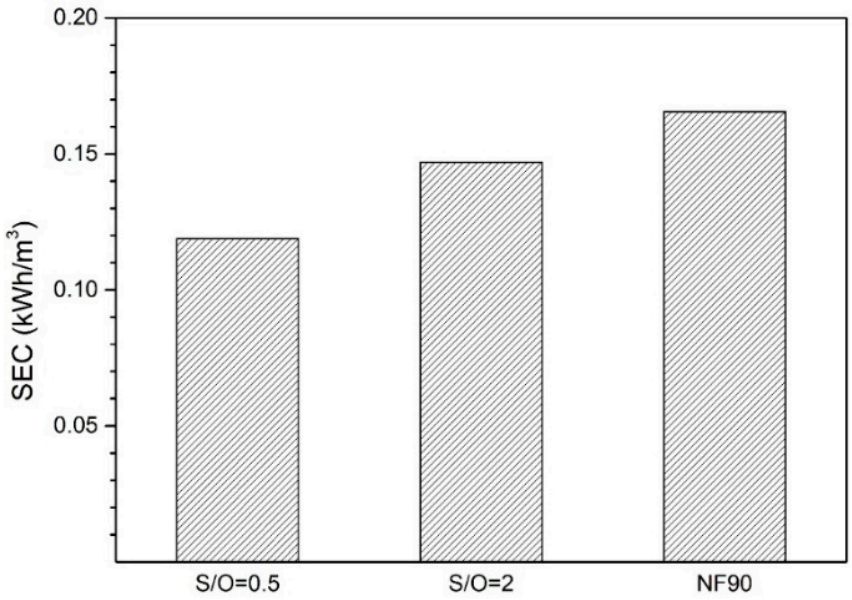

Figure 10. Specific energy consumption of freshwater produced by using different membranes considered in the current study.

Considering the energy cost of 0.15 €/kWh for industrial users in Italy [37], SEC discussed in the above paragraph translate into specific water cost between €0.018–0.024 for each cubic meter of the freshwater obtained. The specific cost for commercial freshwater in the Puglia region is 1.5 €/m^3 which indicates that NF is an attractive option for the production of fresh water from underground water in the region.

4. Conclusions

A commercial polymer membrane and two lab-made inorganic membranes were tested for the desalination of groundwater from a well in the Puglia Region, Italy. Among the three tested membranes, the polymer membrane, NF90, have shown promising performance regarding the selectivity and permeability, with around 80–90% rejection for divalent ions, and 56–85% for micropollutants. From the filtration experiment, around 62% of water can be recovered, the recovered water from NF90 can be potentially used for human consumption or irrigation. On the other hand, the inorganic membranes S/O = 2 and S/O = 0.5 have shown a lower selectivity, the permeate conductivity was 3.8 mS/cm and 2.4 mS/cm, respectively. Due to the high salinity of the permeate water for both inorganic membranes, it is not recommended for drinking. However, the permeate water of S/O = 0.5 could potentially be used for the irrigation of plants with high salinity tolerance. In terms of energy consumption, S/O = 0.5 demonstrated the lowest SEC among the tested membrane which was equivalent to a specific water cost of around 0.02 €/m^3. The specific water cost for the ceramic NF membranes, observed in the current study, is less than 3% of the commercial price of freshwater in the region that demonstrates the excellent economical potential of NF for the treatment of underground water in the region.

Author Contributions: Conceptualization, X.M. and V.B.; methodology, C.A.Q.-J. and A.A.; formal analysis, X.M., C.A.Q.-J. and A.A.; investigation X.M.; writing—original draft, X.M.; writing—review and editing, V.B., C.A.Q.-J. and A.A.; supervision, V.B. and C.A.Q.-J.; funding acquisition, V.B. All authors have read and agreed to the published version of the manuscript.

Funding: This research was funded by the European Commission (H2020-CIRC-2017TwoStage) Grant Agreement n. 776816 ("Project Ô").

Acknowledgments: The authors wish to thank the European Commission for funding.

Conflicts of Interest: The authors declare no conflict of interest.

References and Note

1. Shiklomanov, I.A.; Peter, G. World freshwater resources. In *Water in Crisis: A Guide to the World's Fresh Water Resources*; Oxford University Press: New York, NY, USA, 1993; pp. 13–24.
2. Navarro, B.A.; Goldscheider, N.; Vadillo, I.; Vías, J.; Neukum, C.; Brechenmacher, J.; Cantos, F.C.; Hötzl, H.; Gavilán, P.J.; Perles, M.; et al. *COST Action 620—Vulnerability and Risk Mapping for the Protection of Carbonate (Karst) Aquifers: Final Report*; European Communities: Brussels, Belgium, 2003; pp. 115–196.
3. Lugoli, F.; Leopizzi, M.I.; Bagordo, F.; Grassi, T.; Guido, M.; De Donno, A. Widespread microbiological groundwater contamination in the South-eastern Salento (Puglia-Italy). *J. Environ. Monit.* **2011**, *13*, 192–200. [CrossRef]
4. Meffe, R.; de Bustamante, I. Emerging organic contaminants in surface water and groundwater: A first overview of the situation in Italy. *Sci. Total Environ.* **2014**, *481*, 280–295. [CrossRef] [PubMed]
5. Pendergast, M.M.; Hoek, E.M.V. A review of water treatment membrane nanotechnologies. *Energy Environ. Sci.* **2011**, *4*, 1946–1971. [CrossRef]
6. Hilal, N.; Al-Zoubi, H.; Darwish, N.; Mohammad, A.W.; Abu-Arabi, M. A comprehensive review of nanofiltration membranes:Treatment, pretreatment, modelling, and atomic force microscopy. *Desalination* **2004**, *170*, 281–308. [CrossRef]
7. Lee, K.P.; Arnot, T.; Mattia, D. A review of reverse osmosis membrane materials for desalination—Development to date and future potential. *J. Membr. Sci.* **2011**, *370*, 1–22. [CrossRef]
8. Guillen, G.; Hoek, E.M.V. Modeling the impacts of feed spacer geometry on reverse osmosis and nanofiltration processes. *Chem. Eng. J.* **2009**, *149*, 221–231. [CrossRef]
9. Basile, A. (Ed.) *Handbook of Membrane Reactors: Reactor Types and Industrial Applications*; Woodhead: Cambridge, UK, 2013.
10. Arribas, P.; Khayet, M.; García-Payo, M.; Gil, L.; García-Payo, M. Novel and emerging membranes for water treatment by hydrostatic pressure and vapor pressure gradient membrane processes. In *Advances in Membrane Technologies for Water Treatment*; Elsevier BV: Amsterdam, The Netherlands, 2015; pp. 239–285.
11. Wang, L.K.; Chen, J.P.; Hung, Y.T.; Shammas, N.K. *Membrane and Desalination Technologies*; Humana Press: Totowa, NJ, USA, 2011.
12. Roy, Y.; Warsinger, D.M.; Lienhard, J.H. Effect of temperature on ion transport in nanofiltration membranes: Diffusion, convection and electromigration. *Desalination* **2017**, *420*, 241–257. [CrossRef]
13. Farsi, A.; Boffa, V.; Qureshi, H.F.; Nijmeijer, A.; Winnubst, L.; Christensen, M.L. Modeling water flux and salt rejection of mesoporous γ-alumina and microporous organosilica membranes. *J. Membr. Sci.* **2014**, *470*, 307–315. [CrossRef]
14. Farahbakhsh, K.; Svrcek, C.; Guest, R.K.; Smith, D.W. A review of the impact of chemical pretreatment on low-pressure water treatment membranes. *J. Environ. Eng. Sci.* **2004**, *3*, 237–253. [CrossRef]
15. Tsuru, T. Inorganic porous membranes for liquid phase separation. *Sep. Purif. Methods* **2001**, *30*, 191–220. [CrossRef]
16. Lin, J.Y. Microporous and dense inorganic membranes: Current status and prospective. *Sep. Purif. Technol.* **2001**, *25*, 39–55. [CrossRef]
17. Farsi, A.; Malvache, C.; De Bartolis, O.; Magnacca, G.; Kristensen, P.K.; Christensen, M.L.; Boffa, V. Design and fabrication of silica-based nanofiltration membranes for water desalination and detoxification. *Microporous Mesoporous Mater.* **2017**, *237*, 117–126. [CrossRef]
18. Van der Bruggen, B.; Mänttäri, M.; Nyström, M. Drawbacks of applying nanofiltration and how to avoid them: A review. *Sep. Purif. Technol.* **2008**, *63*, 251–263. [CrossRef]
19. Lin, C.X.C.; Ding, L.P.; Smart, S.; Da Costa, J.C.D.; Da Costa, J.C.D. Cobalt oxide silica membranes for desalination. *J. Colloid Interface Sci.* **2012**, *368*, 70–76. [CrossRef]
20. Boffa, V.; Magnacca, G.; Jørgensen, L.B.; Wehner, A.; Dörnhöfer, A.; Yue, Y. Toward the effective design of steam-stable silica-based membranes. *Microporous Mesoporous Mater.* **2013**, *179*, 242–249. [CrossRef]
21. Gu, Y.; Hacarlioglu, P.; Oyama, S.T. Hydrothermally stable silica–alumina composite membranes for hydrogen separation. *J. Membr. Sci.* **2008**, *310*, 28–37. [CrossRef]
22. Ma, X.; Janowska, K.; Boffa, V.; Fabbri, D.; Magnacca, G.; Calza, P.; Yue, Y. Surfactant-Assisted Fabrication of Alumina-Doped Amorphous Silica Nanofiltration Membranes with Enhanced Water Purification Performances. *Nanomaterials* **2019**, *9*, 1368. [CrossRef]

23. Hilal, N.; Al-Zoubi, H.; Mohammad, A.W.; Darwish, N. Nanofiltration of highly concentrated salt solutions up to seawater salinity. *Desalination* **2005**, *184*, 315–326. [CrossRef]
24. Kaya, C.; Sert, G.; Kabay, N.; Arda, M.; Yuksel, M.; Egemen, Ö. Pre-treatment with nanofiltration (NF) in seawater desalination—Preliminary integrated membrane tests in Urla, Turkey. *Desalination* **2015**, *369*, 10–17. [CrossRef]
25. Llenas, L.; Martínez-Lladó, X.; Yaroshchuk, A.E.; Rovira, M.; De Pablo, J. Nanofiltration as pretreatment for scale prevention in seawater reverse osmosis desalination. *DESALINATION Water Treat.* **2011**, *36*, 310–318. [CrossRef]
26. D.Lgs. 31/2001, Attuazione della direttiva 98/83/CE relativa alla qualita' delle acque destinate al consumo umano, *Gazzetta Ufficiale* n. 52, 3 March **2001**-Supplemento Ordinario n. 41.
27. Licona, K.; Geaquinto, L.D.O.; Nicolini, J.; Figueiredo, N.; Chiapetta, S.; Habert, A.; Yokoyama, L. Assessing potential of nanofiltration and reverse osmosis for removal of toxic pharmaceuticals from water. *J. Water Process. Eng.* **2018**, *25*, 195–204. [CrossRef]
28. Sadrzadeh, M.; Pernitsky, D.; McGregor, M. *Nanofiltration for the Treatment of Oil Sands-Produced Water*; IntechOpen: London, UK, 2018.
29. Gao, F.; Sheng, Y.; Cao, H.; Li, Y.; Su, C.; Cui, X. The synergistic effect of organic foulants and their fouling behavior on the nanofiltration separation to multivalent ions. *DESALINATION Water Treat.* **2016**, *57*, 1–14. [CrossRef]
30. Bowen, W.; Welfoot, J.S. Modelling the performance of membrane nanofiltration—Critical assessment and model development. *Chem. Eng. Sci.* **2002**, *57*, 1121–1137. [CrossRef]
31. Fipps, G. *Irrigation Water Quality Standards and Salinity Management Strategies*; Texas A&M Agrilife Ext.: College Station, TX, USA, 2003.
32. Ayers, R.S.; Westcot, D.W. *Water Quality for Agriculture*; Food and Agriculture Organization of the United Nations: Rome, Italy, 1994.
33. Quist-Jensen, C.A.; Macedonio, F.; Drioli, E. Membrane technology for water production in agriculture: Desalination and wastewater reuse. *Desalination* **2015**, *364*, 17–32. [CrossRef]
34. Wafi, M.K.; Hussain, N.; Abdalla, O.E.-S.; Al-Far, M.D.; Al-Hajaj, N.A.; Alzonnikah, K.F. Nanofiltration as a cost-saving desalination process. *SN Appl. Sci.* **2019**, *1*, 751. [CrossRef]
35. Liu, J.; Yuan, J.; Xie, L.; Ji, Z.-Y. Exergy analysis of dual-stage nanofiltration seawater desalination. *Energy* **2013**, *62*, 248–254. [CrossRef]
36. Ali, A.; Criscuoli, A.; Macedonio, F.; Drioli, E. A comparative analysis of flat sheet and capillary membranes for membrane distillation applications. *Desalination* **2019**, *456*, 1–12. [CrossRef]
37. Statista Prices of Electricity for Industry in Italy from 2008 to 2018 (in Euro Cents Per Kilowatt Hour). Available online: https://www.statista.com/statistics/595826/electricity-industry-price-italy/ (accessed on 31 August 2020).

Paper III

membranes

MDPI

Article

Combined Nanofiltration and Thermocatalysis for the Simultaneous Degradation of Micropollutants, Fouling Mitigation and Water Purification

Katarzyna Janowska [1], Xianzheng Ma [1], Vittorio Boffa [1,*], Mads Koustrup Jørgensen [1] and Victor M. Candelario [2]

[1] Center for Membrane Technology, Department of Chemistry and Bioscience, Aalborg University, Fredrik Bajers Vej 7H, 9220 Aalborg, Denmark; kaj@bio.aau.dk (K.J.); xm@bio.aau.dk (X.M.); mkj@bio.aau.dk (M.K.J.)

[2] Department of Research and Development, LiqTech Ceramics A/S, Industriparken 22C, 2750 Ballerup, Denmark; vcl@liqtech.com

* Correspondence: vb@bio.aau.dk; Tel.: +45-9940-3579

Abstract: Due to progressive limitation of access to clean drinkable water, it is nowadays a priority to find an effective method of water purification from those emerging organic contaminants, which might have potentially harmful and irreversible effects on living organisms and environment. This manuscript reports the development of a new strategy for water purification, which combines a novel and recently developed Al_2O_3-doped silica nanofiltration membrane with a thermocatalytic perovskite, namely cerium-doped strontium ferrate (CSF). The thermocatalytic activity of CSF offers the opportunity to degrade organic pollutants with no light and without input of chemical oxidants, providing simplicity of operation. Moreover, our studies on real samples of secondary effluent from wastewater treatment showed that the thermocatalyst has the ability to degrade also part of the non-toxic organic matter, which allows for reducing the chemical oxygen demand of the retentate and mitigating membrane fouling during filtration. Therefore, the new technology is effective in the production of clean feed and permeate and has a potential to be used in degradation of micropollutants in water treatment.

Keywords: nanofiltration; thermocatalysis; perovskite; micropollutants; water purification; wastewater

Citation: Janowska, K.; Ma, X.; Boffa, V.; Jørgensen, M.K.; Candelario, V.M. Combined Nanofiltration and Thermocatalysis for the Simultaneous Degradation of Micropollutants, Fouling Mitigation and Water Purification. *Membranes* **2021**, *11*, 639. http://doi.org/10.3390/membranes11080639

Academic Editor: Anthony Szymczyk

Received: 19 July 2021
Accepted: 16 August 2021
Published: 19 August 2021

1. Introduction

Sources of global, usable clean drinking water are dramatically decreasing and it is a lifeline to save our planet from a water crisis. Municipal, industrial and agricultural wastewaters are the main sources of micropollutants causing the contamination of natural and drinking water. These compounds such as personal care products, pesticides, pharmaceuticals, hormones, industrial chemicals and environmental estrogens, even at low concentrations (ng L^{-1} or µg L^{-1}), have damaging and irreversible effects on living organisms and the environment [1,2]. Therefore, it is a priority to develop an efficient technology to remove these contaminants from wastewater, considering that, in conventional wastewater treatment plants (WWTPs), physical methods are unproductive for their abatement [3], and biological processes can provide only a limited degradation of such pollutants [4,5]. Therefore, a number of advanced wastewater treatment technologies such as activated carbon adsorption, advanced oxidation processes and membrane technologies have been used for water purification [6]. Above all, membrane-based technologies are recently gaining attention as they produce water of superior quality, they are less sensitive to feed quality fluctuations, and their footprint is much smaller compared to conventional water treatment processes [4]. Out of membrane technologies, especially nanofiltration (NF) has been found as a promising cost-effective alternative method for

removing and concentrating low-molecular-weight organic micropollutants [7,8]. The pore sizes of NF membranes are typically between 1 and 2 nm, so they can molecularly sieve hydrated multivalent ions and organic micropollutants [9,10]. NF is distinguished by low operating pressure and high permeability, which benefits in the form of relatively low investment, operation and maintenance costs [11]. Nevertheless, there are some limitations of this process such as the non-complete rejection of water pollutants, membrane fouling, and the production of a toxic concentrate (retentate), which needs to be treated before disposal [2,6,8,12,13].

This manuscript reports the development of a novel strategy for water purification that involves the integration of membrane filtration and advanced oxidation. For filtration experiments, we used a ceramic membrane consisting of alumina tubular support coated with an Al_2O_3-doped NF silica layer, which has been previously reported [14], showing good retention of organic pollutants. Al_2O_3 doping was used to increase the chemical stability of the silica thin layer [14,15]. Moreover, the tubular configuration and the mechanical resistance of this membrane are suitable to perform the NF experiment in the presence of thermocatalytic particles, which might clog or scratch commercial polymeric membrane modules. Advanced oxidation processes (AOPs) utilize highly reactive oxygen species (ROS) such as OH• and O_2•-, which mineralize most of the pollutants into less or non-toxic products (e.g., H_2O and CO_2) in aqueous systems [3,16,17]. Among AOPs, thermal catalysis offers the opportunity to degrade organic pollutants with no light and without input of chemical oxidants. Therefore, in our experiments, the concentration of micropollutants and organic matter in the membrane retentates were reduced by treatment with a perovskite thermocatalyst, namely, cerium-doped strontium ferrate (CSF), either during or after filtration. Bisphenol A (BPA) was chosen as a model pollutant to spark water samples, because it is a common water contaminant with a well-documented endocrine-disrupting activity and toxicity [18]. Moreover, common biological treatments are not effective for BPA degradation [19]. On the other hand, we reported full abatement of BPA in water by treatment with CSF perovskite in our previous study [20].

The purpose of this work was to integrate a ceramic membrane with perovskite in order to effectively retain and degrade BPA and improve the quality of feed and permeate. We also performed tests with real secondary effluent from treatment wastewater, which contain large amounts of non-toxic organic matter. Organic matter may have a negative influence on the thermocatalytic abatement of micropollutants and can cause clogging of membranes' pores at the detriment of membrane permeance [21]. It is responsible for membrane fouling and for the chemical oxygen demand of the retentate. Therefore, the influence of the thermocatalyst on reduction of non-toxic organic matter content and fouling is also discussed. Finally, we performed a two-step experiment to check the impact of thermocatalyst on BPA abatement and organic matter degradation for effluent concentrate in order to compare it with one-step filtration with thermocatalyst addition.

2. Materials and Methods

2.1. Cerium-Doped Strontium Ferrate Perovskite Synthesis

Initially, 1.8 g strontium nitrate (Carl Roth, purity $\geq$ 99%), 4.04 g iron (III) nitrate (Sigma-Aldrich, purity $\geq$ 98%) and 0.65 g cerium (III) nitrate (Sigma-Aldrich, purity 99%) were completely dissolved in 200 mL of distillated water, using a 1 L glass beaker as container. Then, 7.68 g citric acid (Carl Roth, purity $\geq$ 99.5%) were added in order to reach a citric acid-to-metal cations ratio of 2, whereas the reducers-to-oxidizers ratio (Φ) was regulated at its stoichiometric value through the addition of 9.25 g of ammonium nitrate (Sigma-Aldrich, purity $\geq$ 99.5%), according to the valence concepts based on propellant chemistry [22]. The pH of the solution was adjusted to 6.0 using ammonium hydroxide (Sigma-Aldrich, 25 wt %), in order to favor citrate anions-metal cations complex formation, and the glass beaker was placed on a hot plate and kept under 80 °C for the evaporation of the water under continuous magnetic stirring. When a sticky gel was obtained, the hot plate was set to the maximum temperature (310 °C) in order to start the gel self-ignition. After

the combustion, the as-burned powder was calcined in 1000 °C for 5 h with a heating rate of 5 °C min^{-1}. After calcination, about 2 g of $Sr_{0.85}Ce_{0.15}FeO_{3-\delta}$ powder were obtained.

2.2. Membrane Fabrication

The membrane preparation method is described in detail by Ma et al. [14]. Note that 5% mol Al_2O_3-doped silica NF membrane used for tests was fabricated via the sol-gel method using a cationic surfactant, namely, N,N,N-Trimethylhexadecan-1-aminium bromide (CTAB) as pore-forming agent. The molar ratio of surfactant/oxide was kept at 0.5, because, based on the previous study, the membrane prepared under such conditions exhibited the best selectivity towards organic pollutants and salts. A two-step approach was applied for the sol synthesis. The first step of synthesis was the hydrolysis of TEOS, which was achieved by letting to react a mixture of TEOS (98%, Sigma-Aldrich, St. Louis, MO, USA), ethanol (99.9%, VWR Chemicals, Radnor, PA, USA), deionized water, and nitric acid (69%, Sigma-Aldrich, St. Louis, MO, USA), with a molar ratio of 1:4:2.5:0.04, at 60 °C for 3 h. Then, in the second step of the synthesis, CTAB (99%, Sigma-Aldrich, St. Louis, MO, USA) was added to the pre-hydrolyzed TEOS solution to achieve the desired CTAB: (SiO_2 + Al_2O_3) molar ratio. After the complete dissolution of CTAB, aluminum isopropoxide (AIP) (98%, Sigma-Aldrich, St. Louis, MO, USA) was directly added to the mixture to obtain a 5 mol% Al_2O_3 concentration in the final consolidated membrane material. The mixture was continuously stirred at 60 °C until all the AIP was dissolved and a transparent yellowish solution was obtained). Sol was diluted by 1:20 volume ratio with ethanol and subsequently filtered with a 0.2 µm syringe filter (Minisart RC, 25 mm, Sigma-Aldrich, St. Louis, MO, USA) to remove dust particles and impurities before the coating. The membrane was coated on commercial y-alumina tubular support with y-alumina intermedia layer (250 × 10 × 7 mm (L × OD × ID), Pervatech B.V., Rijssen, The Netherlands). The membrane was fabricated by dip-coating of the alumina-doped silica sols onto the supporting substrates. Specifically, the inside of the supports was coated vertical by a lab-made device at a dipping/withdrawing rate of <2.5 cm/min. After drying at room temperature for 24 h, the membranes were calcined at 450 °C for 2 h at the heating and cooling rate of 2 °C min^{-1}.

2.3. SEM

The morphology of the membrane cross-section and surface was investigated by SEM analysis using an EVO 50 XVP microscope (Zeiss, Köln, Germany) with LaB6 source. The samples were mounted on metallic stubs with double-sided conductive tape and ion coated with a gold layer (thickness ~25 nm) by a sputter coater (Baltec SCD 050, Pfäffikon, Switzerland) for 60 s under vacuum at a current intensity of 60 mA to avoid any charging effect.

2.4. Effluent Sampling

Secondary effluent was sampled from the Wastewater Treatment Plant Aalborg West (AAW) 57.049422° N, 9.864735° E in Denmark in January 2021. Sampling permission was granted by Aalborg Forsyning, Kloak A/S. Samples were transported to the laboratory within 1 h after sampling and kept in the fridge until experiments. Samples were used for NF permeance tests without and with addition of thermocatalyst and for experiments with concentrate.

2.5. Nanofiltration Apparatus

The experimental cross-flow filtration set-up is shown in Figure 1, and it follows the system described by Farsi et al. [23]. The feed was pumped to the NF membrane by a feed pump giving pressure 6 bar. Monotubular membrane (250 × 10 × 7 mm (L × OD × ID), Pervatech B.V., The Netherlands) was sealed completely in a stainless steel membrane module. The effective membrane surface was 55 cm^2. The permeate mass flow was measured by a balance (Mettler Toledo, Mono Bloc series, Greifensee, Switzerland) connected

to a computer to continuously log the weight of the permeate. The feed pressure was measured before and after the membrane by two pressure transmitters (Danfoss, MBS 4010, Nordborg, Denmark) and an electronic heat sensor (Kamstrup A/S, Skanderborg Denmark) measured feed temperature before membrane module. A rotary lobe pump (Philipp Hilge GmbH & Co, Novalobe, Germany) generated the cross-flow rate measured by a microprocessor-based flow rate transmitter (Siemens, MAG 50000, Munich, Germany). It was adjusted to 1.6 ± 1 m s^{-1} for all the experiments. The retentate stream was controlled by a manual valve. The system was operated for 3 h to ensure that the system was operated at steady-state condition. During filtration, samples were collected from each stream (feed, permeate) at various times to observe system changes during time. Filtration experiments were done at temperature 50 °C. A typical test started by filling up the feed tank with 1.8 L of solution and setting the system at the specified operational conditions.

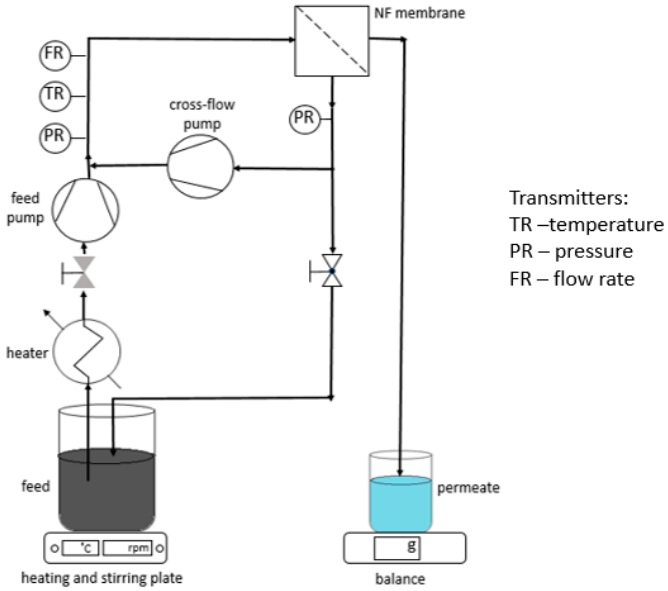

Figure 1. Scheme of the nanofiltration setup used in this study.

2.6. COD Analysis

COD (chemical oxygen demand) analysis was performed using COD kits (Hach®) 5–60 mg/L and 15–150 mL/L and Hach Lange DR3900 apparatus. Then, 2 mL of samples were added to each vial from the proper kit and placed in a heating block for 2 h at 148 °C. After cooling down to 20 °C, the vials were placed one after another in Hach Lange to measure COD in mg L^{-1}.

2.7. Determination of BPA Concentration in Water Samples

In each experiment, collected samples of feed were filtered using RC 0.45 µm syringe filters. Then, the liquid phases of feed and permeate were analyzed through HPLC with UV detection (Phenomenex, with a Kintex® 5 µm EVO C18 100 Å LC column (150 × 4.60 mm), mobile phase flow of 1 mL min^{-1} (acetonitrile/water = 60/40 *v*/*v*%), UV detector at 230 nm) in order to determine the concentration of the contaminant in the sample. A calibration curve was determined using several solutions of BPA in concentrations between 1 and 10 mg L^{-1}.

3. Results

3.1. SEM of Membrane

Figure 2 shows the SEM cross-section of the Al_2O_3-doped silica membrane used in this study. The micrograph shows a continuous film covering the multilayered alumina support. From the picture, the thickness of the top layer measured to be 0.5 µm. Based on

analysis at the low-temperature porosimeter [14], the Al_2O_3-doped silica material coated on the alumina support has main and maximum pore size of 1.3 nm and 2.5 nm, respectively, and therefore it is suitable to act as a NF membrane. Moreover, CSF particles have a flake-like structure with thickness of about 0.2 µm and lateral dimensions that are several micrometers large. Therefore, Al_2O_3-doped silica membrane can easily retain CSF particles at the feed side during filtration.

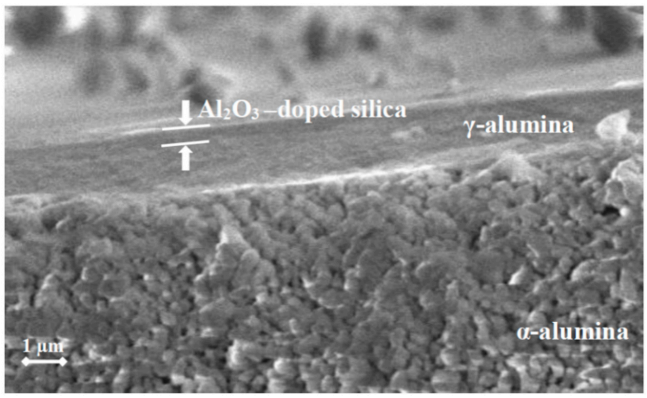

Figure 2. Cross-sectional SEM micrograph of the membrane used in this study. The Al_2O_3-doped silica NF layer is coated over a mesoporous γ-alumina interlayer and a macroporous α-alumina support.

3.2. BPA Rejection

The experiment studying the BPA rejection and impact of temperature on water permeance was performed using 1.8 L of deionized water with a starting BPA concentration of 10 mg L^{-1} as membrane feed. The cross flow was set up to 1.6 ± 0.1 m s^{-1} and the feed was pumped with a trans-membrane pressure of 6 bar. From Figure 3, it can be seen that no impact of temperature on BPA rejection has been observed. Pollutant rejection remains constant, reaching values near to 100% at all the tested temperatures: 30 °C (98.7%), 40 °C (99.5%), 50 °C (98.6%), 55 °C (98.8%), 60 °C (98.9%). However, the water permeance of the membrane increased with increase of temperature in the range 30–60 °C as follows: 30 °C (1.09 L (h m^2 bar)$^{-1}$), 40 °C (1.40 L (h m^2 bar)$^{-1}$), 50 °C (1.91 L (h m^2 bar)$^{-1}$), 55 °C (2.02 L(h m^2 bar)$^{-1}$), 60 °C (2.17 L (h m^2 bar)$^{-1}$). This twofold increase of water permeance from 30 to 60 °C is consistent with the data reported by Tsuru et al. [24] for other types of ceramic NF membranes.

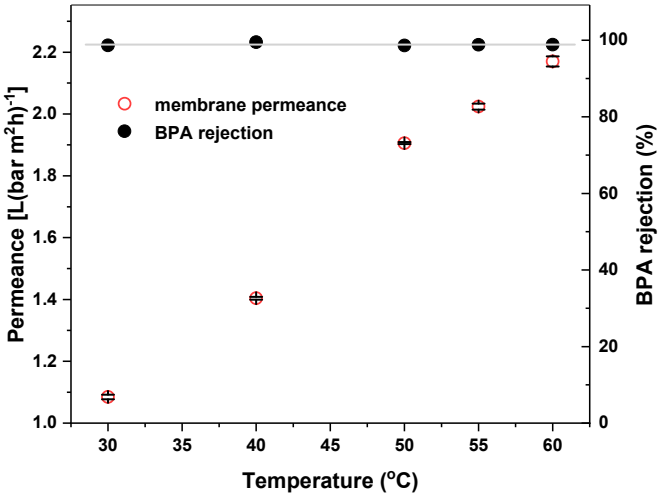

Figure 3. Impact of temperature on water permeance and BPA rejection for the Al_2O_3-doped silica NF membrane used in this study. Black bars indicate the error for the permeance values.

3.3. BPA Abatement during Filtration

The experiments to investigate the thermocatalytic abatement during filtration were performed at a temperature of 50 °C, because our previous studies showed that CSF can catalyze fast degradation of BPA at this temperature [20]. The feed volume was 1.8 L, a cross flow of 1.6 ± 0.1 m s^{-1} was applied and the transmembrane pressure was 6 bar. The feed was heated and after reaching a temperature of 50 °C the proper amount of BPA was added to reach a concentration of pollutant of 10 mg L^{-1}. After running the system for 2 h, the thermocatalyst was added in the retentate to reach a concentration of 1 g L^{-1} and the system was operated for another 3 h.

In Figure 4a, it can be seen that during the first 2 h the concentration of BPA in the feed was stable at about 10 mg L^{-1}, with a slight increase, which corresponds to the volumetric concentration factor (VCF), i.e., the ratio of the initial feed volume to the feed volume after a certain filtration time. Indeed, in our filtration experiment, VCF was only 1.069 after 2 h of filtration. Hence, the BPA concentrations in the feed during the first two hours indicate that this micropollutant is stable at the filtering temperature. On the contrary, after adding the CSF thermocatalyst, the concentration of BPA immediately decreases, reaching 4 g L^{-1} after 3 h of operation, despite a VCF = 1.241 for this filtration time.

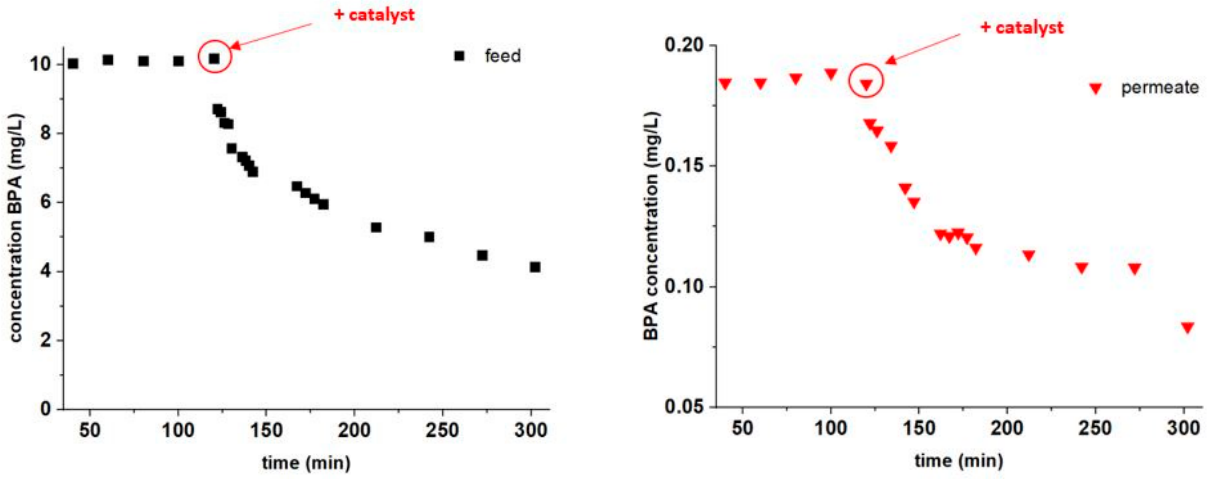

(**a**) (**b**)

Figure 4. Degradation experiment at 50 °C with addition of CSF: (**a**) BPA concentration in the membrane feed as a function of the filtration time; (**b**) BPA concentration in the permeate as a function of the filtration time. Red arrows and circles indicate the time when CSF was added to the membrane feed solution.

Figure 4b shows the development in concentration of BPA in the permeate over time. It can be seen that, during the first 2 h, the permeate concentration of BPA is stable, around 0.19 mg L^{-1}, with a slight increase, which corresponds to the increase in concentration at the retentate side. After adding the thermocatalyst to the feed, the concentration of BPA in the permeate significantly decreases, reaching about 0.1 mg L^{-1} after 3 h. This experiment proves that the addition of thermocatalyst to the NF system leads not only to the abatement of BPA at the feed side, but it also improves the quality of the permeate. Indeed, the membrane selectivity remains constant at (98.1 ± 0.2)% during this filtration experiment (when excluding the outlying value measured for the permeate at 300 min). Therefore, the abatement of BPA concentration at the feed side, upon adding the CSF powder, corresponds to a decrease in BPA concentration at the permeate side. Moreover, the addition of CSF powder did not undermine BPA rejection, suggesting that CSF particles had not damaged the Al-doped silica NF layer (e.g., by friction) during the experiment.

3.4. Fouling Mitigation

The experiments to investigate the influence of thermocatalyst on the reduction of non-toxic organic matter and fouling were conducted by filtering the secondary effluent collected from the Aalborg Wastewater Plant West (WWTP). The properties of effluent are listed in Table 1.

Table 1. Properties of effluent.

Parameter	Unit	Value
pH (22.0 °C)		7.48 ± 0.01
Conductivity (22.5 °C)	mS/cm	1.15 ± 0.01
COD	mg/L	33.4 ± 0.7

As can be seen in Figure 5, when the NF membrane is used to filter a real wastewater effluent, the flux of the permeate decreases along the filtration time. The 80% of permeate flux decline can be explained by the membrane being fouled by the organic matter present in the wastewater effluent (COD 33.4 mg L^{-1}). On the other hand, the flux decline of the permeate was only 20% when 1 g L^{-1} of CSF was added to the wastewater effluent during filtration. Moreover, the fouling was studied to determine which fouling type occurred during each experiment. A method based on a simple regression fitting [25] was used to determine the type of fouling mechanisms in experiments on the filtration with cross flow, as explained in detail in the Supplementary Materials. It was found that, for both the effluent with and without thermocatalyst, the main fouling type is intermediate pore blocking, for which the best (≈1) R^2 correlations were found. It can be seen in Figure 5 that modelled data correspond well with the experimental data for filtration of effluent with (J_{SS} = 2.704 L m^{-2} h^{-1}, K_i = 0.009) and without thermocatalyst (J_{SS} = 0.816 L m^{-2} h^{-1}, K_i = 0.004). The intermediate pore blocking appeared to give slower fouling formation for experiments with thermocatalyst, which is explained by the lower content of organic matter to fouling the membrane as a result of organic matter degradation by the thermocatalyst. After about 100 min of filtration, the models deviate from intermediate pore blocking models, which may be a result of cake formation [25], which in this case can correspond to deposition of CSF particles on the membrane surface.

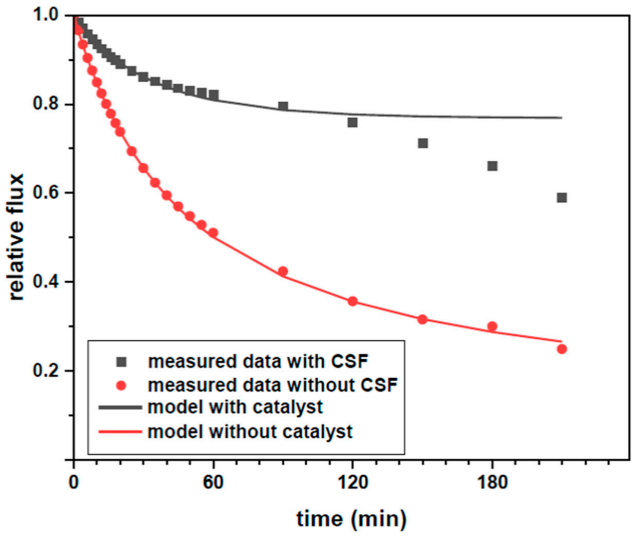

Figure 5. Comparison of change of relative flux in time for effluent with and without thermocatalyst; bullets indicate experimental points; lines correspond to an intermediate pore blocking model (Supplementary Materials).

3.5. Thermocatalytic Treatment of the NF Concentrate

A second way to integrate CSF with NF is to use thermocatalysis as a separate step after concentration, thus saving energy by reducing the volume of wastewater which needs to be heated. Therefore, we performed a new experiment in which 900 mL of wastewater effluent were concentrated to 180 mL by filtration at 6 bar over the Al_2O_3-doped silica membrane. The sample was sparked with BPA in order to reach a BPA concentration of ~10 mg L^{-1} after concentration. After concentration, 50 mL samples of the concentrate were treated at 50 °C with CSF at concentrations of 1, 2 and 10 g L^{-1} over 5 h. As can be seen in Figure 6, treatment with CSF thermocatalyst in a batch reactor causes 35% abatement of COD after 5 h of treatment. COD abatement does not change significantly by increasing CSF concentration from 1 to 10 g L^{-1}. This result is consistent with the fact that the dissolved organic matter consists of different types of chemical species, some of which are highly recalcitrant to degradation, such as part of the humic substances. On the other hand, the abatement of BPA increases following the concentration of CSF, as shown in Figure 7. However, these tests show also that the thermocatalyst is less efficient in the abatement of BPA in real matrixes, which contain large quantities of dissolved organic matter, than when it was tested with model solutions of BPA dissolved in deionized water.

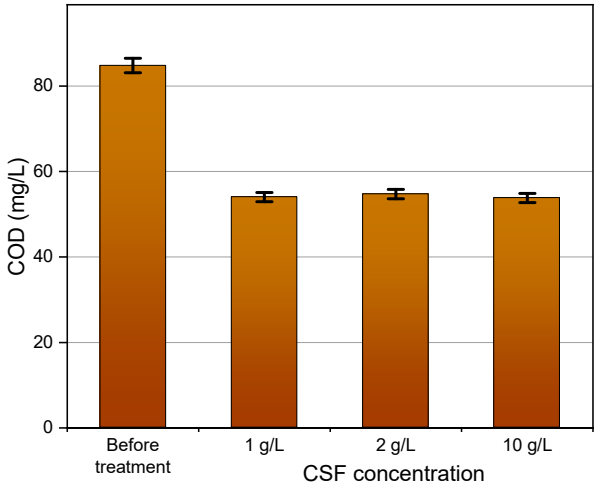

Figure 6. Chemical oxygen demand (COD) in the concentrated wastewater effluent before and after treatment with different amounts of CSF for 5 h.

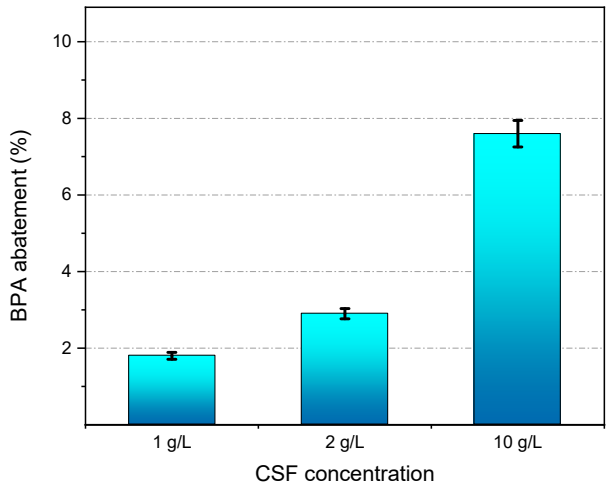

Figure 7. Abatement of BPA in the concentrated wastewater effluent after treatment with different amounts of CSF for 5 h.

4. Discussion

In this study, we presented a new method of water purification using the recently developed Al_2O_3-doped silica NF membrane combined with cerium-doped strontium ferrate (CSF), as thermocatalyst for the abatement of water pollutants. The new process was investigated in the degradation of bisphenol A (BPA), which is a common water contaminant with endocrine-disrupting activity. Concerning the NF membrane, we observed no impact of temperature on BPA rejection, which remains >98% at all the tested temperatures (30–60 °C). Instead, water permeance showed a twofold increment by increasing the feed temperature form 30 to 60 °C. Such temperature-permeance dependence in ceramic NF membranes can be explained by considering the change in solvent viscosity and that permeation in micropores occurs by a combination of viscous flow and activated transport [24]. Hence, the increase of the feed temperature is beneficial for membrane permeance and for the thermocatalytic abatement at the same time [20].

Two possible configurations were tested in this study, each of them with some specific advantages. Addition of CSF at the membrane feed during filtration allows for micropollutant abatement, while mitigating membrane fouling and improving the quality of the permeate. On the other hand, pre-concentration of the wastewater by nanofiltration allows for a strong reduction of the thermal energy needed for the thermocatalytic process, and decreases investment and running costs of the abatement step, since a smaller wastewater volume needs to be treated [26]. The two different configurations can be selected based on the type of wastewater, on its temperature, and on the presence of low-grade waste heat or renewable waste heat.

The experiments reported in this paper can also highlight some of the challenges for the implementation of this technology on a real scale. Firstly, non-toxic dissolved organic matter, which is typically present in wastewaters at concentrations much higher than the micropollutants, has a negative effect on both the water permeance of the membrane [27] and the thermocatalytic performances of CSF in the abatement of micropollutants. In this study, we show that CSF can degrade part of the dissolved organic matter and that, when added in the membrane feed, had also a positive impact on fouling. However, we also observed that CSF was able to degrade about 60% of BPA in deionized water after 3 h at 50 °C and less than 8% of BPA in concentrated wastewater (COD~85 mg L^{-1}) after 5 h at 50 °C. Therefore, thermocatalyst and process parameters should be optimized, taking into account the presence of non-toxic organic matter in real wastewater systems. A second challenge is the process upscaling. In this work, CSF was synthetized in a few grams batches by the solution-combustion method, which is notoriously not amenable to scale up. Nevertheless, Deganello et al. have indicated some strategies for large-scale synthesis of perovskites [27] and the industrial production of CSF is one of the tasks of the project NanoPerWater (EUREKA, Eurostars Cut-off 12, Project number: 113625). For the sake of comparison, all the thermocatalytic tests in this work were performed with dispersed CSF powders. Nevertheless, the recovery and reuse of the thermocatalyst is also a crucial aspect for this technology; especially when CSF is used in a separate abatement step after NF pre-concentration, and thus it cannot be retained by a membrane. For this reason, a possible implementation of this technology consists in the immobilization of the catalyst in a fixed-bed reactor for the abatement of micropollutants from wastewater effluent after pre-concentration over a NF membrane, which is indeed the scope of the recently funded NanoTheC-Aba project (JPI, 1st Aquatic Pollutants Joint Call 2020, Project number: ID 402). Concerning the economy of the new process, Ma et al. [14] have calculated that the Al_2O_3-doped silica NF membrane can operate at a specific energy consumption <0.15 kWh per m^3 of permeate, which makes this step potentially attractive when organic contaminants need to be removed from wastewater. Nevertheless, the thermocatalytic step requires at least 1.167 kWh (m^3 °C)$^{-1}$ for heating wastewater, making the overall process expensive, unless the wastewater stream to be treated already has a temperature suitable for CSF activation, or low-grade waste heat is available on site (which is the case for many industrial processes), or it is possible to exploit solar thermal energy.

5. Conclusions

For the first time, a thermocatalytic perovskite, namely Ce-doped strontium ferrate (CSF), was combined with a NF ceramic membrane for the treatment of wastewater. We showed that the addition of CSF to the membrane feed causes degradation of BPA and reduces BPA traces in the permeate. When the system was tested with a real wastewater effluent, CSF was able to reduce membrane fouling. From analysis of flux over time using different fouling models, it was found that the main fouling type occurring in our experiments is intermediate pore blocking. Our data show also that CSF can effectively degrade part of the non-toxic organic matter present in the water, which can explain its ability to mitigate membrane fouling. CSF can be also used to reduce the COD of wastewater after concentration by NF, although its ability to degrade BPA, and presumably the other micropollutants, is reduced by the scavenging effect of large concentrations of non-toxic organic matter, which also interacts with the reactive oxygen species generated by the thermocatalyst. Despite the abovementioned challenges, the new technology does not require light sources or additions of chemicals, contrary to other hybrid NF-advanced oxidation processes, e.g., those based on photocatalysis or Fenton technologies, respectively. Hence, integration of NF with thermocatalysis has the potential to rise as a new strategy for the treatment of wastewaters contaminated by micropollutants.

Supplementary Materials: The following are available online at https://www.mdpi.com/article/10.3390/membranes11080639/s1: Paragraph S1: Analysis of fouling models; Table S1: Results of R2 for each fouling method for filtration with and without catalyst.

Author Contributions: V.B. conceived the concept. K.J. and X.M. carried out materials synthesis and permeation tests. K.J., M.K.J., V.B. and V.M.C. analyzed data. K.J. wrote the paper with editorial contributions from V.B., M.K.J., V.M.C. and X.M. All authors have read and agreed to the published version of the manuscript.

Funding: This research was funded by the European Union's Horizon 2020 research and innovation program under the Marie Skłodowska-Curie grant agreement N. 765860.

Data Availability Statement: Data are contained within the article or Supplementary Materials.

Conflicts of Interest: The authors declare no conflict of interest.

References

1. Valbonesi, P.; Pro, M.; Vasumini, I.; Fabbri, E. Science of the Total Environment Contaminants of emerging concern in drinking water: Quality assessment by combining chemical and biological analysis. *Sci. Total Environ.* **2021**, *758*, 143624. [CrossRef] [PubMed]
2. Shahkaramipour, N.; Tran, T.N.; Ramanan, S.; Lin, H. Membranes with Surface-Enhanced Antifouling Properties for Water Purification. *Membranes* **2017**, *7*, 13. [CrossRef]
3. Chen, H.; Ku, J.; Wang, L. Thermal catalysis under dark ambient conditions in environmental remediation: Fundamental principles, development, and challenges. *Chin. J. Catal.* **2019**, *40*, 1117–1134. [CrossRef]
4. Werber, J.R.; Osuji, C.O.; Elimelech, M. Materials for next-generation desalination and water purification membranes. *Nat. Rev. Mater.* **2016**, *1*, 16018. [CrossRef]
5. Anderson, M.G.; Mcdonnell, J.; Ximing, C.; Cline, S.A.; Balance, W.W.; Rockstrom, J.; Daily, G.C.; Ehrlich, P.R.; Reidy, C.A.; Dynesius, M.; et al. The Challenge of Micropollutants in Aquatic Systems. *Science* **2006**, *313*, 1072–1077.
6. Xu, R.; Qin, W.; Tian, Z.; He, Y.; Wang, X.; Wen, X. Enhanced micropollutants removal by nanofiltration and their environmental risks in wastewater reclamation: A pilot-scale study. *Sci. Total Environ.* **2020**, *744*, 140954. [CrossRef] [PubMed]
7. Escalona, I.; Fortuny, A.; Stüber, F.; Bengoa, C.; Fabregat, A.; Font, J. Fenton coupled with nanofiltration for elimination of Bisphenol A. *Desalination* **2014**, *345*, 77–84. [CrossRef]
8. Li, C.; Sun, W.; Lu, Z.; Ao, X.; Li, S. Ceramic nanocomposite membranes and membrane fouling: A review. *Water Res.* **2020**, *175*, 115674. [CrossRef]
9. Wang, P.; Wang, F.; Jiang, H.; Zhang, Y.; Zhao, M.; Xiong, R.; Ma, J. Strong improvement of nanofiltration performance on micropollutant removal and reduction of membrane fouling by hydrolyzed-aluminum nanoparticles. *Water Res.* **2020**, *175*, 115649. [CrossRef]
10. Abdel-Fatah, M.A. Nanofiltration systems and applications in wastewater treatment: Review article. *Ain Shams Eng. J.* **2018**, *9*, 3077–3092. [CrossRef]

11. Farsi, A.; Malvache, C.; de Bartolis, O.; Magnacca, G.; Kristensen, P.K.; Christensen, M.L.; Boffa, V. Design and fabrication of silica-based nanofiltration membranes for water desalination and detoxification. *Microporous Mesoporous Mater.* **2017**, *237*, 117–126. [CrossRef]
12. García, N.; Purcell-milton, F.; Gun, Y.K. Recent progress and future prospects in development of advanced materials for nano fi ltration. *Mater. Today Commun.* **2020**, *23*, 100888. [CrossRef]
13. Chon, K.; Cho, J. Fouling behavior of dissolved organic matter in nanofiltration membranes from a pilot-scale drinking water treatment plant: An autopsy study. *Chem. Eng. J.* **2016**, *295*, 268–277. [CrossRef]
14. Ma, X.; Janowska, K.; Boffa, V.; Fabbri, D.; Magnacca, G.; Calza, P.; Yue, Y. Surfactant-assisted fabrication of alumina-doped amorphous silica nanofiltration membranes with enhanced water purification performances. *Nanomaterials* **2019**, *9*, 1368. [CrossRef] [PubMed]
15. Tsuru, T. Inorganic porous membranes for liquid phase separation. *Sep. Purif. Methods* **2001**, *30*, 191–220. [CrossRef]
16. Li, N.; Wang, X.; Zhang, H.; Zhang, Z.; Ding, J.; Lu, J. Comparing the performance of various nanofiltration membranes in advanced oxidation-nanofiltration treatment of reverse osmosis concentrates. *Environ. Sci. Pollut. Res.* **2019**, *26*, 17472–17481. [CrossRef]
17. Wang, J.L.; Xu, L.E.J.I.N. Advanced Oxidation Processes for Wastewater Treatment: Formation of Hydroxyl Radical and Application Advanced Oxidation Processes for Wastewater Treatment: Formation of Hydroxyl Radical. *Crit. Rev. Environ. Sci. Technol.* **2012**, *42*, 251–325. [CrossRef]
18. Arca-Ramos, A.; Eibes, G.; Feijoo, G.; Lema, J.M.; Moreira, M.T. Potentiality of a ceramic membrane reactor for the laccase-catalyzed removal of bisphenol A from secondary effluents. *Appl. Microbiol. Biotechnol.* **2015**, *99*, 9299–9308. [CrossRef]
19. Zielińska, M.; Cydzik-Kwiatkowska, A.; Bułkowska, K.; Bernat, K.; Wojnowska-Baryła, I. Treatment of Bisphenol A-Containing Effluents from Aerobic Granular Sludge Reactors with the Use of Microfiltration and Ultrafiltration Ceramic Membranes. *Water. Air Soil Pollut.* **2017**, *228*, 282. [CrossRef]
20. Janowska, K.; Boffa, V.; Jørgensen, M.K.; Quist-Jensen, C.A.; Hubac, F.; Deganello, F.; Coelho, F.E.B.; Magnacca, G. Thermocatalytic membrane distillation for clean water production. *NPJ Clean Water* **2020**, *3*, 1–7. [CrossRef]
21. He, Z.; Lyu, Z.; Gu, Q.; Zhang, L.; Wang, J. Ceramic-based membranes for water and wastewater treatment. *Colloids Surfaces A Physicochem. Eng.* **2019**, *578*, 123513. [CrossRef]
22. Deganello, F.; Tyagi, A.K. Solution combustion synthesis, energy and environment: Best parameters for better materials. *Prog. Cryst. Growth Charact. Mater.* **2018**, *64*, 23–61. [CrossRef]
23. Farsi, A.; Boffa, V.; Qureshi, H.F.; Nijmeijer, A.; Winnubst, L.; Christensen, M.L. Modeling water flux and salt rejection of mesoporous γ-alumina and microporous organosilica membranes. *J. Membr. Sci.* **2014**, *470*, 307–315. [CrossRef]
24. Tsuru, T.; Izumi, S.; Yoshioka, T.; Asaeda, M. Temperature Effect on Transport Performance by Inorganic Nanofiltration Membranes. *AIChE J.* **2000**, *46*, 565–574. [CrossRef]
25. Mora, F.; Karla, P.; Quezada, C.; Herrera, C.; Cassano, A. Impact of Membrane Pore Size on the Clarification Performance of Grape Marc Extract by Microfiltration. *Membranes* **2019**, *9*, 146. [CrossRef]
26. Miralles-Cuevas, S.; Oller, I.; Agüera, A.; Pérez, J.A.S.; Sánchez-Moreno, R.; Malato, S. Is the combination of nanofiltration membranes and AOPs for removing microcontaminants cost effective in real municipal wastewater effluents? *Environ. Sci. Water Res. Technol.* **2016**, *2*, 511–520. [CrossRef]
27. Oller, I.; Miralles-cuevas, S.; Agüera, A.; Malato, S. Monitoring and Removal of Organic Micro-pollutants by Combining Membrane Technologies with Advanced Oxidation Processes. *Curr. Org. Chem.* **2018**, *22*, 1103–1119. [CrossRef]

Paper IV

VUV-UVC Coupled Membrane Distillation for Recirculating of inland Mariculture Effluents in Israel

Xianzheng Ma,[1] Lana Flanjak, [1] XinXin Chen, [1] Cejna Anna Quist-Jensen,[1] Aamer Ali,[1] Peter Roslev, [1*]

Vittorio Boffa,[1*]

[1] *Department of Chemistry and Bioscience, Aalborg University, Fredrik Bajers Vej 7H, 9220 Aalborg, Denmark.*

*Corresponding Author: vb@bio.aau.dk; pr@bio.aau.dk;

Abstract

Mariculture effluents are characterized by high salinity and high concentrations of dissolved organic matter. Anti-parasitic and anti-fungal agents, such as formaldehyde, are typically added to the pounds in intensive fish farms. However, the direct discharging of such effluents can lead to serious environmental consequences, therefore, a sustainable approach is needed for the treatment of mariculture effluent. Recent studies have found that thermal-driven membrane distillation (MD) is promising for water desalting, due to the nearly complete salt rejection and allowing for higher recovery factors than reverse osmosis. In this study, an effluent from an inland mariculture plan in Eilat (Israel) was taken sparked with 20 ppm of formaldehyde fed to a polymeric hollow fiber membrane. The MD membrane showed almost complete abatement of salinity while recovering up to 90% of the initial feed. Salts in the concentrate were recovered by precipitation. However, the membrane showed only little rejection for formaldehyde. Thus, VUV/UVC photolysis was applied to degrade the formaldehyde in the MD permeate. By coupling MD and VUV/UVC photolysis process, a high degradation efficiency can be observed, and the concentration of formaldehyde dropped below the detection limit (0.5 ppm) within the first 20 min of the photolysis process.

1. Introduction

With the growing demand for seafood products and the reduction of natural fishery resources, aquaculture has become one of the fastest-growing industries in the sector of food production (1). In 2020, aquaculture production has reached around 21.4 million tons, which accounts for nearly half of the total annual marine production (2). Consequently, the impact of the mariculture industry on the quality of the water in the oceans is now not negligible. In high-density fish farming facilities, fish

feeds, drugs, and other chemical products are periodically introduced into the water (3). The resulting effluents are not only abundant with nutrients, dissolved organics, and colloids but they are also characterized by high salinity (4). The direct discharge of the effluents into the coastal area will lead to pollution, eutrophication, and deterioration of the marine ecosystem (5). For the sustainable development of the mariculture industry, appropriate treatment is needed before effluents can be recycled, reused, or discharged. Conventional biochemical approaches such as the activated sludge process or aquaponics system are effective at reducing or reusing the organic matter of the freshwater aquaculture effluents. Nevertheless, the mariculture effluents are challenging for many biochemical processes due to the high salinity (6)(7).

Over the years, membrane technologies have been considered for the treatment of mariculture wastewater after the biological steps. The mainstream membrane desalination technologies such as reverse osmosis (RO) could provide an opportunity to recover freshwater from the effluent. However, the RO has a limited water recovery factor (about 35%-85%) due to the increase of osmotic pressure in the feed during the filtration process (8)(9). The disposal of the brine produced by the RO units represents a further problem (9)(10). In recent years, the thermal-driven membrane technology, membrane distillation (MD), has shown great potential for desalination applications. Compare to RO, MD can achieve much higher water recovery factors while delivering nearly complete salt rejection. In a typical MD process, a hydrophobic membrane with a pore size below 1 μm is applied as a barrier between the feed and the permeate, and the feed solution is heated to create a temperature gradient across the membrane (11). Due to the hydrophobic nature of the membrane, liquid can not transport through the membrane, instead, the water vapor permeates via the membrane pores from the feed and

condensed on the permeate side (11)(12). Over time, the feed solution is concentrated and fresh water can be collected from the permeate side. The feed solution can be concentrated up to the saturation point where the solute can be precipitated (13). Therefore, MD can not only be used to recover freshwater but also to recover valuable minerals or molecules from the feed solution (13)(14). Therefore, the introduction of MD in mariculture facilities can potentially achieve zero-liquid discharge (15).

Although MD is highly effective at retaining the nonvolatile components in the feed, it can not reject volatile compounds. However, many volatile compounds are potentially generated or accumulated in aquaculture systems. One example is formaldehyde, which has an extensive history of use in aquaculture as a disinfection agent to prevent parasites and fungal infections (16). The consensus is that the discharge of formaldehyde-enriched effluents will harm the marine ecosystem (17). Advanced oxidation processes (AOP) have become increasingly attractive for micropollutant removal. The AOP relies on the generation of hydroxyl radicals (OH•), which can oxidize the organic micropollutants into mainly water and carbon dioxide. The hydroxyl radicals can be derived from the primary oxidants, Fenton-like processes, or photo/thermal catalytic reactions (18). Yet, most of the AOP requires additional chemical input, which could increase the cost and cause secondary pollution. Vacuum-UV (VUV) devices can emit photons with a wavelength in the range of 200 to 10 nm (UVC). Recent studies have shown that VUV/UVC-based technologies have great potential in removing organic pollutants in water, because of the simple implementation and their functioning without additional chemicals. For instance, Gonçalves, et al. reported around 95% of clotrimazole (4ppm) degradation was obtained after 32 min of irradiation (25 J $cm^{2\ -1}$) (19). This study aims to explore the synergistic

integration of MD with VUV/UVC for the treatment of a mariculture effluent for the simultaneous production of distilled water and the recovering of the minerals in the concentrate.

2. Materials and Experiment

2.1 MD experiment

The water samples of the mariculture effluent for the MD experiment were collected from the National Center for Mariculture, Eilat, Israel. In this experiment, A lab-scale DCMD setup equipped with a commercial MD module (Microdyn-Nadir, MD 020 CP 2N) was applied for this study, and the detailed configuration of the MD system has been elaborated in a previous study (19). The modules had an active filtration area of 0.1 m^2 and consisted of polypropylene hollow fibers with an average pore size of 0.2 μm. The starting volume of the feed and the drawing solutions were 2 L of and 0.7 L, respectively. A heating bath was set to produce a temperature of 40℃, 55℃, and 70℃ to the feed solution. While the temperature of the drawing solution was kept at 15°C by a cooling bath. The feed stream was pumped inside of the hollow fibers, while the permeate stream was circulated at the outside of the hollow fibers. The flows of the feed and the permeate solutions were provided by a peristaltic pump with a flow rate of 20L h^{-1}. A countercurrent flow configuration was selected to maximize the temperature gradient across the membrane. The temperatures for both inlet and outlet of the feed and permeate side were measured by digital thermometers during the experiments. The permeability of the MD system was measured by the increasing weight of the water in the permeate tank via a digital balance. While the pH of the feed and the conductivity of the permeate were also logged via a MATLAB program.

2.2 Water characterization

The salinity of both feeds and permeate solution was investigated by a conductivity meter, while the pH of the permeate solution during the photolysis process was measured by a pH meter. The concentration of the formaldehyde was determined based on the Hantzsch reaction with β-diketone, 4-amino-3-pentene-2-one (Fluoral-P). Formaldehyde reacts with Fluoral-P and produces 3,5-diacetyl-1,4-dihydroluthydine that can be detected by spectrometry and fluorimetry (Compton et al. 1980; Loh et al. 2007). Fluoral P (Sigma, Denmark) was dissolved in acetonitrile and added to samples acidified to pH 4 with phosphate buffer. Absorbance (412 nm) and fluorescence (Ex/Em 485/535 nm) was determined after 30 min using a UV/VIS spectrophotometer (Thermo Scientific™ GENESYS™ 20 Visible Spectrophotometer) and a Perkin Elmer Victor X2 multilabel plate reader, respectively. The quantification of formaldehyde was not affected by the presence of NaCl in the samples at concentrations below 28 ppt.

2.3 Crystal characterization

To investigate the salt crystal formation during the MD process, an optical microscope (ZEISS, Axiolab 5) was applied to observe the water sample from the feed solution. The morphology and the composition of the crystal participation were collected from the feed solution and were examed by X-ray diffraction (XRD) and inductively coupled plasma spectroscopy (ICP), respectively. The XRD measurements were performed by Empyrean XRD, PANalytical, with a monochromator Cu Kα radiation (1.5406 Å). Spectra were acquired in the range from 5° to 75° at 40 kV with a scanning rate of 8° min^{-1}. On the other hand, the composition of the obtained salt crystals was analyzed by

redissolving the dried salts in DI water to achieve a concentration of 1g L^{-1}, and the potential presented cation concentration in the solution was measured by ICP (PerkinElmer® Optima 8000 Optical Emission Spectrometer). The calibration of the ICP was down by the standards from PlasmaCAL Q.C. No 4 (SCP Science).

2.4 VUV/UVC irradiation

The degradation experiments in this study were conducted by a lab-made VUV/UVC photolysis reactor. Before the experiment, the permeate solution obtained from the MD process was diluted with ID water to achieve a final volume of 3.5 L. The detailed structure of the reactor was described in a previous study, in brief, the reactor consisted of a stainless-steel cylinder feed tank that connects to the photolysis reactor that contains an amalgam VUV/UVC lamp (1050mm × 19mm) (19). The solution was circulating in the system by a centrifugal pump with a flow speed of around 2L min^{-1}, while a cooling system was applied to keep a constant temperature. The VUV/UVC lamp was able to emit the UVC and VUV with a 4:1 ratio, simultaneously, which can produce the radiation flux of 56 W and 14 W, respectively. Each degradation experiments last for 64 min while water samples were collected during the experiments.

3. Results and discussion

3.1 Membrane distillation of the mariculture discharge

The first set of experiments was designed to determine the desalination ability of the hollow fiber module to desalinate the mariculture effluent. Before the experiments, the effluent samples were

filtered over a 50 μm paper filter. The filtration tests were performed with a starting feed solution of 2 L, which was kept at different a temperature (40℃, 55℃, 70℃) for each experiment, while 0.7 L of DI water was circulating on the permeate side with a cooler operated at 15℃. Figure 1A shows the water flux of the MD system under the three operation temperatures over the filtration time. Generally, the water flux under different temperatures was relatively stable throughout the experiment. The fluxes of permeate across the membrane were about 0.6 LMH, 1.5 LMH, and 2.6 LMH when the feed tank temperature was set to 40℃, 55℃, and 70℃, respectively. This is not surprising, indeed, the driving force of the MD process is the vapor pressure difference caused by the temperature gradients across the membrane. During the experiment, the flux has shown a very slight decreasing trend over time, the is could be caused by the increase of the osmotic pressure due to the concentration of the feed. However, for MD, the impact of the osmotic pressure is relatively minor, since the vapor pressure is the dominating driven force. The vapor pressure positive correlates with the temperature, and therefore, the increase of the flux can be observed with the increase in the temperature. The water recovery factors vs filtration time during these experiments are shown in Figure 1B. The water recovery is stable with a nearly linear development over time reaching values of between 80% and 90 % for the three experiments. With the increase in the temperature, the rate of water recovery also increases due to the higher water flux. By the end of the MD process of each operating temperature, crystals have become visible in the feed solution. A detailed analysis of the elaborated in the next section.

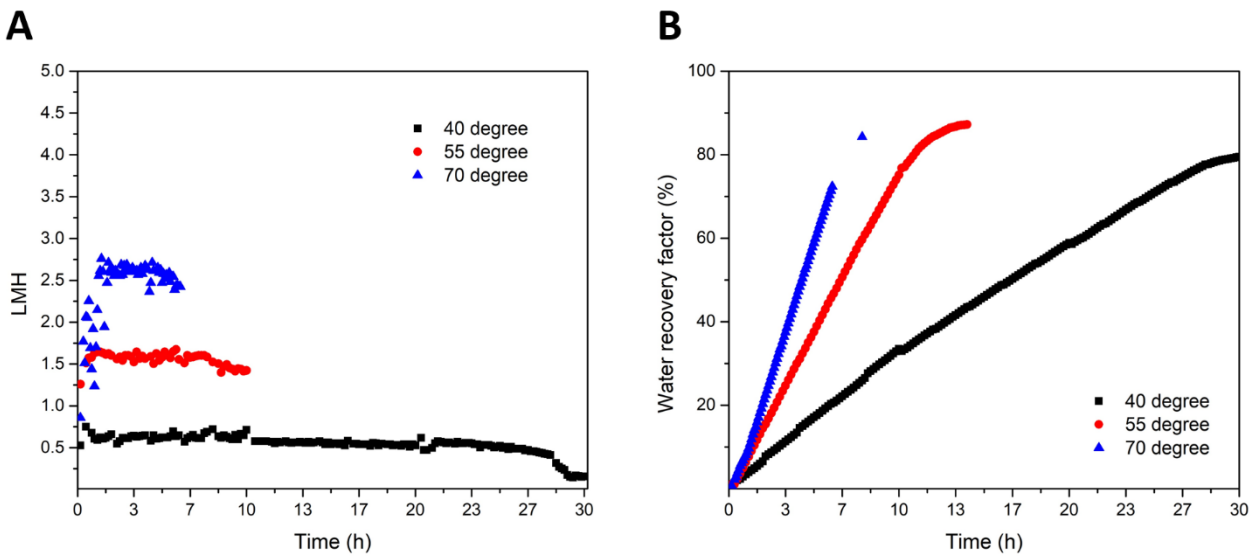

Figure 1: (A) The flux and the water recovery factors (B) of the MD system under the operating temperatures of 40°C, 55°C, and 70°C over time.

The membrane has also shown a high salt rejection at all the tested temperatures. The change in permeate conductivity is shown in Figure 2. The final permeate conductivity for all temperatures was at around 100 µs cm^{-1}. The permeate conductivity is nearly negligible compared with the feed conductivity (42000 µs cm^{-1}), which indicates almost all salt ions have been retained by the MD. The high rejection shows that the membrane has a high degree of resistance toward wetting. However, the permeate conductivities have a general trend of first increasing and then decreasing over time. It is worth noticing that the peak of each permeate conductivity is also increasing slightly with the operating temperature of the feed. The highest permeate conductivity values were 100 µs cm^{-1}, 107 µs cm^{-1}, and 113 µs cm^{-1}, for the feed heating temperature of 40°C, 55°C, and 70°C, respectively. The increase in conductivity could be explained by the permeation of the conductive volatile components such as NH_3, which is present in low concentrations in the feed. Indeed most of it should be removed in the nitrification process and integrated into the mariculture system. As the temperature increases, the vapor

pressure of the volatile components also increases, resulting in a higher concentration of the conductive volatile components in the permeate, hence a higher conductivity. Over time, when most of the conductive volatile components from the feed have permeated through the membrane, and the evaporation rate of the water surpasses the volatile components, a decrease in conductivity can be observed due to the dilution from the water.

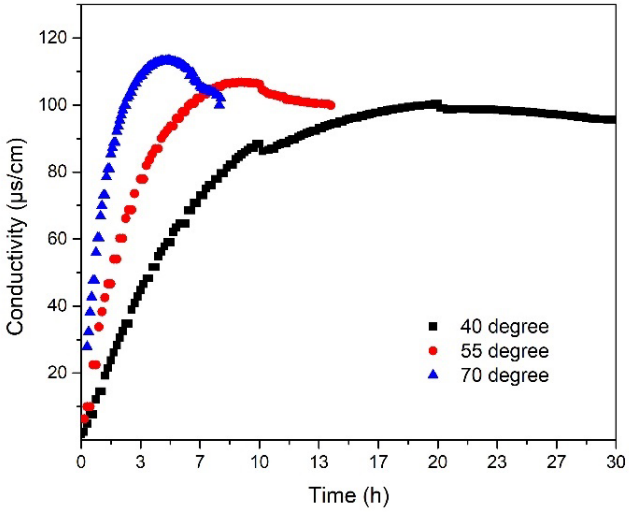

Figure 2: The development of permeate conductivity at the feed operating temperatures of 40°C, 55°C, and 70°C over time.

In the mariculture industry, formaldehyde has been extensively used as an antifungal and antiparasitic agent. Although no formaldehyde was detected in the mariculture effluents, in this study, to investigate the MD at retaining volatile pollutants, 20 ppm of formaldehyde was sparked into the feed solution as a model pollutant to simulate the fish farming process. Figure 3 A shows the change in formaldehyde concentration over time for the three operating temperatures. Overall, the MD has shown poor retention of formaldehyde, the final formaldehyde concentration of the permeate was 7.1, 15.8. and 10.9 ppm for the operating temperature of 40°C, 55°C, and 70°C, respectively. The formaldehyde concentrations of the permeate solutions are developed linearly over time, indicating a relatively

constant evaporation rate of formaldehyde from the feed solution. The net formaldehyde concentration in the water permeating the membrane was calculated from the concentrations in the drawing solution corrected for the initial volume of the drawing solution (700 mL) and plotted in Figure 3B. It can be seen that the net formaldehyde concentration increase with the temperature. The average net formaldehyde concentration raises from 8.3 to 16.2 ppm when the feed tank temperature increases from 40℃ to 70℃, which can be ascribed to the increases in formaldehyde vapor pressure with the temperature. The net permeates formaldehyde concentration for all operating temperatures is lower than the 20ppm of initial feed formaldehyde concentration indicating that the formaldehyde has a low evaporation rate than water vapor at the tested temperature range. The remaining formaldehyde is mostly retained.

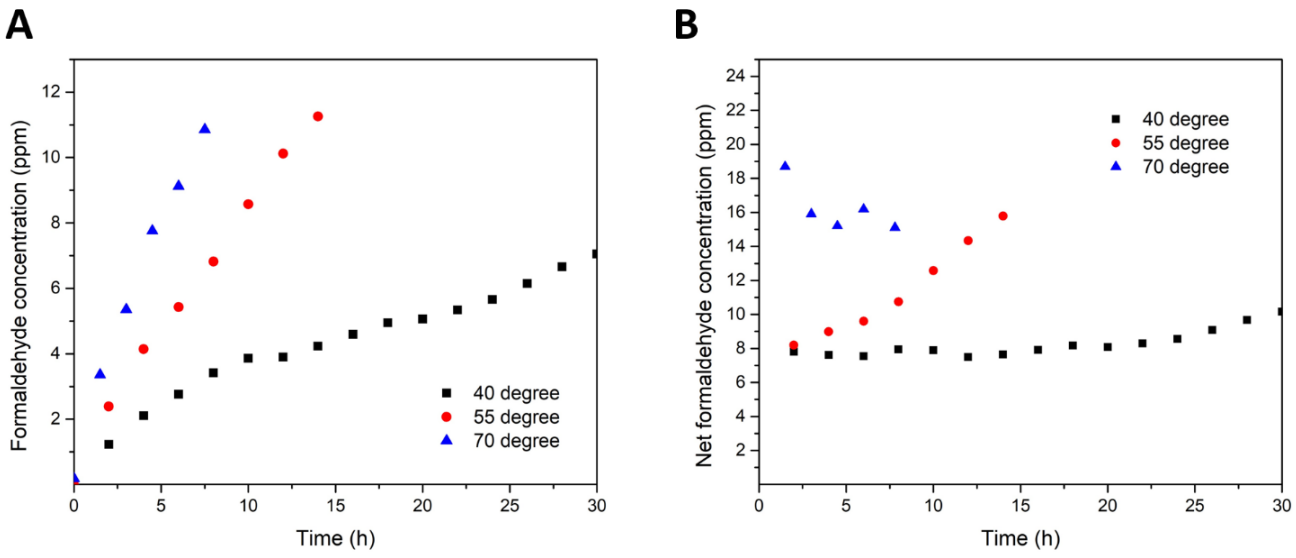

Figure 3: Formaldehyde concentration in the drawing solution (A) and the net formaldehyde concentration in the permeate (B) at the feed tank operating temperatures of 40℃, 55℃, and 70℃.

3.2 Crystallization of salts

In the MD process, when the feed concentration exceeded the saturation point, precipitation of the salts can become visible. Therefore, MD can not only be used for the recovery of distilled water at the permeate side but also minerals and molecules from the concentrate. To investigate the potential of salt crystals recovery from the feed and the effect on membrane scaling, the crystal formation during the MD process was observed by optical microscope, and the salt crystals that were obtained during the MD experiment were analyzed by ICP and XRD. The feed sample from the operating temperature of 70 °C was taken and examined under the microscope every 15 min after 6.5h to observe the crystal formation. It can be seen from the microscope images in Figure 4 that there are two types of crystal formed in the feed solution before and after 7h. The crystals that are formed before 7h have no clearly defined geometry, it can be assumed that salts with low solubilities, e.g. carbonates precipitate at this stage. With the progression of the crystal formation, an agglomeration can be observed for the first type of salt at 7h. After 7h, crystals with cubic shape start to form in the feed solution. This shape is indicative of the formation of NaCl. In the next 30min, the crystals growth and agglomerate.

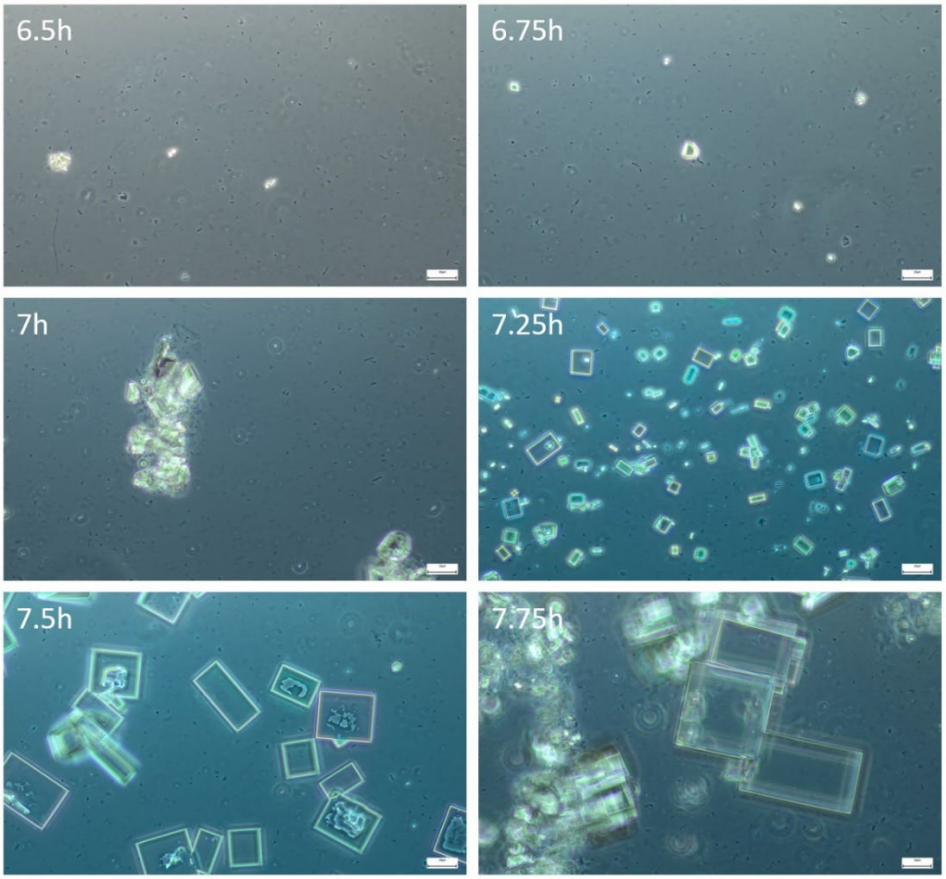

Figure 4: The salt crystals formation microscope image of the feed solution at 70℃ between 6.5h to 7.75h.

The salt crystals that have obtained from all operating temperatures were collected from the feed by centrifugal at 1500rpm and dried at room temperature. The composition of the salts was determined by dissolving the dried salt in DI water to achieve a 1g L^{-1} solution, and the concentration of the cations was measured by ICP.

Table 1: The cation weight percentage of the obtained salt solution under different feed operating temperatures.

Feed temperatures(℃)	**Na^+ (wt%)**	**K^+ (wt%)**	**Ca^{2+} (wt%)**	**Mg^{2+} (wt%)**
40	5.78	0.40	15.34	0.61
55	21.77	0.81	7.09	1.32
70	21.03	0.76	7.16	1.21

As shown in Table 2, the cations with the highest concentration are Na^+, K^+, Ca^{2+}, and Mg^{2+}. Transition metal ions are not reported in the table because their concentration was below the detection limit. For the salt sample obtained keeping the feed tank at 40℃, the Ca^{2+} has the highest relative concentration, followed by Na^+, Mg^{2+}, and K^+. Salts obtained from the concentration of feed, while keeping the tank at 55℃ and 70℃ have similar cation compositions: Na^+ has the highest concentration, followed by Ca^{2+}, Mg^{2+}, and K^+. The composition difference between the salt obtained from different temperatures could be resulting from the water recovery difference. The experiment stopped and salts were collected at recovery factors of 79%, 87%, and 84% for the experiments with a feed tank at 40℃, 55℃, and 70℃. This indicates initially mostly calcium salts, e.g. calcium carbonate precipitates (before reaching a recovery factor of 79%), then, mostly NaCl crystals are formed.

3.3 Formaldehyde degradation by VUV/UVC

The membrane showed poor retention for formaldehyde: Indeed, after the MD process, the formaldehyde concentration of the permeate still ranges between 4 and 8 ppm. To remove the formaldehyde in the permeate, VUV/UVC photolysis is applied in this study. In general, the degradation of the formaldehyde results from the forming of hydroxyl free radicals by the VUV/UVC irradiation-induced water and oxygen molecule homolysis, as shown in the equations. (20) In the reaction, the product could include hydroxide, hydrogen, and oxygen free radicals, also protons and electrons. The generated species can not only degrade organic micropollutants but also reduce potential heavy metal ions.

$$H_2O + hv(\lambda = 185nm) \rightarrow H\cdot + OH\cdot \quad (1)$$

$$H_2O + hv(\lambda = 185nm) \rightarrow H^+ + OH\cdot + e^- \quad (2)$$

$$O_2 + hv(\lambda = 185nm) \rightarrow 2O\cdot \quad (3)$$

To determine the formaldehyde degradation efficiency of our VUV/UVC photolysis reactor, water samples were taken periodically and the concentration of the compound in the reaction was plotted in Figure 6 A as a function of the irradiation time. In general, the VUV/UVC reactor shows high efficiency in removing formaldehyde. At 0 min of the photolysis process, the concentration of formaldehyde was 4.0ppm, 8.0ppm, and 7.3 ppm for the permeate solution obtained with the feed tank at 40℃, 55℃, and 70℃, respectively. An exponential decrease in the formaldehyde concentration can be noticed during the photolysis process, and 97%. 73% and 77% of the formaldehyde were degraded after 8 min of irradiation for the permeate obtained from 40℃, 55℃, and 70℃, respectively. After 16 min, the concentration of formaldehyde in the 3 permeates dropped below the detection limit. The pH of the permeate water was also monitored during the VUV/UC photolysis process. It can be seen in Figure 6B that the pH has a similar trend to the degradation curve of the formaldehyde. At 0 min, all permeate from different temperatures have a pH in the range of 7.3 and 7.6. Over time, an exponential decrease in the pH can also be observed. The pH decreased to about 6.7 within the first 10min of the photolysis experiment and kept in the range of 6.5-6.6 throughout the rest of the experiments. The decrease of the pH could be resulting in the formation of formic acid and carbonates from the degradation of the formaldehyde, additionally, the generation of H^+ can take place during the photolysis process, as shown in equation (2), which contributes to the decrease of pH.

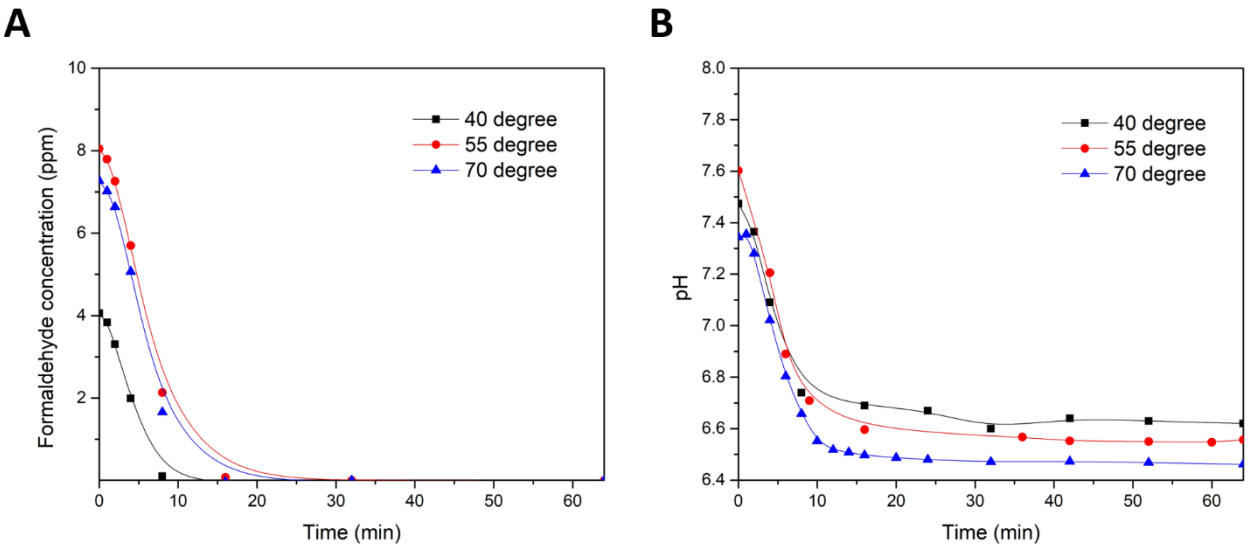

Figure 5: The change of the formaldehyde concentration (A) and pH (B) of the permeate solution obtained from feed operating temperatures during the VUV/UC photolysis process.

4. Conclusion

In this study, the potential of applying the MD for the desalination of an inland mariculture effluent and VUV/UVC photolysis reactor for the detoxification of the MD permeate was investigated. To test the efficiency of the MD system, the MD system was operated at a feed temperature of 40℃, 55℃, and 70℃ reading recovery factors up to 90%. The MD process has shown nearly complete desalting in all the tests. Precipitation of salt crystals was observed in the feed solution during concentration. The salt species that can be obtained from the MD process largely depend on the solubility of the salt and the water recovery factor of the MD process. Calcium carbonates precipitate first, followed by NaCl. Despite the high salt rejection, the membranes were permeable to formaldehyde, due to the volatile nature of this compound. Therefore, the VUV/UVC photolysis reactor was applied for the degradation of the formaldehyde. It can be seen that the photolysis can fully degrade the formaldehyde

from all permeate samples within 20 min. To the best of our knowledge, this is the first time that these two techniques, namely MD and VUV/UVC advanced oxidation, are combined.

Author Contributions: conceptualization, X.M., V.B., and P.R.; methodology, CAJQ, and A.A.; formal analysis, X.M, L.F. CAJQ and X.C.; investigation X.M. and L.F.; writing original draft, X.M.; writing—review and editing, V.B, P.R. CAJQ, and A.A.; supervision, V.B, and P.R.; funding acquisition, V.B.

Funding: "Project Ô" (H2020-CIRC-2017TwoStage, Grant Agreement n. 776816).

Acknowledgments: The authors wish to thank the European Commission for funding.

Conflicts of Interest: The authors declare no conflict of interest.

References

1. Lu S, Wang Q, Gao M, Zhao C, She Z, Zhao Y, et al. Effect of aerobic/anoxic duration on the performance, microbial activity and microbial community of sequencing batch biofilm reactor treating synthetic mariculture wastewater. Bioresour Technol. 2021;333:125198.
2. Zheng L, Liu Q, Liu J, Xiao J, Xu G. Pollution Control of Industrial Mariculture Wastewater: A Mini-Review. Water. 2022;14(9).
3. Wang X, Cuthbertson A, Gualtieri C, Shao D. A review on mariculture effluent: Characterization and management tools. Water. 2020;12(11):1–24.
4. Lymbery AJ, Doupé RG, Bennett T, Starcevich MR. Efficacy of a subsurface-flow wetland using the estuarine sedge Juncus kraussii to treat effluent from inland saline aquaculture. Aquac Eng. 2006;34(1):1–7.
5. Song D, Xu J, Fu Y, Xu L, Shan B. Polysulfone/sulfonated polysulfone alloy membranes with an improved performance in processing mariculture wastewater. Chem Eng J. 2016;304:882–9.
6. He H, Chen Y, Li X, Cheng Y, Yang C, Zeng G. Influence of salinity on microorganisms in activated sludge processes: A review. Int Biodeterior Biodegrad. 2017;119:520–7.
7. Spradlin A, Saha S. Saline aquaponics: A review of challenges, opportunities, components, and system design. Aquaculture. 2022;555(February):738173.
8. Wilf M, Bartels C. Optimization of seawater RO systems design. Desalination. 2005;173(1):1–12.
9. Morillo J, Usero J, Rosado D, El Bakouri H, Riaza A, Bernaola FJ. Comparative study of brine

management technologies for desalination plants. Desalination. 2014;336(1):32–49.

10. Peters T, Pintó D. Seawater intake and pre-treatment/brine discharge - environmental issues. Desalination. 2008;221(1–3):576–84.

11. Khayet M. Membranes and theoretical modeling of membrane distillation: A review. Advances in Colloid and Interface Science. 2011.

12. Liao Y, Zheng G, Huang JJ, Tian M, Wang R. Development of robust and superhydrophobic membranes to mitigate membrane scaling and fouling in membrane distillation. J Memb Sci. 2020;601:117962.

13. Quist-Jensen CA, Macedonio F, Horbez D, Drioli E. Reclamation of sodium sulfate from industrial wastewater by using membrane distillation and membrane crystallization. Desalination2017;401:112–9.

14. Quist-Jensen CA, Ali A, Mondal S, Macedonio F, Drioli E. A study of membrane distillation and crystallization for lithium recovery from high-concentrated aqueous solutions. J Memb Sci. 2016;505:167–73.

15. Panagopoulos A, Haralambous KJ. Minimal Liquid Discharge (MLD) and Zero Liquid Discharge (ZLD) strategies for wastewater management and resource recovery-Analysis, challenges and prospects. J Environ Chem Eng. 2020;8(5):104418.

16. Leal JF, Neves MGPMS, Santos EBH, Esteves VI. Use of formalin in intensive aquaculture: properties, application and effects on fish and water quality. Rev Aquac. 2018;10(2):281–95.

17. Jung SH, Kim JW, Jeon IG, Lee YH. Formaldehyde residues in formalin-treated olive flounder (Paralichthys olivaceus), black rockfish (Sebastes schlegeli), and seawater. Aquaculture.

2001;194(3–4):253–62.

18. Leong S, Razmjou A, Wang K, Hapgood K, Zhang X, Wang H. TiO2 based photocatalytic membranes: A review. J Memb Sci. 2014;472:167–84.

19. Gonçalves NPF, del Puerto O, Medana C, Calza P, Roslev P. Degradation of the antifungal pharmaceutical clotrimazole by UVC and vacuum-UV irradiation: Kinetics, transformation products and attenuation of toxicity. J Environ Chem Eng. 2021;9(5):106275.

20. Abbaszadeh Haddad F, Moussavi G, Moradi M. Advanced oxidation of formaldehyde in aqueous solution using the chemical-less UVC/VUV process: Kinetics and mechanism evaluation. J Water Process Eng. 2019;27:120–5.

ISSN (online): 2446-1636
ISBN (online): 978-87-7573-831-1

AALBORG UNIVERSITY PRESS